Study of Wellbore Stability With Varying Borehole Orientation Through Stress Condition Modeling

by

Dharmendra Kumar Gupta

COLLEGE OF ENGINEERING STUDIES

Submitted

In partial fulfillment of the requirement of the degree of

Doctor of Philosophy

to

UNIVERSITY OF PETROLEUM AND ENERGY STUDIES

DEHRADUN

April, 2011

Dedicated

To

Upstream Community

ACKNOWLEDGEMENTS

I take this opportunity to express my gratitude to Dr. S.J.Chopra, Chancellor, UPES for his blessings & encouragement throughout the work. I would like to express my deepest thanks and gratitude to Dr.Parag Diwan,Vice Chancellor, UPES for being an outstanding motivator & supervisor who inspired me to work in drilling area. I am thankful to Shri G.C Tewari Pro Vice Chancellor, UPES for his best wishes. Of course the foremost, I thank my guide Prof. B.P.Pandey Ex Dean Emeritus UPES for his support at critical times. His insights and enthusiasm have been inspirational for me at all times. His constant encouragement and invaluable suggestions made this work possible. I am grateful to Prof D.N.Saraf & Prof Badhoni for fruitful suggestions based on his rich experience.

I would like to express my gratitude to Dr.Shri Hari , Dean ,COES, UPES for his cooperation and providing a good working atmosphere during my work . I acknowledge and thank Mrs Deepa Verma ,Head Institution Development ,UPES for sponsoring me to complete IWCF course. I wish to thank everyone who added to the value of the work described in this thesis and to the pleasure I gained from it**.**

I am beholden to Mr.A.K. Hazarika Ji CMD, ONGC who allowed me to work at Ahmadabad Asset; Mr B.S.Bisht (DGM well) GEOPIC, ONGC for their continuous support & discussions. I specially thank Mr. Abhishek Upadhyay (DGM Drilling) Crain Energy for his constructive discussions related to Wellbore instability problems.

I am extremely thankful to Dr. P.C.Nawani, Director, National Institute of Rock Mechanics ,Bangalore who allowed me to work in rock mechanics laboratory .Dr.Ajay Nathani,Senior Scientist, Dr. Nagarajan (head, Rock machines lab) help on TRIAXIAL Machine for finding rock mechanical properties. I also thank Mr Amit Parihar , for making my stay comfortable at Bangalore. Dr. Dinesh Zope (Head Reservoir)Reliance Industries Ltd; Prof. Mahendra Singh (IITR) Head of Rock mechanics department ;Dr. Vijay

Dangwal ,PWD Dehradun , my discussions with them greatly improved my work as well as my understanding of earth stresses. My sincere thanks to Dr. R.Islam, Scientist-F, Wadia Institute of Himalayan Geology for fruitful discussions.

I would like to extend my gratitude to Dr. Pradeeep Joshi, HOD for allowing me to participate in teaching rock mechanics and drilling engineering for various bachelor and master degree programs in UPES. In particular, I would like to thank Prof. Arun Chandel for his fruitful discussions and timely help. My colleagues Shayam Pandey, R.K.Tripathi, Deepak Kumar & Ajay Kumar always helped me as & when required. I would like to thank Prof.S.K. Nanda, Dr.Devraju, Prof.K.S.Mishra & Prof.Sokari Braide for helping in understanding geological faults and tectonic activities, Prof. Ravi Kiran helped in Mat Lab and Prof Prakash in C-Proraming. A special thanks goes to Dr. Meenakshi Singhal for pains taking efforts in editing the draft. Thanks to Mr Birendra ,Mrs Pooja ,Ms Anita & Mr Anup for their help with typing, administrative and publishing matters.

The friendship of Prof S.C.Gupta , Dr.Kamal Bansal , Dr.Nihal A.S helped me through quite a few difficult days. It has been a pleasure to be a part of their lives together. The main instrumental during the work is my student Mr. Suresh Ayyappan (M.Tech. PE). He deserves my whole hearted best wishes for wonderful career ahead.

Finally, I am thankful to almighty God, my parents Shri Ramsharan Das Gupta & Smt Vimla Gupta ,my in-laws Shri Ramsharan Rusia & Smt Meena Rusia & family members for their support over the years and that has always been a great source of confidence. Last, but not least, my better half Mrs. Deepti Gupta and kids Khyati & Athrav, hold special mention for their love & understanding during field work and in the making of this dissertation complete.

Dharmendra Kumar Gupta

DECLARATION

I hereby declare that this submission is my own work and that, to the best of my knowledge and belief, it contains no material previously published or written by another person nor material which has been accepted for the award of any other degree or diploma of the university or other institute of higher learning, except where due acknowledgment has been made in the text.

Dharmendra Kumar Gupta

Abstract

Wellbore stability is of critical importance in the success of drilling operations. One of the main goals of any drilling mission is to drill the well as cost-effective as possible. Wellbore instability can be detrimental to this goal. Therefore, wellbore stability analysis has been included in well planning stage of many companies.

Wellbore stability is a function of several factors such as inclination and azimuth, in situ stresses, mud weight, rock strength parameters, etc. Some of these factors are controllable and some are not. Among the controllable factors are inclination, azimuth and mud weight. By changing these parameters, one can reduce stability problems significantly. Theoretically, it is possible to design the well trajectory in a way to face least stability problems. ***In this dissertation linear elastic constitutive model along with Mohr-Coulomb failure criterion have been utilized to perform stability calculations for different inclinations and azimuths.***

The use of inclined and horizontal wells in the exploitation of natural resources has increased considerably and so the need of wellbore stability while drilling arises. This is particularly true for long reach, highly deviated and horizontal wells where the cost of downtime is very high. During the development phase engineers seek to optimize wellbore stability through determination of optimal well trajectories and safe mud weights. The implications of borehole instability to lost drilling time and equipment have prompted operators and service companies to apply Petroleum Geomechanics principles to define working limits for mud weights to avoid tensile or compressive failure. The theoretical analysis involved in borehole stability is quite complex and requires a great deal of mathematical insight.

Wellbore stability modeling is relevant to the full lifecycle of oil exploration and production. Increasingly, drilling programs are incorporating a more proactive approach to mitigate this frequent and expensive source of drilling cost over-runs (McLennan and Abou-Sayed, 2002). Rather than using trial-

and-error methods to maintain wellbore integrity, geomechanical modeling techniques are using available data to provide a solid technical foundation from which to manage the drilling process. Most stability problems occur in shale formations. The main causes are high original pore pressure and drilling-induced pore pressure perturbations, along with chemical interactions between the formation and the drilling fluids. In addition to well-known shear failure, tensile failure of shales is one of the most troublesome and hard-to-predict forms of wellbore destabilization. This failure is typified as wellbore spalling, splintered cavings or another caving morphology. Modeling of the near-wellbore stress environment requires consideration of the complex interaction of wellbore mechanical and hydraulic forces.

Stress is a concept fundamental to Rock Mechanics principles and applications

1. There is a pre-existing state in the rock mass and we need to understand it, both directly, and as a stress state applies to analysis and design.
2. During rock excavation, the stress state can change dramatically. This is because rock, which previously contained stress, has been removed and the load must be redistributed.

Geomechanical Instability

Geomechanical instability refers to mechanical conditions such as wellbore collapse or failure. In general, wellbore instability is related to drillpipe sticking, tight spots, caving production, wellbore collapse and unscheduled sidetracks. These conditions are mostly caused by unknown rock stress conditions and lead to increased costs during drilling and completion operations.

The proposed methodology assumes the validity of linear elastic theory for porous media in order to predict geomechanical rock behavior. In addition to this, to reduce solution uncertainties in the model a set of data is used, which

is obtained from drilling reports, well logging, laboratory tests, well tests such us LOT (Leak off Test), FIT (Formation Integrity Test) and microfracturing. The main goal of this method is to obtain representative models to be used while drilling, so it would be possible to prevent instability problems and to reduce non productive time and drlling costs.

Geomechanics behind Minimum Mud Weight (MW_{min})

The mud weight window is bounded on the lower side by the minimum mud pressure required to prevent excessive shear failure of the wellbore wall. Minimum Mud Weight also sometimes called collapse pressure. Geomechanical concept behind MMW is that it helps in preventing the magnitude of deviatoric stresses to exceed the shear strength of the subsurface rock formations so that shear failure can be prevented.

When mud weight is too low than the MW_{min}, it means low wellbore pressure. Sometimes portion of the walls of the formation drilled earlier collapse due to pressure imbalances and mix with the cuttings. Under low wellbore pressure the tangential or circumferential or hoop stress is high and ultimately difference between hoop stress $\sigma\theta\theta$ and radial stress σrr (i.e. deviatoric stresses) in some areas around the wellbore is large enough to develop shear failure of the wellbore. This failure is known as wellbore collapse.

Normally the induced stresses are compressive and create shear stress within the rock. The more equal these stresses, the more stable the rock.

Geomechanics behind Maximum Mud Weight (MW_{max})

The mud weight window is bounded on the higher side by the maximum mud pressure required to prevent tensile failure of the wellbore wall. The mud weight should not exceed the frature gradient. There are numerous definitions of fracture gradient but in practice this is the mud weight at which excessive lost circulation occurs. Maximum Mud Weight is also sometimes called Fracture Pressure. Geomechanical concept behind $\mathbf{MW_{max}}$ is that it helps in

preventing the magnitude of radial stresses to exceed the fracture strength of the subsurface rock formations so that tensile failure can be prevented.

When mud weight is too high than the MWmax, it means high wellbore pressure. Too high a wellbore pressure will open fractures in the formations resulting in loss of mud. Under high wellbore pressure the tangential or circumferential or hoop stress goes into tension resulting in axial fractures. The induced hoop stress decreases and may become negative resulting in rock failure in tension. This failure is known as wellbore burst. The term wellbore burst is always associated with Formation Breakdown Pressure.

CONTENTS

References

Appendix

- **Appendix A**

  C-Program to calculate the transposed In-Situ Stress
  C-Program to calculate the Induced Wellbore Stress
  C-Program to calculate both transposed and Induced Wellbore Stress

- **Appendix B**

  Experimental Exposure at National Institute of Rock Mechanics, Bangalore

List of Figures

List of Tables

List of Symbols

σ_v	Vertical stress
σ_H and σ_h	Two horizontal stresses
σ_1	Maximum principal stress
σ_2	Intermediate principal stress
σ_3	Minimum principal stress
$\sigma_{\theta\theta}$, σ_{rr} and σ_{zz}	wellbore induced stresses
σ_x, σ_y and σ_z	Transposed In-situ Stresses
MW_{max}	Maximum Mud Weight
MW_{min}	Minimum Mud Weight
θ	Circumferencial Wall Angle
τ	shear stress
α	hole deviation angle, from vertical
β	hole azimuth
ρ_m	Mud Density (ppg)
ρ_b	Rock bulk Density (ppg)
ν	Poisson' ratio
Cb	Bulk compressibility
Cr	Rock matrix compressibility
φ	Internal friction angle
Φ	Porosity
Δ	Represents change in a value
C	Cohesion
Pf	Formation pressure, psi
Pw	Wellbore pressure when fracture is created
T	Tensile strength
Vclay	clay volume (%)
Vp and Vs	Compressional and Shear wave velocities of the rock,

List of Abbreviations

API	American Petroleum Institute
BHA	Bottom hole assembly
BHO	Bottom hole orientation
BHP	Bottom hole pressure
DC	Drill collar
DDR	Daily drilling report
DST	Drill string test
DSV	Down hole safety valve
ECD	Equivalent circulating density
EMW	Equivalent mud weight
FG	Formation pressure equivalent density
FRAC	Fracture
HPHT	High pressure high temperature
ID	Internal diameter
KOP	Kick off point
LOT	Leak off test
LWD	Logging while drilling
MD	Measured depth
MPI	Magnetic particle inspection
MW	Mud weight
MWD	Measurement while drilling
NDT	Non destructive testing
NPT	Non productive time
OBM	Oil based mud
OD	Outside diameter
PPG	Pounds per gallon
PSI	Pounds per square inch
RIH	Run in hole
RPM	Revolutions per minute
SCR	Slow circulation rate
SF	Safety factor
SICP	Shut in casing pressure
SIDPP	Shut in drill pipe pressure
SPM	Strokes per minute
TFA	Total force area
TOC	Top of cement
TVD	Total vertical depth
UBD	Under balanced drilling
WOH	Weight on hook
WBM	Water based mud

Chapter 1
INTRODUCTION

1.1 RISING ESSENTIAL NEED FOR WELLBORE STABILITY

Oil fields are usually drained from several platforms that extensively influence the development costs. The required number of platforms can be reduced by using non-vertical production wells. The deviated and horizontal wells enlarge the drainage area from a single point. This increases the productivity, and may subsequently decrease the number of planned platforms. In some cases, deviated boreholes are drilled to reach a substantial distance horizontally away from the drilling location (*i.e*., extended reach drilling). This is mainly used to access many parts of the reservoir from one location, which will also reduce the required number of platforms. Moreover, deviated boreholes are sometimes essential to reach locations that are not accessible through vertical boreholes. However, drilling non- vertical boreholes brings out new problems, such as cuttings transport, casing setting and cementing, and drill string friction. An increased borehole angle will also increase the potential for borehole instability during drilling.

Nevertheless, drilling vertical boreholes will not guarantee the stability of the well. In all areas of the world, borehole instability causes substantial problems, even in vertical boreholes. For instance, in the Wanaea field of the Australian Northwest Shelf, the development plan proposed deviated and horizontal wells to minimize stability problems (Kingsborough *et al.,* 1991).

Wellbore stability is dominated by the *in situ* stress system. When a well is drilled, the rock surrounding the hole must take the load that was previously taken by the removed rock. As a result, the *in situ* stresses are significantly modified near the borehole wall. This is presented by increased stress around the wall of the hole, that is stress concentration. The stress concentration can lead to rock failure of the borehole wall, depending up on the existing rock strength. The basic problem is to know, and to be able to predict, the reaction of the rock to the altered mechanical loading.

In order to avoid borehole failure, drilling engineers should adjust the stress concentration properly through altering the applied internal wellbore pressure (*i.e*., mud pressure) and the orientation of the borehole with respect to the *in situ* stresses. In general, the possible alteration of the borehole orientation is limited. It is therefore obvious that wellbore instability could be prevented by mainly adjusting the mud pressure. Traditionally, the mud pressure is designed to inhibit flow of the pore fluid into the well, regardless of the rock strength and the field stresses. In practice, the minimum safe overbalance pressure (well pressure–pore pressure) of typically 100-200 psi, or a mud density of 0.3 to 0.5 lb/gal over the formation pore pressure, is maintained (*e.g.,* French and McLean, 1992; Awal *et al*., 2001). This may represent no problem in competent rocks, but could result in mechanical instability in weak rocks. In general, the mud pressure required to support the borehole wall is greater than that required to balance and contain fluids, due to the *in situ* stresses which are greater than the formation pressure. Stress-induced borehole failures can be grouped into the following three classes, as shown in Figure 1.1

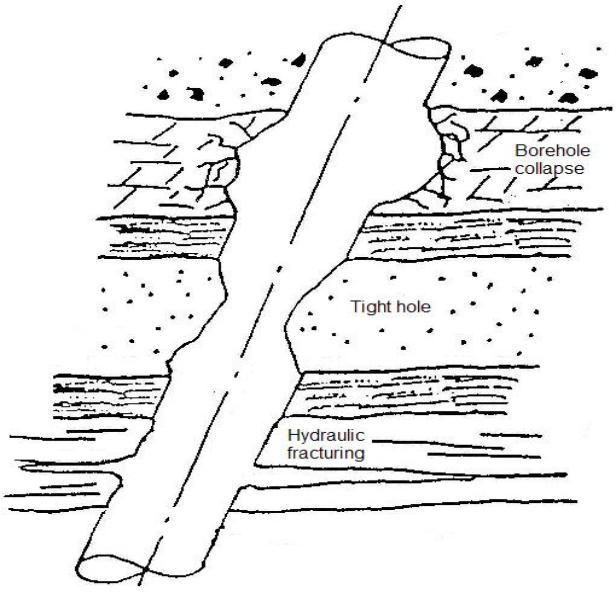

Figure 1.1 Typical stability problems during drilling.

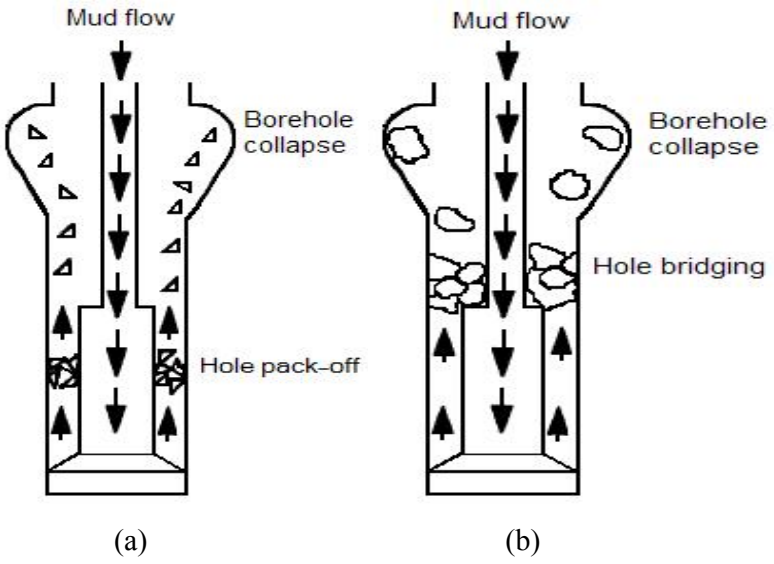

Figure 1.2 Stuck pipe problem due to borehole collapse.

(a) Hole pack-off. (b) Hole bridge.

Symptoms of hole enlargement or collapse in brittle rock failure are due to poor cementing, difficulties with logging response and log interpretation, and poor directional control. Poor cementing of the casing could lead to problems for perforating, sand control, production and stimulation. Furthermore, when the hole starts to collapse, small pieces of the formation may settle around the drill string and pack off the annulus (*i.e.*, hole pack-off), while medium to large pieces fall into the borehole and might jam the drill string . These may prevent pulling the string out of the hole (*i.e.*, stuck pipe), and so the planned operations are suspended. Stuck pipe problems due to borehole collapse is illustrated in Figure 1.2

Hole size reduction due to ductile rock failure presented by the plastic flow of rock into the borehole. This usually occurs in very weak shale, sandstone, salt and some chalk formations. Symptoms of this condition are repeated requirements of reaming and may result in stuck pipe.

Severe loss of drilling fluid to the formation from fracturing often causes well control problems. The lost circulation will reduce the applied mud pressure and may result in inflow of pore fluid. The formation fluid will flow from high pressure zone (kick zone) to a lower pressured zone (loss zone), which is known as underground blowouts

Unplanned operations due to stress induced borehole failure resulting in loss of time and occasionally equipment account for at least 20% of drilling costs (Ewy *et al*., 1994; Santarelli *et al*., 1996; Aadnoy and Ong, 2003). For instance, Charlez and Onaisi (1998) presented two examples of stuck pipes due to wellbore instability. In both examples sidetracking of the well was essential and the cost was in the range of $2M for each case.

1.2 PARAMETERS THOSE AFFECT WELLBORE STABILITY

Primarily borehole instability is governed by *in situ* stresses, pore pressure and rock strength. In addition to these dominant parameters, borehole stability may directly or indirectly be influenced by the following parameters or effects:

(a) mud chemistry (b) temperature effects and (c) time-dependent effects.

Most of the overburden consists of shaly formations. In highly reactive shale sections, mud chemistry is of extreme importance in addition to the mechanical aspects of instability. The mud composition changes as shales slough and disperse into the mud column, or by chemical interactions between the minerals in the formation and the mud. This indeed will alter the mud properties and rheology. Therefore, chemical additives are typically introduced in the mud according to the minerals in the formations. In highly reactive shales, oil-based mud is preferred as it is more inhibitive than water based mud. However, the disposal of oil-based mud requires a special management to avoid the pollution of the environment, which has restricted its applications

Temperature changes associated with mud circulation during drilling may alter the rock properties . The change in rock properties may reduce or enhance borehole failure depending on the thermal effect. Maury and Sauzay (1987) reported that temperature fluctuations may also influence the stress distribution around the borehole. As the temperature increases, the tangential and vertical stresses will increase. However, temperature fluctuations will not influence the stress anisotropy around the borehole as the thermal effect should alter the tangential and vertical stresses by an equal amount .

Reactive shale instability is also time-dependent, and is governed by two intrinsic mechanisms: (a) consolidation and (b) creep. Consolidation is due to pore pressure gradients induced by fluid communication between the mud and pore fluid. Creep is described by a change of strain at a constant effective stress level. Both of these mechanisms will result in hole size reduction. In practice, it is difficult to distinguish between creep and consolidation effects. In general, consolidation will occur shortly after loading, while creep will govern later deformation (Fjaer *et al.*). The mud pressure and properties, and the temperature in the rock may vary during drilling operations, which in turn enhance borehole instability. All these

parameters make it more difficult to directly pursue the time-dependent effects. The best approach is to quickly isolate the rock with a casing to minimize the potential borehole instability.

1.3 MOTIVATION FOR STUDYING WELLBORE STABILITY

The days of easily available oil are rapidly running out. Deep and deviated wells are becoming more and more common. One needs to understand the stress behavior of formation rock in order to control the stability of such wells. Wellbore instability is a costly problem, and is especially challenging in extended reach wells / high pressure high temperature wells. The responsible factor is the state of stresses, which is influenced by mechanical (in-situ), hydraulic (pore pressure change), and thermal effects.

Wellbore stability problems in drilling cost to the drilling industry around $10 billion dollars per year worldwide. Despite tremendous efforts pursued over the past years, wellbore stability problems continue to be experienced by the drilling communities. The practical consequences of wellbore instability are often the collapse of borehole wall" (Aadnoy and Ong, 2003).

Borehole collapse could be predicted by adopting compressive failure analysis in conjunction with a constitutive model for the stresses around the borehole. The selection of a failure criterion for wellbore stability analysis is difficult and confusing. It is unclear to drilling engineers as which failure criterion should be used in the wellbore stability analysis.

"Preferably a failure criterion should be based upon knowledge of the failure mechanism, but this is not always so. In fact, many failure hypotheses have been propounded as a result of theoretical reasoning only and could not be verified by experimental evidence" (Bieniawski, 1967). The most commonly used failure criteria in wellbore stability analysis are Mohr-Coulomb criterion and Drucker-Prager criterion. These failure criteria are based on quite different failure hypotheses.

In this work I have studied the basic fundamentals of stress and rock failure mechanics as well as examine failure criteria. The subject of borehole failure is quite complex and confusing. Therefore, I will only consider the mechanical instability of the wellbore to improve borehole failure predictions.

1.4 EARTH STRESSES

The knowledge of earth stresses involved in geomechanical analysis of wellbore stability is essential to understand the geomechanical data's.

1.4.1. In-situ Earth Stress

Prior to drilling, subsurface rocks are exposed to a balanced or near balanced stress environment. The naturally occurring stress in place is called the In-situ stress. Stress is normally compressive due to the weight of the overburden. For this reason, in rock mechanics compressive stress is defined to be positive.

1.4.2 Overburden Stress - S_v

Overburden stress is the pressure exerted on a formation at a given depth due to the total weight of the rocks and fluids above that depth. Most formations are formed from a sedimentation/ compaction geologic history. Formations may vary significantly from the earth's surface to any depth of interest. Shallow shales will be more porous and less dense than shales at great depths.

As the overburden squeezes the rock vertically, it pushes horizontally. Constraint by surrounding rock creates horizontal stress.

1.4.3 Horizontal Stress - (S_{Hmax} , S_{hmin})

When drilling near massive structures such as salt domes or in tectonic areas, the horizontal stresses will differ and are described as a minimum (S_{hmin}) and a maximum (S_{Hmax}).

1.4.4 Effective Stresses

The rock matrix does not support the full load of overburden and horizontal stress. Part of the load is supported by the fluid in the pore (pore pressure). The net stress is the effective stress felt by the rock matrix. Effective stress is used in rock mechanics to determine the stability of the wellbore. Thus effective stress is defined by the difference between external stress acting on the rock matrix and pore pressure.

$$\text{Effective stress} = \text{Total Stress} - \text{Pore Pressure}$$

1.5 IMPORTANCE OF STRESSES AROUND BOREHOLE

Prior to drilling, the mechanical stresses in the formation are less than the strength of the rock. The chemical action is also balanced, or occurring at a rate relative to geologic time (millions of years). Rocks under this balanced or near-balanced state are stable. After drilling, the rock surrounding the wellbore undergoes changes in tension, compression and shear loads as the rock forming the core of the hole is removed.

Under these conditions, the rock surrounding the wellbore can become unstable, begin to deform, fracture and cave into the wellbore or dissolve into the drilling fluid. Excessive rock stress can collapse the hole resulting in stuck pipe. Hole squeezing mobile formations produce tight hole problems and stuck pipe. Cavings from failing formation makes hole cleaning more difficult and increases mud and cementing costs.

Hence understanding and determination of induced stresses around the borehole becomes very vital in the Wellbore Stability Analysis.

1.6 ROCK PROPERTIES AND MECHANICAL BEHAVIORS

Rock physical and mechanical properties are very important parameters for geological engineering design. Rock physical properties include density,

porosity, and permeability, etc. Rock mechanical properties mainly include elastic modulus, Poisson's ratio and rock strength.

1.6.1 Density

Rock density (ρ) is a measure of mass of the rock contained in a given unit volume (density = mass/volume). It is usually expressed in g/cm^3. Rock density is also called bulk density. Since most of rocks are porous media, bulk density of porous rocks depends on not only the density of the solid matrix material, but also the density of pore fluids. For underground rocks, as depth increases the rock compaction increases, causing porosity reduction. This induces an increase in rock density as depth increases.

1.6.2 Porosity

Porosity (Φ) is an important property to analyze oil and gas reservoir and aquifer storage. Porosity is defined to be the ratio of a volume of void spaces within a rock to the total bulk volume of the rock.

1.6.3 Permeability

Permeability is the most important physical property of a porous medium. Permeability measures quantitatively the ability of a porous medium to conduct fluid flow. Permeability has dimensions of an area, and it is measured in units of Darcy (1 Darcy = 0.98 X 10^{-12} m^2), or more commonly the milli-darcy.

1.6.4 Elastic modulus

Elastic modulus (also called Young's modulus) is an important parameter to describe stress and strain relationship. For most rocks, the uniaxial stress-strain curve before failure takes approximately the linear form. This can be presented by:

$$\sigma = E\varepsilon \tag{1.1}$$

where **σ** is the stress; **έ** is the strain; the constant, E, is called elastic modulus. A material is linearly elastic if the above relation holds accurately.

Elastic modulus describes the capacity of rock deformation or the stiffness of a rock. For a high elastic modulus rock, it is less deformable (i.e. stiff). The initial part of the complete stress-strain curve will be steep. For a low elastic modulus (soft) rock, it is more deformable, and the initial part of the complete stress-strain curve will be gentle (Hudson and Harrison 1997).

Rock static elastic modulus can be obtained from lab core tests of either uniaxial or triaxial compressive experiment (Meng et al. 2002). Rock dynamic elastic modulus (Ed) can be solved from the following equations by knowing the rock elastic compressional and shear wave velocities:

$$v_p = \sqrt{\frac{E_d}{\rho_b}\frac{(1-\nu)}{(1+\nu)(1-2\nu)}} \tag{1.2}$$

$$v_s = \sqrt{\frac{E_d}{\rho_b}\frac{1}{2(1+\nu)}} \tag{1.3}$$

where Vp and Vs are the compressional and shear wave velocities of the rock, respectively; **ρ** b is the rock bulk density; v is the Poisson's ratio of the rock. Rock elastic velocities can be obtained by seismic survey or sonic well log. The dynamic elastic modulus can be converted into static modulus by empirical correlations (Du et al. 2001). The dynamic modulus also can be expressed as the following forms if one knows the interval transit time:

$$E_d = \frac{\rho_b}{t_p^2}\frac{(1+\nu)(1-2\nu)}{(1-\nu)}$$

$$E_d = \frac{2\rho_b(1+\nu)}{t_s^2} \tag{1.4}$$

where tp and ts are the compressional and shear interval transit time, respectively.

In general, the dynamic values of elastic modulus have been found to be significantly greater than the static values. It was also noted that the discrepancy was far greater for soft rocks, such as sandstone, than for hard rocks, such as granite (Howarth 1984). The discrepancies between the dynamic and static moduli have been widely attributed to microcracks and pores in the rocks.

1.6.5 Poisson's ratio

Poisson's ratio is the ratio of transverse strain to corresponding axial strain on a material stressed along one axis. For a rock core subjected to axial load, Poisson's ratio (v) can be expressed as:

$$\nu = -\frac{\varepsilon_l}{\varepsilon_a} \tag{1.5}$$

where ε*l* is the lateral strain; ε*a* is the axial strain. Therefore, Poisson's ratio can be determined by measuring the lateral and axial deformations of the uniaxial compressive test in rock samples.

Poisson's ratio can also be calculated from the velocities of the elastic wave:

$$\nu = \frac{\frac{1}{2}(v_p / v_s)^2 - 1}{(v_p / v_s)^2 - 1} \tag{1.6}$$

where Vp and Vs are the compressional and shear velocities, respectively.

Experimental results show that Poisson's ratio in a rock depends on lithology, confining stress, pore pressure, and porosity of the rock. Normally Poisson's ratio is about 0.2 for sandstones, about 0.3 for carbonate vrocks, and greater than 0.3 for shales.

1.7 RESEARCH OBJECTIVES

The overriding objectives of this research work are:

- To develop conceptual learning of most confusing & complicated area of Geomechanics
- To investigate the effect of stresses on wellbore stability under varying borehole orientation.

1.8 ABOUT THE WORK

The work done in this thesis is presented into three parts. Those are briefly discussed below.

1.8.1 Model Development

Geomechanical Model Development emphasizes the estimation techniques of in-situ earth stresses, transposition of in-situ earth stresses from global earth co-ordinates to wellbore co-ordinates and the variation of induced wellbore stresses along the periphery of the wellbore. The wellbore stability analysis is carried out using present field procedures and techniques involved in the geomechanical model development.

1.8.2 C- Programming

Since manual calculations for wellbore stability analysis takes too much time due to lengthy procedure, I have developed C-Programs to simplify the calculation work to determine the induced wellbore stresses for various borehole orientation.

1.8.3 Computational Analysis

Using C-Programs, the induced wellbore stresses for various well profiles i.e. vertical, directional and horizontal wellbore are determined. Then stress plots are developed with the help of Matlab for various wellbore orientations. It can be easily inferred from these stress plots that stress concentration varies drastically as a function of position around the wellbore.

Chapter 2

LITERATURE REVIEW

Since last two decades Geo-Mechanical Earth Modeling (GMEM) is the main focused research area to oil industry due to non productive timing & huge cost involved .Wellbore stability is of critical importance in the success of drilling operations. One of the main goals of any drilling mission is to drill the well as cost-effective as possible. Wellbore instability can be detrimental to this goal. Therefore, wellbore stability analysis has been included in well planning stage of many companies.

Wellbore stability is a function of several factors such as inclination and azimuth, in-situ stresses, mud weight, rock strength parameters, etc. Some of these factors are controllable and some are not. Among the controllable factors are inclination, azimuth and mud weight. By changing these parameters, one can reduce stability problems significantly. Theoretically, it is possible to design the well trajectory in a way to face least stability problems.

M.R. Mclean and M.A Addis et al (1990) discussed the effect of strength criteria on mud weight recommendations. They proposed a Homogenous, Isotropic, Linear –Elastic wellbore stability analysis for the prediction of the onset of failure and consequently the mud weights required to prevent hole instability. They reported that the hole problems during the drilling phase of operations are often the consequence of mechanical wellbore stability. This leads to higher than the necessary drilling costs. These two authors study assesses the influence of two commonly proposed failure criteria on mud

weight selection. The failure criteria selected was shown to have an extremely significant effect on the computed safe mud weights. Examples related to field situations were presented which highlight the anomalies and contrary evidence relating to the suitability of failure criteria.[1]

M.A Moinuddin and K.Khan et al (2006) presented a wellbore stability analysis of vertical, directional and horizontal well using field data. They redeveloped an old offshore field produced using vertical and directional wells by drilling horizontal wells. Quantification of drilling problems in sixty wells show that majority are tight holes along with stuck pipes and hole pack offs problems. The major loss of productivity is due to stuck pipes. A preliminary study of shale in sections where problems occur, show no chemical reactivity. Petrographic analysis confirmed the fissile and brittle nature of shale with presence of open, partially healed micro fractures and partings. Rock mechanical simulation predicted the safe mud weight window for horizontal wells, depending on azimuth. However, all the horizontal wells analyzed in their study were drilled using the same mud weight window. Therefore, field based parameters like initial mud weight used for drilling, mud weight increment and problems per well were used to analyze wellbore instability, identify different instability mechanisms and design safe mud weight window for drilling horizontal wells. These parameters were used first on the drilling data of vertical wells to develop the procedure for the analysis of wellbore instability and identify the mechanisms of instability. The developed procedure was then applied to the drilling data of directional wells to show the dependence of mud weight on the inclination and azimuth of the well. Finally, the procedure was applied to horizontal wells data along with the concept of critical washouts to infer the safe mud weight window. The safe mud weight window is validated on another set of drilling data showing 90% success rate. Their analysis confirms the existence of anisotropy in horizontal stresses and is extremely useful in cases where there is significant variation in mechanical properties of different layers of reservoir rock.[2]

A.M.Paiaman, B.D. Al-Anazi et al (2008) presented optimizing wellbore inclination and azimuth to minimize instability problems. In this paper, the authors considered linear elastic constitutive model along with Mohr-Coulomb failure criterion to perform stability calculation for different inclinations and azimuths. They show that drilling wells parallel to minimum in-situ horizontal stress causes less stability problems. Also the effect of in-situ stress field on wellbore stability has been investigated by them and they reported that in the case of high difference between the in-situ stresses, the optimum path for a well is a low inclination and an intermediate azimuth. The authors emphasize that curing wellbore stability problems needs a thorough knowledge of the mechanism responsible for causing instability. Misconception in failure mechanism recognition can even deteriorate the problem rather than solving it out. Therefore, it is of great importance to exactly determine what mechanism has caused the problem. Wellbore instability problems are usually tackled with a combination of constitutive models and failure criteria. Constitutive models are a set of equations used to determine the stresses around the borehole wall after drilling the well. They range from simple linear elastic models to sophisticated thermo-poro-elsato-plastic models. The linear elastic model assumes the formation to be homogenous and isotropic and do not account for the plastic behavior of the rock. All the constitutive models have, only, studied the effect of a few parameters on the stability of the wellbore and have ignored the rest. There is no unifying constitutive model which can handle all the parameters that affect the stability of the wellbore. There are various failure criteria which are used to determine the onset of failure in the rocks. Some use only minimum and maximum principal stresses and some use all of the principal stresses. They can be divided to linear and nonlinear criteria. In linear criteria, the relationship between the shear stress and normal stress is linear and in nonlinear criteria is not. For example, Mohr-Coulomb is a linear criterion and Hook & Brown is nonlinear. The authors used a combination of linear elastic constitutive model and Mohr-Coulomb failure criteria has been employed to analyze the effect of inclination and azimuth as well as in-situ stress field on the stability of the wellbore. Two cases have been assumed for

the in-situ stress field. The difference between these two cases is that, in the second case, the difference between the horizontal stresses is higher. [3]

Rama Rao, S.Grandi, M.N. Toksov et al (2003) presented geomechanical modeling of in-situ stresses around a borehole. In this paper, authors present a modelling of the in-situ stress state associated with the severe hole enlargement of a wellbore. Geomechanical information is relevant to assure wellbore stability, i.e., to prevent damages in the formation and later on, the casing. Many of the drilling parameters, as mud weight or the optimal orientation of the borehole, require some knowledge of the mechanical behavior of the rock. The lack of these kind of data in exploratory areas, where there are usually insufficient constraints for the geological model, increases even more the risk, hence the costs. The presented model uses the concepts of poroelasticity theory to compute the stationary 2D, brittle response of the formation around a borehole that is submitted to effective compressive horizontal stresses. The numerical solution is obtained using a finite element approximation. The initial stress state at the far field was estimated combining a frictional-failure theory with the observations of dipmeter caliper in a particular borehole that presents elongations in a preferential direction. The direction and relative extension of the observed breakouts at a particular depth are modeled successfully using formation realistic parameters and dimensions, although the exact shape of the borehole (at all angles) was unknown. For the particular case study, the orientation of the breakout is NE-SW, at about 82 degrees azimuth. Therefore, the maximum horizontal stress lies at approximately 350 degrees azimuth. The ratios of horizontal principal stresses to vertical stress that best honor the observations are SHmax = 2.3Sv and Shmin = 1.7Sv. The compressive strength necessary for the rock to fail, as indicated by the caliper data under this stress field, is about 140 MPa. [4]

Z. Mingxin, Y. Shiduo et al (2009) presented comprehensive geomechanic study which helps mitigate severe stuck pipe problems in development drilling in bohai bay, china. Guan Jia Pu Oil Field is located in the western part of Bohai Bay, China. The field was developed with high angle and horizontal

wells drilled from an artificial island. The development drilling had experienced severe stuck pipe problems in a short period, which resulted in hole collapse, equipment being left in hole and sidetracking. This paper presents a comprehensive geomechanic study with the aim of identifying the root cause of the stuck pipe problem and developing mitigating measures for future drilling. A rigorous review of the drilling experience in the field revealed that the stuck pipe incidents mainly occurred 1) in high angle and horizontal wells in Sa He Jie shale overlying the main reservoir; 2) during tripping out of hole whilst no problem was reported during drilling; and 3) with the stuck pipe wells appeared to be not correlated with a particular wellbore azimuth. Mechanical Earth Models based on an isotropic mechanical property assumption were then constructed using mainly well logs and data extracted from the drilling and completions reports. Wellbore stability analyses were conducted for the stuck pipe and non-stuck pipe wells which demonstrated that extensive borehole failure in Sa He Jie shale was the main cause of stuck pipe. The arc of calculated borehole failure was greater than 90 due to the use of insufficient mud weight. This could have generated large size shale cavings which would be difficult to circulate out of the hole. For non-stuck pipe wells, the calculated borehole failure extent was much less. Mechanical deformation and strength anisotropy of Sa He Jie shale were evaluated in laboratory using ultrasonic measurements and scratch testing equipment on large shale caving blocks. It was observed that the strength along the bedding planes of the shale was much weaker than the intact shale material. A numerical model was then applied to assess the effect of mechanical anisotropy on wellbore stability. Bedding plane failure in Sa He Jie shale affects wellbore stability for high angle band horizontal wells (deviation greater than 60) drilled close to the minor horizontal stress direction. The additional mud weight to counteract bedding plane failure is approximately 0.03SG. Based on the study, a mud weight program was proposed for a planned well, which had been drilled without significant geomechanics-related problems.[5]

P.J. Mclellan et al (1996) presented assessing the risk of wellbore instability in horizontal and inclined wells. The authors state that Wellbore instability can lead to expensive operational problems during the drilling, completion and production of horizontal and inclined wells. This paper reviews the direct and indirect symptoms of wellbore instability, its root causes, and various empirical and deterministic modeling approaches to predict the risk of hole collapse or convergence. In general, linear elastic models that are only concerned with stability at the wellbore wall often give overly pessimistic predictions. An alternative approach, using the extent of the "yielded" zone around an unstable wellbore and the kinematics of rock detachment, is proposed for practical risk assessments. A case history for an open hole completed horizontal well in a limestone reservoir under high drawdown is described. [6]

P.M Collins et al (2002) presented geomechanics and wellbore stability design of an offshore horizontal well, North Sea. This paper describes a comprehensive geomechanical assessment of the P2-NE Field in the North Sea. The objective was to review the available core, log, and drilling data to characterize the geomechanical performance of the P2- NE Field in order to explain observed behaviour, and extrapolate this to future drilling, particularly for Well P2-NE- 2 Horizontal. This study focussed on the inclined Well P2-NE-2 Pilot, which was drilled specifically to obtain reservoir data for the subsequent horizontal well. The geomechanical analysis is based upon the general geological setting, deductions made from field data, and geomechanical core tests. Wellbore stability analyses were conducted, using the mechanical properties and regional stresses as input. Geomechanical tests and petro physical logs were used to obtain realistic profiles of mechanical properties. Anomalously, the reservoir mudstones were of considerable strength, exceeding the strengths of the sandstones. Weak zones were found in the sandstone that would be stable while drilling if an adequate mud weight were used. These zones would likely be sand producers during production. This is because the rock stresses would continue to increase, due to the continued pressure decline during depletion. To obtain stress data, a minifrac

test from an adjacent field was analyzed. This provided the breakdown pressure, fracture propagation pressure, the ISIP, and most importantly the fracture closure pressure. The principal horizontal stress orientations were determined from borehole breakout analyses, and compared to residual strain relaxation tests on core. Other observed borehole elongations included wellbore washouts and keyseating. Finally, a stability analysis was conducted for the horizontal well, in order to assess the effect of increasing the mud weight. The primary objective was to determine the minimum mud weights required for wellbore stability during drilling, and these were found to be considerably less than those predicted without a geomechanics analysis. Fracture gradients set a maximum for the Equivalent Circulating Density(ECD). Zones with high sanding potentials were identified, based on the rock strength analyses. [7]

G. Keaney, K.Adesina et al (2006) presented wellbore stability with consideration of pore pressure and drilling fluid interactions. A poroelastic wellbore stability model incorporating pore pressure and its variation with time is proposed. A finite element method has been developed to couple solid deformation and fluid flow around the wellbore. Pore pressure and drilling mud interaction is modeled by considering different boundary conditions. A comparison between the elastic solution and the proposed solution demonstrates that the elastic solution has a much larger total tangential stress near the wellbore. Furthermore, it is shown that the excessive pore pressure near wellbore, if not properly balanced with additional annular fluid pressure, can create tensile failure or spalling in low permeability rocks. [8]

A.S. Raba, D.E.Hembling et al (2007) presented a geomechanical facies-based approach to optimize drilling and completion strategy of an unconsolidated sandstone reservoir, Saudi Arabia. Drilling horizontal wells, single and multilateral, is nowadays common practice for Saudi Aramco in most of its oil and gas reservoirs in Saudi Arabian fields. This study highlights the application of a geomechanic study to evaluate well stability, drilled into a friable eolian oil-bearing sandstone reservoir. Saudi Aramco’s reservoir

management was eager to find the optimum mud type and azimuthal direction to place long reach horizontal wells, so as to minimize the risk of stress-induced borehole breakouts, optimize drilling mud weights, aid in making informed decisions about adequate completion design, and ensure sustainable production under depletion mode. The reservoir rocks in this field are characterized as a wet, eolian depositional system with four distinct depositional facies: dune, sand sheet, paleosol and playa. Grouping the lithology into these four recognizable depositional facies significantly enhanced the understanding of facies dependent rock properties and related wellbore integrity. Hence, a critical objective of the study was to combine the knowledge of reservoir and material properties with detailed analyses of the present day in situ stress field. Upon determination of the in situ stress field in the study area, wellbore stability in the principal horizontal stress directions (Shmin and SHmax) was calculated and compared and the resulting optimum direction was recommended. The effect of mud on rock strength was evaluated and the mud type that caused less rock-strength reduction was selected. The study concluded that under undepleted conditions horizontal wells should be drilled with oil-based mud parallel to the field-derived maximum principal horizontal stress (SHmax) azimuth in order to maximize borehole stability and minimize required mud weights during drilling and completion. The results from this detailed study was to be incorporated into Saudi Aramco's reservoir management decision tree, in order to maximize wellbore integrity during drilling and completion such that least damage occured to the reservoir during drilling.[9]

John Fuller, K.Qiu, et al (2008) presented geomechanics enables the success of horizontal well drilling in libya: Drilling highly deviated or horizontal wells can be prone to instability problems. This paper describes a case in Libya on which significant difficulties were encountered during drilling the first horizontal development well in a field in Murzuq basin. The first two branches of the well were lost due to severe instability problems. A comprehensive geomechanic study was carried out to understand the causes of the wellbore failure and to improve drilling design and drilling performance on further

development wells in the field. The study specifically included: Performing a systematic data audit and integration to identify specific uncertainties in the input data and identify data gaps and performing a comprehensive drilling event review to investigate what happened during drilling and what were the major instability problems. All drilling events were organized, categorized and input into a database. A graphical presentation of the drilling events review was generated.

This procedure reduced the uncertainty of the model and the resulting wellbore stability predictions. This improves understanding and awareness of the various drilling hazards and enables effective utilization of the wellbore stability information during drilling. The analysis identified the cause of wellbore instability, as being inadequate mud weight while drilling the overlying shale formation in the deviation build-up section. The design of the second horizontal well was optimized based on this study. The well was drilled successfully without problems and, in fact, ahead of drilling schedule. This case demonstrated that a comprehensive geomechanic analysis can greatly improve drilling performance and reduce drilling costs.

Horizontal wells can increase production rates and ultimate recovery, and reduce the number of platforms or wells required to develop a reservoir. The geometry also helps to delay water or gas breakthrough, bypass environmentally sensitive areas and reduce stimulation costs. To achieve avoidance of water coning and delay of water breakthrough, Akakus Oil Operations started to drill the first horizontal development well H1 in a field in Libya in 2006. However, unexpected drilling difficulties were encountered and the first two branches of the well were lost. Prior to this project, quite a significant number of exploration and development vertical wells had been drilled in the same block without experiencing any major problem. A wellbore stability study was carried out to understand the cause of wellbore failure in the horizontal well, to optimize the drilling design and performance for the next horizontal development wells to be drilled in the same field. The initial requirement for a wellbore stability analysis is a Mechanical Earth Model

(MEM). Two wells with quite complete suites of data were identified. The two wells included the first horizontal well H1 and another nearby vertical offset well V1. First, the dataset was checked for consistency and edited when necessary to resolve any anomalies. At the same time, a review of the drilling data from well H1 and its sidetracks (named as Branch 1, Branch 2 and Branch 3, respectively, hereafter) was performed.

The purpose of the review was to gather information that would be used to identify and characterize the instability events experienced in the well. Then, the audited data were used to generate the MEM of each well. The MEMs built for wells H1 and V1 were validated comparing the wellbore instability predictions from the models to the instability indications of daily drilling reports, microresistivity images and caliper data. The MEM created for well V1, based on location proximity, was considered to be the most geomechanically representative model for the planned horizontal well H2. The MEM of the well V1 was propagated to the well H2. Wellbore stability analysis was subsequently carried out on the well H2 and potential drilling risks related to its trajectory were identified. A wellbore stability forecast was created for the planned horizontal well H2. The forecast included a summary of key drilling hazards for the planned well trajectory; a contingency plan for each hazard including an analysis of the consequences to the rest of the wellbore; a mud weight window profile and supplementary information for drilling the well H2. Key objectives of the forecast was to raise awareness of the various hazards likely to be encountered and to improve understanding of the deformation mechanism causing the instability. By applying above findings and recommendations, the driller could effectively respond to any wellbore instability during drilling.[10]

L.M. Warlick, Perumalla et al (2009) presented evaluation of wellbore stability during drilling and production of open hole horizontal wells in a carbonate field. Drilling horizontal wells is a common practice for Saudi Aramco in most of its oil and gas reservoirs of Saudi Arabian clastic and carbonate fields. While previously all wells in this field were cased and

perforated, during the planning stage for increasing production, the question raised was whether openhole horizontal well completion was feasible over the life of the field (i.e., when taking near-wellbore drawdown and far field production-induced reservoir depletion into consideration. The direct benefit would be that openhole completion greatly reduced the development costs for the 300 plus production wells planned for the field. A rock mechanics study was undertaken to provide a comprehensive understanding of wellbore stability of openhole horizontal wells throughout their life span from drilling through production during field development. Two objectives identified for the study were: 1) assessment of wellbore stability and critical drawdown rates during production to avoid well collapse, and 2) the optimal well deviation, azimuth and required mud weight during drilling to minimize wellbore instability problems. To increase accuracy of the results and greatly reduce uncertainty, cores from both reservoirs were retrieved in order to have representative samples of the formations of interest. A testing program was undertaken to determine the static and dynamic mechanical properties, compressive rock strength, rock failure characteristics and thick-wall-cylinder strength. The effect of water on rock strength was tested as well, to evaluate if water encroachment posed additional risk to the mechanical integrity of the formation. In addition, the required geomechanical model in particular in-situ stress field, magnitude and direction was determined from several data sources: stress-induced wellbore failure analyses (from oriented caliper and, wellbore image log analyses, microfrac testing, direct pore pressure measurements, wireline log data and analysis of the general regional stress information for the area surrounding the field. The study showed that openhole completion is feasible for most well azimuths in both reservoirs. However it was determined that the tar bearing intervals of both reservoirs are not competent enough to be completed openhole due to the risk of wellbore collapse. The recommendation was therefore to avoid the tar bearing intervals and to consider casing those zones as applicable. The rock strength showed minimal effect as a result of exposure to water; therefore, water flooding would be a concern from a wellbore integrity point of view. A field-specific compressive rock strength-wireline sonic log correlation was developed and

calibrated with results from the lab tests. The flank wells were found to tolerate more drawdown pressure than crest wells, due to higher rock strength in the flank as compared to the crest. Additionally, it was recommended that the wells be drilled in the direction of minimum principal horizontal stress to maximize borehole stability and minimize required mud weights during drilling and completion. The results from this extensive study were incorporated into Saudi Aramcos reservoir management decision tree.

Wellbore instability problems are being experienced during the drilling of horizontal wells in highly stressed formations such as shale, unconsolidated sandstone, and weak carbonates. The instability problems can be a simple washout to total collapse of the hole, and these problems are related to the mechanical properties (strength and deformation under stress), the drilling fluids properties, the in-situ stress field, and time dependant deformation. Openhole completion may be possible in weak carbonate if the in-situ stress field is not critical in terms of magnitude and mode (normal, strike-slip, or inverse). For example, a rock mechanics study on a shallow carbonate formation in Saudi Arabia has revealed unconfined compressive strengths less than 2,000 psi; however the results of wellbore caliper monitoring as a function of production time showed no changes in wellbore size and therefore all horizontal wells were completed openhole.

The structure of the oil field analyzed in this study is a conventional northwest trending asymmetric anticline. To develop the field to its target production, Saudi Aramco's reservoir management team planned to drill a number of horizontal wells to ensure maximum reservoir contact. Because mechanical integrity of the wellbore for openhole completion strategy is of critical importance, Saudi Aramco decided to have a geomechanics evaluation conducted to understand if and how well integrity can be maximized through utilization of the right mud weights and well directions, such that stable conditions during drilling and production would be guaranteed. The objective was to evaluate the feasibility of openhole completion; therefore the wellbore stability throughout the life span of the well was the focus of the study.

Additionally, it is important to optimize the mud weights during drilling to minimize wellbore instabilities and to recommend optimal well orientations and maximum values for drawdown and depletion to allow for stable well throughout the production phase. Hence, the objective of the study was to combine the knowledge of reservoir and material properties with a detailed analysis of the present day in-situ stress field in order to assess conditions during drilling and production mechanical rock failure might occur at the wellbore wall and could become so severe that it would no longer be manageable.[11]

G.G Donovan, T.J. Bourgeois et al (2007) presented applied rock mechanics in drilling of depleted reservoirs in deepwater gulf of mexico .This paper describes the method used in one Deepwater Gulf of Mexico field for analyzing rock properties in order to define a stable pressure window to maximize the efficiency of the drilling process. The method combined wellbore stability modeling, formation evaluation, log and laboratory derived rock properties, well site pressure integrity testing, geophysical data, and acoustic log analysis. As a complement to a carefully structured drilling program, this synergistic approach resulted in extended reach wells that were drilled with no wellbore-related down time. The process began with a definition of the pore pressure cells, both in magnitude and position, generally delineated by studying the seismic profile along the projected wellbore and analyzing acoustic log and pressure testing data. The pore pressure data, earth stress field information, and rock properties were used to model the minimum wellbore pressure for stable drilling. A study of the changing sea floor profile along the well path was used to adjust the overburden pressure, which was then combined with rock properties to estimate the in-situ stresses, resulting in an estimate of the fracture gradient, or the maximum allowable wellbore pressure to avoid drilling fluid losses. Modeling tools was discussed along with a commentary on the validity of log derived mechanical properties. The approach is applied to drilling operations on two extended reach wells and the paper documents the entire design and analysis process.

The subject wells are located in a deepwater field that was discovered in 1985. Following the drilling of the initial 20 surface wells and ten wells were drilled to the objectives and completed from 1997 to 2000. As the first wells declined in productivity, an additional six wells were drilled and completed. The two wells of interest here were drilled through zones whose reservoir pressure had declined during the production process. Typically, drilling through depleted zones is problematic because the hydrostatic pressure required to minimize compressive failure in adjacent shales can exceed their fracture gradient, initiating tensile failures that may induce catastrophic drilling fluid losses. [12]

Donald Lee, Bryan Collins et al (2003) presented a scheme using a mechanical earth model and integrated drilling team to reduce well costs and drilling risks in san martin field. This paper briefly describes a process developed to reduce drilling risks and well costs and gives details on its application to three deviated development wells in Camisea, Peru. Previous offset vertical and deviated wells in this area encountered wellbore instability, drilling fluid loss, and reactive shales. In some cases these events made it necessary to drill multiple sidetrack wells. The process provided specific advantages while drilling technically difficult trajectories. Integral to the process was development of a mechanical earth model (MEM) for prediction of drilling events and down hole drilling risk management. The model, created using data from multiple disciplines (seismic, drilling, geology, wireline logs, core testing), enabled the drilling team to understand potential drilling hazards and quickly act to mitigate risks, as well as to make rapid informed decisions while drilling. Examples demonstrate how the process compared forward predictions with actual results and how the model was updated during drilling. The first well reached total depth (TD) 5 days ahead of schedule even though the trajectory was in a difficult stress azimuth and several nondrilling problems occurred. Teamwork and communication among the drilling location and four offsite offices played a critical role in the decision process. Predrill predictions matched post-drill information in most cases. Lessons learned from the first well were applied to subsequent well plans. This process can be applied to any exploratory or development well, but high-risk, high-cost wells receive

maximum benefit. Although wellbore instability resulting from tectonic stress was the main risk in this field, the process is equally valid for drilling issues such as overpressured regimes, underbalanced drilling or extended-reach wellbores. [13]

Weiren Lin, Hisao Ito et al (2008) presented estimation of minimum principal stress from an extended leak-off test onboard the chikyu drilling vessel and suggestions for future test procedures. To understand the physics of faulting and rupture propagation for the great M8-class Nankai earthquakes that recur approximately every 100 years, a comprehensive drilling project was underway: the Nankai Trough Seismogenic Zone Experiment (NanTroSEIZE; Tob and Kinoshita, 2007) ,which is part of the Integrated Ocean Drilling Program (IODP). Stress levels along seismogenic faults must be known in order to understand processes controlling the timing, energetic and extent of earthquake ruptures. For scientific drilling projects such as NanTroSEIZE it is very important to determine the in situ stress state at the decollement and the mega splay fault in the Nankai Trough. Preliminary experiments to determine the orientations and magnitudes of principal stresses in the Nankai Trough were undertaken during the NanTroSEIZE Stage 1 expeditions using borehole image analysis (stress-induced breakouts and tensile fractures; Kinoshita et al., 2008) and indirect, core-based methods such as an elastic strain recovery (ASR; Lin et al. 2006). These experiments would provide necessary and important information about in-situ stress. However, to improve reliability and reduce experimental uncertainties in these stress determinations, it was necessary to have direct in-situ measurements of stress magnitudes; in particular the minimum principal stress at depth. These direct measurements are best obtained using methods involving the initiation and propagation of hydraulic fractures at depth, such as the traditional hydraulic fracturing test, a leak-off test (LOT), or an extended leak-off test (XLOT, sometimes ELOT) (Zoback et al., 2003). In this paper it was shown that with the advent of the riser drilling vessel Chikyu, the XLOT is applicable and effective in deep scientific ocean drilling projects (ODP). During previous ODP expeditions and non-riser IODP expeditions, LOT or XLOT (which are sometimes used to determine drilling parameters such as optimal mud density) have not been

conducted because the borehole was open to the seafloor. Thus, it has been impossible to pressurize a short interval of open hole below the casing as needed to conduct a LOT or XLOT without utilizing time-consuming and frequently unreliable drill-pipe-deployed packers. In contrast, the new drilling vessel Chikyu provides a riser-drilling capability that allows pressuring the entire casing string with drilling mud immediately after the casing is cemented in place. Therefore, NanTroSEIZE Stage 2 was expected to present the first opportunity for a scientific ocean drilling program to use LOT or XLOT procedures without using a packer, providing direct information on the in situ magnitude of the minimum principal stress at minimal cost and risk. [14]

M.E Magee, K.L Burgdorff et al (2004) presented wellbore breakout analysis in the southeast moran field, papua new guinea. Abnormally high pore pressure regimes and severe wellbore instabilities in the Ieru Formation and its underlying shales in the Moran Field in the actively deforming Papua New Guinea (PNG) Fold Belt region cause long non-productive times. Many of the Moran wells encountered severe wellbore instabilities that resulted in stuck pipe, excessive cuttings, pack-off, lost bottom hole assemblies, and well control problems. Mechanical sidetracks were often required to reach target. Mechanical rock failure along the borehole wall induced by inappropriate mud weights was often the primary factor that led to these drilling problems and cost overruns. To characterize the physical state of the reservoir and over-burden formations and stress coupling for the Southeast Moran area, a geomechanical model based on the analysis of wireline logs, downhole measurements, and drilling experiences gathered from Moran-3X and two sidetrack wells was built. This model was used to design optimal mud weights for maintaining wellbore stability in the proposed SE Moran-1 well. After the SE Moran-1X well was drilled and logged, the analysis confirmed the accuracy of the geomechanical model by reproducing borehole conditions as seen in image logs.

The geomechanical model consists of the magnitude and orientation of the three principal stresses, the pore pressure, and the uniaxial compressive rock strength. Analysis of available electrical borehole image data collected in

Moran-3X and its two sidetrack wells included mapping stress-induced wellbore breakouts and drilling-induced tensile fractures. In addition, estimation of the least principal stress values from leak-off tests, calculation of the vertical stress from density logs, pore pressure information from direct measurements, and rock strength from empirical log-derived relationships were made. The maximum horizontal stress was constrained by modeling the stress and pressure conditions with the rock strengths that were consistent with the observed wellbore failures. To validate the geomechanical model comparison was made of predictions of wellbore breakout development to breakouts observed in image logs and from the drilling experience in the Moran-3X sidetrack wells. Then a safe mud weight for the proposed SE Moran-1X well using this geomechanical model was determined. Stress-induced wellbore breakouts occur when the compressive stress concentration around the borehole wall exceeds the rock strength.

In a vertical well, in a region where overburden stress is a principal stress, breakouts may form on opposite sides of the wellbore at the azimuth of the minimum horizontal far-field compression, as this is where the compressive hoop stress is greatest. If a well is inclined to the principal stresses, the location of the breakouts is a complex function of the orientation of the wellbore and the orientations and magnitudes of the in situ stresses. Drilling-induced tensile fractures occur in the borehole wall where the circumferential hoop stress is negative and exceeds the tensile strength of the rock. These fine-scale features occur only in the wall of the borehole, due to the localized stress concentration, and do not propagate away from the hole. The fractures form either parallel to the borehole axis in vertical wells, or in an en echelon pattern that is inclined with respect to the borehole axis in deviated wellbores. Tensile fractures will remain axial in a deviated wellbore if the well is drilled approximately parallel to the maximum horizontal stress. [15]

It is observed that most of the research has been carried out using advance rock mechanics laboratories and softwares for field applications i.e. commercial purpose .It is also observed that no significant work has been done in the field GMEM & Wellbore Stability analysis in our country. An attempt

has been made to carry out detailing simplified approach to analyze of GMEM & wellbore stability problems. Emphasize is given on the step by step manual procedure of wellbore stability calculations. I am sure it will help to develop strong base for advance research in this area.

Chapter 3
THEORY & APPLIED BACKGROUND OF INDUCED STRESS CONDITION IN PETROLEUM RELATED ROCK MECHANICS

3.1 IMPORTANCE OF STRESS

The important parameter in the geomechanical model is knowledge of the current state of stress. Wellbore failure occurs because the stress concentrated around the circumference of a well exceeds the strength of a rock.

3.1.1 Stress changes in depleting reservoirs

Drilling and hydraulic fracturing are affected by the poro elastic stress changes accompanying depletion. When there is a need to drill through depleted reservoirs to reach deeper formations, a variety of drilling problems could occur. Unless relatively low mud weights are used, there could be unintentional hydraulic fracturing and lost circulation in the depleted reservoir due to the decrease of the least principal stress in the depleted zone (but not adjacent formations). There can also be differential pipe sticking due to the difference between the mud weight and pore pressure in the depleted formations. If much lower mud weights are used to avoid these problems in the depleted zone, wellbore instability could be a significant problem above and below it.

3.2 STRESS IN THE EARTH'S CRUST

Curing wellbore stability problems needs a thorough knowledge about the mechanism upon which the instability has occurred. Misconception in failure mechanism recognition can even deteriorate the problem rather than solving it out. Therefore, it is of great importance to exactly determine what mechanism has caused the problem. Compressive stress exists everywhere at depth in the earth. Stress magnitudes depend on depth, pore pressure and active geologic processes that act at a variety of different spatial and temporal scales. There are three fundamental characteristics about the stress field that are of first-order importance:

- Knowledge of stress at depth is of fundamental importance for addressing a wide range of practical problems in geomechanics within oil, gas and geothermal reservoirs and in the overlaying formations.
- The *in situ* stress field at depth is remarkably coherent over a variety of scales.
- It is relatively straightforward to measure, estimate or constrain stress magnitudes at depth using techniques that are practical to implement in oil, gas and geothermal reservoirs.

In short, the *in situ* stress field in practice is determinable, comprehensible and needed to address a wide range of problems in reservoir geomechanics.

3.3 STATE OF STRESS AT A DEPTH

We have to define only four parameters to fully describe the state of stress at depth namely three principal stress magnitudes, and one stress orientation.

i. Sv, the vertical stress, corresponding to the weight of the overburden
ii. SHmax, the maximum principal horizontal stress
iii. Shmin,the minimum principal horizontal stress and

iv. one stress orientation, usually taken to be the azimuth of the maximum horizontal compression, SHmax.

This obviously helps make stress determination in the crust (as well as description of the in situ stress tensor) a much more tractable problem.

3.4 E. M. ANDERSON'S CLASSIFICATION SCHEME

We have to consider the magnitudes of the greatest, intermediate, and least principal stress at depth (*S*1, *S*2, and *S*3) in terms of *S*v, *S*Hmax and *S*hmin in the manner originally proposed by E. M. Anderson.

As illustrated in Figure 3.1 and Table 3.1, the Anderson scheme classifies an area as being characterized by normal, strike-slip or reverse faulting depending on whether

i. The crust is extending and steeply dipping normal faults accommodate movement of the *hanging wall* (the block of rock above the fault) downward with respect to the *footwall* (the block below the fault)

ii. Blocks of crust are sliding horizontally past one another along nearly vertical strike-slip faults

iii. The crust is in compression and relatively shallow-dipping reverse faults are associated with the hanging wall block moving upward with respect to the footwall block

iv. The Anderson classification scheme also defines the horizontal principal stress magnitudes with respect to the vertical stress

v. The vertical stress, *S*v, is the maximum principal stress (*S*1) in normal faulting regimes, the intermediate principal stress (*S*2) in strike-slip regimes and the least principal stress (*S*3) in reverse faulting regimes.

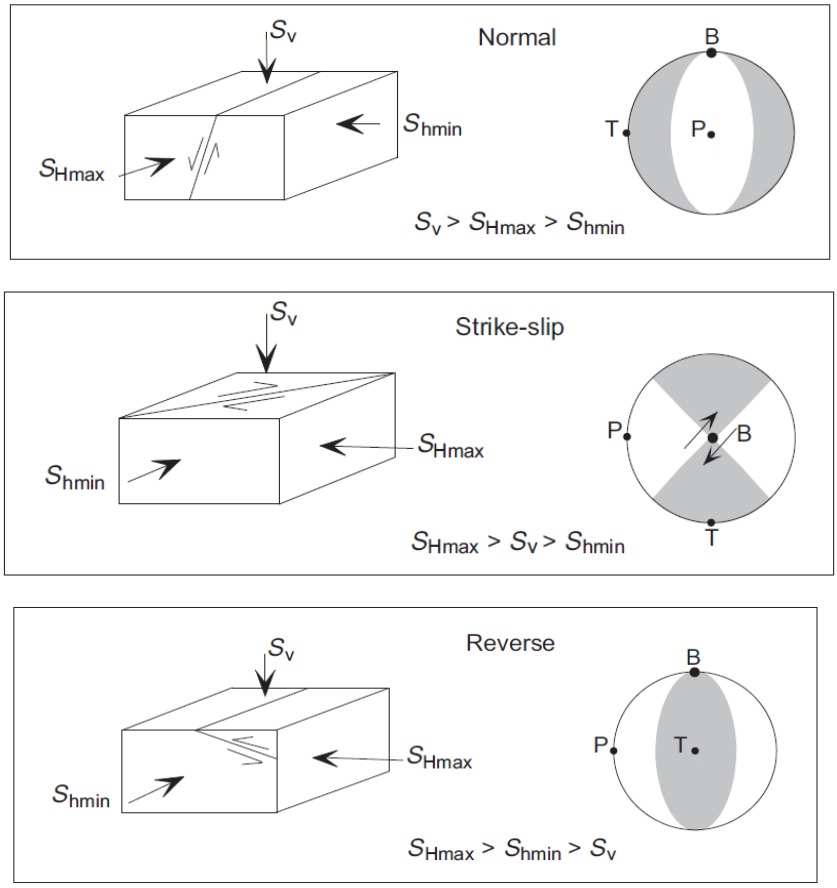

Figure 3.1: E. M. Anderson's classification scheme for relative stress magnitudes in normal, strike-slip and reverse faulting regions.

Table 3.1

Regime	Stress		
	S_1	S_2	S_3
Normal	S_v	S_{Hmax}	S_{hmin}
Strike-slip	S_{Hmax}	S_v	S_{hmin}
Reverse	S_{Hmax}	S_{hmin}	S_v

According to the Anderson classification scheme, the horizontal principal stresses may be less than, or greater than, the vertical stress, depending on the geological setting. The relative magnitudes of the principal stresses are simply related to the faulting style currently active in a region.

- As illustrated in above Figure 3.1, the vertical stress dominates in normal faulting regions (S1 = Sv), and fault slip occurs when the least horizontal principal stress (Shmin) reaches a sufficiently low value at any given depth depending on Sv and pore pressure.
- Conversely, when both horizontal stresses exceed the vertical stress (S3 = Sv) crustal shortening is accommodated through reverse faulting when the maximum horizontal principal stress (SHmax) is sufficiently larger than the vertical stress.
- Strike-slip faulting represents an intermediate stress state (S2 = Sv), where the maximum horizontal stress is greater than the vertical stress and the minimum horizontal stress is less (SHmax ≥ Sv ≥ Shmin). In this case, faulting occurs when the difference between SHmax and Shmin is sufficiently large.

3.5 VARIATION OF STRESS MAGNITUDES IN VARIOUS STRESS REGIMES

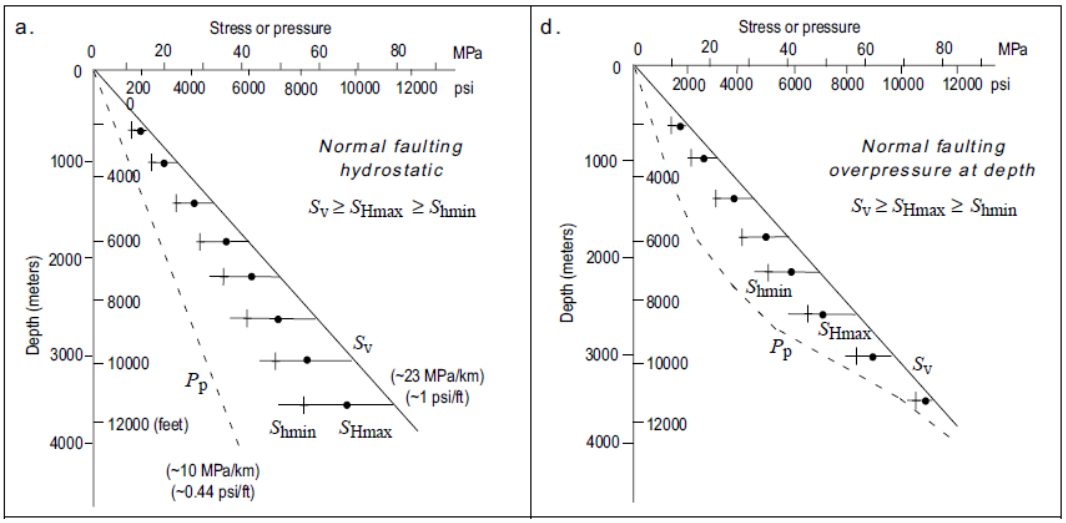

Fig 3.2 Variation of stress magnitudes with depth in normal-faulting stress regime for hydrostatic (a) and overpressure conditions (d).

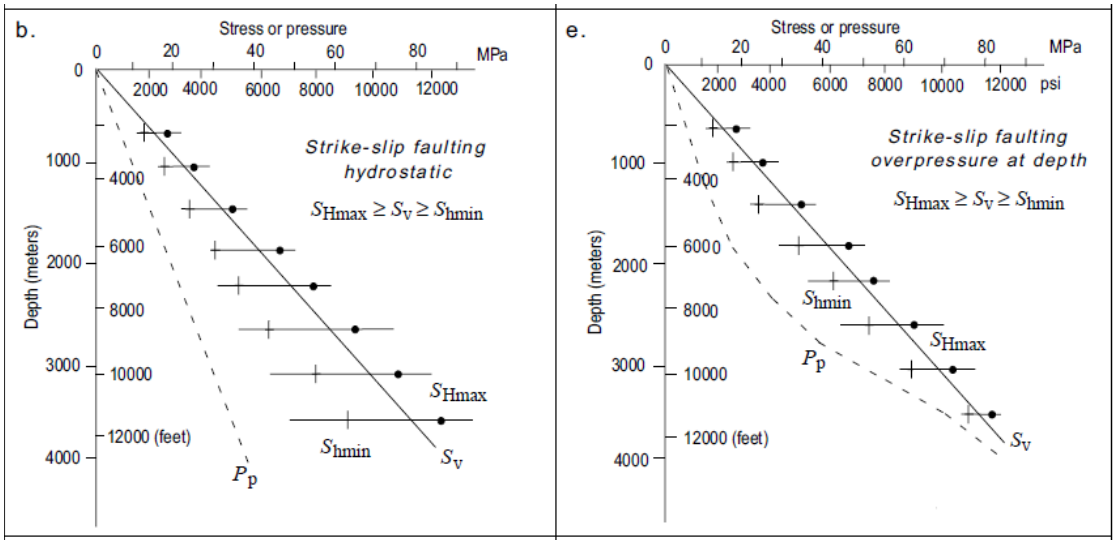

Fig 3.3 Variation of stress magnitudes with depth in strike slip-faulting stress regime for hydrostatic (b) and overpressure conditions (e).

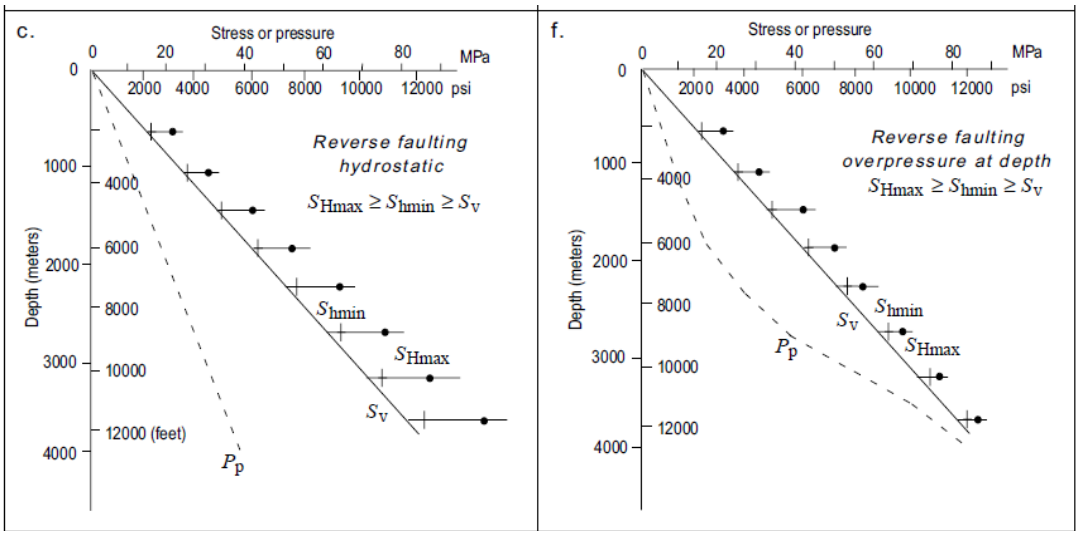

Fig 3.4 Variation of stress magnitudes with depth in strike slip-faulting stress regime for hydrostatic (c) and overpressure conditions (f).

3.6 IN-SITU STRESS MEASUREMENTS

The In-Situ Stresses are the three principal in situ earth stresses namely (S1,S2,S3) and they are determined in the context of (SHmax , Sv , Shmin).The determination of these stress values are very essential in the calculation of induced stresses at the wellbore wall.

A general overview of the strategy that will use for characterizing the stress field is as follows:

1. Assuming that the overburden is a principal stress (which is usually the case), *S*v can be determined from integration of density logs
2. The orientation of the principal stresses is determined from wellbore observations , recent geologic indicators and earthquake focal mechanisms
3. *S*3 (which corresponds to *S*hmin, except in reverse faulting regimes) is obtained from mini-fracs and leak-off tests
4. Pore pressure, *P*p, is either measured directly or estimated from geophysical logs or seismic data
5. Having observations of wellbore failures (breakouts and drilling-induced tensile fractures) allows for much more precise estimates of *S*Hmax.

3.7 THEORY BEHIND ROCK MECHANICS

The rock mechanics theory behind the geomechanical wellbore stability are presented below:

3.7.1 Elasticity

Most materials have an ability to resist and recover from deformations produced by external forces. This ability is called elasticity. It is the foundation for all aspects of rock mechanics. The term elasticity indicates the linear relationship between the external forces and the corresponding deformations. The region of validity for linear elasticity is often exceeded in practical situations.

In petroleum related rock mechanics, much of the interest is furthermore focused on rocks with a significant porosity as well as permeability. The elastic theory for solid materials is not able to fully describe the behavior of such materials and the concept of poroelasticity has therefore to be taken into account. The elastic response of a rock material may also be time dependent, so that the deformation of the material changes with time, even when the external conditions are constant.

3.7.2 Stresses

In rock mechanics the sign convention states that compressive stresses are positive. The historical reason for this is that the stresses dealt with in rock mechanics are mostly compressive.

The area A' of the cross-section at b) is, however, smaller than A. Hence the stress $\sigma = F/A'$ at b) is larger than the stress at a), i.e. the stress depends on the position within the stressed sample.

The orientation of the cross-section relative to the direction of the force is also important. Consider the cross-section at c) in Fig3.5 with area . Here the force is no longer normal to the cross-section.

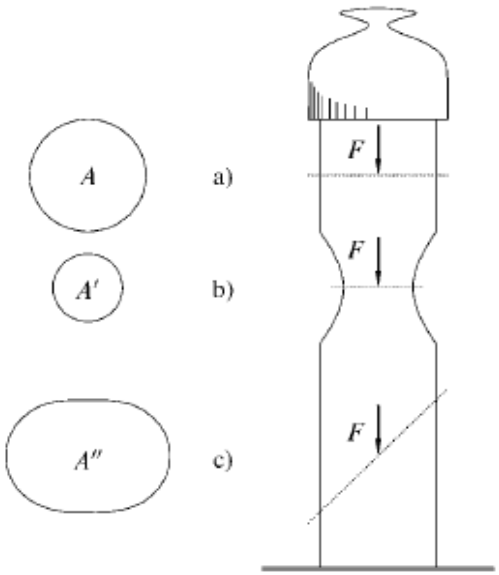

Fig 3.5 Illustration of Forces and Stress

We may then decompose the force into one component F_n that is normal to the cross-section, and one component F_p that is parallel to the section (fig 3.7 below)

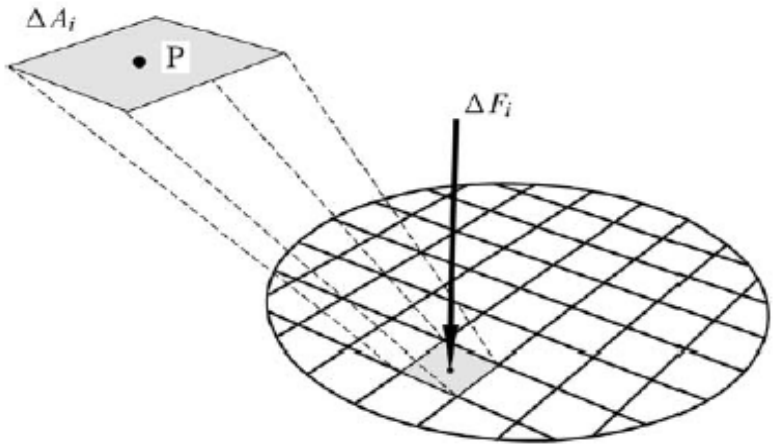

Fig 3.6. Local Stress

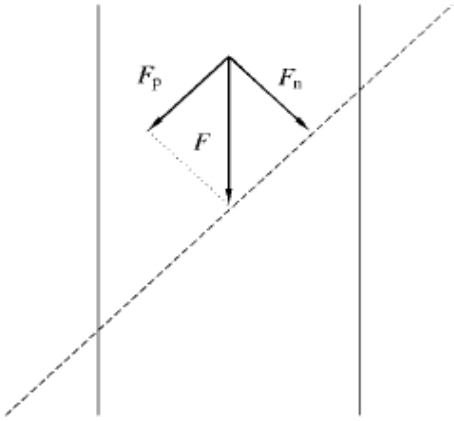

Fig 3.7 Decomposition of forces

The quantity σ is called the normal stress and is given by

$$\sigma = \frac{F_n}{A''} \tag{3.1}$$

While the quantity τ is called shear stress and is given by

$$\tau = \frac{F_p}{A''} \tag{3.2}$$

Thus, there are two types of stresses which may act through a surface, and the magnitude of each depends on the orientation of the surface.

3.7.3 Stress Tensor

To give a complete description of the stress state at a point P within a sample, it is necessary to identify the stresses related to surfaces oriented in three orthogonal directions.

The stresses related to a surface normal to the x-axis may be denoted σ_x , τ_{xy} and τ_{xz}, representing the normal stress, the shear stress related to a force in y-direction, and the shear stress related to a force in the z-direction, respectively. Physically, there will be only one shear stress associated with

this surface. However, the orientation of the shear stress has to be identified, and this is most conveniently done by identifying its y- and z-components: τ_{xy} and τ_{xz}. Similarly, the stresses related to a surface normal to the y-axis are denoted σ_y , τ_{yx} and τ_{yz}, while the stresses related to a surface normal to the z-axis are denoted σ_z, τ_{zx} and τ_{zy} . Thus there are all together nine stress components related to the point P:

$$\begin{pmatrix} \sigma_x & \tau_{xy} & \tau_{xz} \\ \tau_{yx} & \sigma_y & \tau_{yz} \\ \tau_{zx} & \tau_{zy} & \sigma_z \end{pmatrix} \tag{3.3}$$

Above expression is called the stress tensor. It gives a complete description of the stress state at the point P.

3.7.4 Principal Stresses in Two Dimension

For special orientations of the coordinate system, the stress tensor has a particularly simple form. To reveal this form, we shall initially study stresses in two dimensions. This is more than just an academic exercise; many problems of practical interest are effectively two dimensional.

Consider the normal (σ) and shear (τ) stresses at a surface oriented normal to a general direction θ in the xy-plane, as shown in Fig. 3.8. The triangle on the figure is at rest, such that no net forces act on it. Cancellation of forces implies that:

$$\sigma = \sigma_x \cos2\,\theta + \sigma_y \sin2\,\theta + 2\tau_{xy} \sin\theta \cos\theta \tag{3.4}$$

$$\sigma = \tfrac{1}{2}(\sigma_x + \sigma_y) + \tfrac{1}{2}(\sigma_x - \sigma_y)\cos 2\theta + \tau_{xy} \sin 2\theta \tag{3.5}$$

$$\tau = \sigma_y \sin\theta \cos\theta - \sigma_x \cos\theta \sin\theta + \tau_{xy} \cos\theta \cos\theta - \tau_{yx} \sin\theta \sin\theta \tag{3.6}$$

$$\tau = \tfrac{1}{2}(\sigma_y - \sigma_x) \sin 2\theta + \tau_{xy} \cos 2\theta \tag{3.7}$$

By proper choice of θ, it is possible to obtain $\tau = 0$. From Eq. (3.7) we see that this happens when:

$$\tan 2\theta = \frac{2\tau_{xy}}{\sigma_x - \sigma_y} \tag{3.8}$$

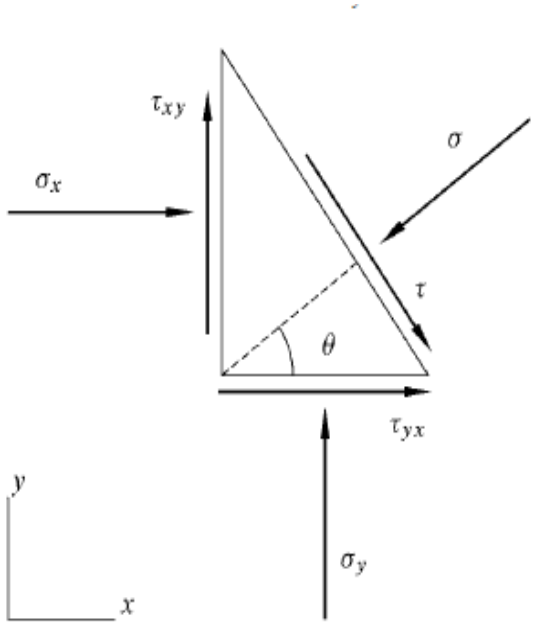

Fig 3.8. Force equilibrium on a triangle. The arrows shows the direction of the forces on the triangle, assuming that all the stress components are positive.

Eq. (3.8) has two solutions, θ_1 and θ_2. The two solutions correspond to two directions for which the shear stress τ vanishes. These two directions are called the principal axes of stress.

The corresponding normal stresses, σ_1 and σ_2, are called the principal stresses and are found by introducing Eq. (3.8) into Eq. (3.5):

$$\sigma_1 = \frac{1}{2}(\sigma_x + \sigma_y) + \sqrt{\tau_{xy}^2 + \frac{1}{4}(\sigma_x - \sigma_y)^2}$$
$$\sigma_2 = \frac{1}{2}(\sigma_x + \sigma_y) - \sqrt{\tau_{xy}^2 + \frac{1}{4}(\sigma_x - \sigma_y)^2} \qquad (3.9)$$

It is convenient to choose the notation such that $\sigma_1 \geq \sigma_2$. Thus, in the direction θ_1, which identifies a principal axis, the normal stress is σ_1 and the shear stress is zero. In the direction θ_2, which identifies the other principal axis, the normal stress is σ_2 and the shear stress is zero. The principal axes are orthogonal.

3.8 MOHR'S STRESS CIRCLE

It is often convenient to reorient the coordinate system such that the x-axis is parallel to the first principal axis and the y-axis parallel to the other. Then the stresses σ and τ in a general direction θ relative to the x-axis become, from Eqs. (3.5) and (3.7):

$$\sigma = \frac{1}{2}(\sigma_1 + \sigma_2) + \frac{1}{2}(\sigma_1 - \sigma_2)\cos 2\theta$$
$$\tau = -\frac{1}{2}(\sigma_1 - \sigma_2)\sin 2\theta \tag{3.10}$$

Plotting corresponding values of σ and τ in a diagram (Fig 3.9a), we obtain a circle called the Mohr's circle. The radius of the circle is $(\sigma 1 - \sigma 2)/2$ and the centre is at the point $(\sigma 1 + \sigma 2)/2$ on the σ-axis.

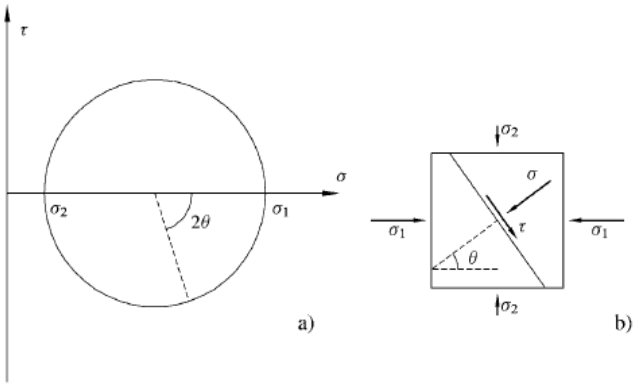

Fig 3.9 Mohr's Circle

The stresses σ and τ in any direction θ (Fig 3.9 b) correspond to a point on the Mohr's circle. It is seen from Fig. 3.10a that the largest absolute value for the shear stress is $(\sigma 1 - \sigma 2)/2$ and occurs for $\theta = \pi/4$ (= 45°) and $\theta = 3\pi/4$ (= 135°). A special case arises if $\sigma 1 = -\sigma 2$ and the centre of the Mohr's circle is located at the origin of the σ–τ co-ordinate system. In this case the maximum shear plane is free of normal stresses and this state of stress is known as *pure shear*; this condition provides the basis for some of the failure criteria used in metal plasticity. The Mohr's circle is a very useful tool in the analysis of conditions for rock failure.

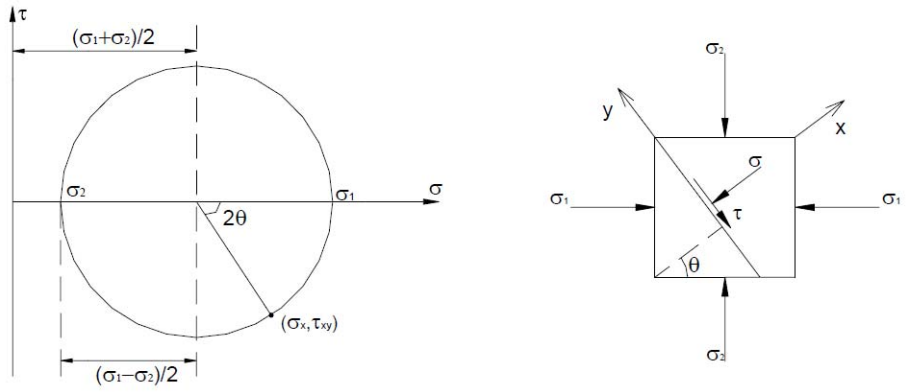

Fig. 3.10: Mohr's circle and stress components across a plane. (a) Construction of Mohr's circle. (b) The stress components acting on a plane correspond to a point on Mohr's circle.

3.8.1 Stress analysis in three dimensions

The two-dimensional analysis considers the equilibrium only in two directions, say the x and y directions and thus three independent stress components (i.e., σx, σy and τxy) are required to specify the state of stress at a point. The general analysis is three-dimensional and involves six independent stress components (i.e., three normal stresses and three shear stresses) in order to describe the state of stress at a point, as discussed previously. The actual values of these components depend on the orientation of the infinitesimal cube. Thus, the directions where the normal stress components have maximum and minimum values should be considered. This takes place when the shear stress components on all the faces of the cube vanish. These directions, therefore, are principle stress axes and the stress tensor at the point will have the following simple form:

$$\sigma = \begin{pmatrix} \sigma_1 & 0 & 0 \\ 0 & \sigma_2 & 0 \\ 0 & 0 & \sigma_3 \end{pmatrix}, \tag{3.11}$$

where σ1 is the maximum principal stress, σ2 is the intermediate principle stress, and σ3 is the minimum principle stress (i.e., σ1 ≥ σ2 ≥ σ3). As a result, there are three principle stresses and their orientations that must be determined in order that the state of stress at a point is defined. In three-dimensional analysis, a direction in space is identified by the direction cosines (Fig 3.11.)

$$\lambda_x = \cos\alpha_x,\ \lambda_y = \cos\alpha_y,\ \lambda_z = \cos\alpha_z, \tag{3.12}$$

where α_x, α_y and α_z are the angles between the chosen direction and the x-, y- and z-axes, respectively. The vector λ = (λx, λy, λz) is a unit vector in the chosen direction, and so

$$\lambda_x^2 + \lambda_y^2 + \lambda_z^2 = 1. \tag{3.13}$$

The principle stresses can be found by solving the following determinant equation for σ P (Goodman, 1989, p. 403):

$$\begin{vmatrix} \sigma_x - \sigma_p & \tau_{xy} & \tau_{xz} \\ \tau_{xy} & \sigma_y - \sigma_p & \tau_{yz} \\ \tau_{xz} & \tau_{yz} & \sigma_z - \sigma_p \end{vmatrix} = 0. \tag{3.14}$$

This will give a cubic equation:

$$\sigma_p^3 - I_1\sigma_p^2 - I_2\sigma_p - I_3 = 0, \tag{3.15}$$

Where

$$\begin{aligned} I_1 &= \sigma_x + \sigma_y + \sigma_z, \\ I_2 &= \sigma_x\sigma_y + \sigma_y\sigma_z + \sigma_z\sigma_x - \tau_{xy}^2 - \tau_{yz}^2 - \tau_{zx}^2, \\ I_3 &= \sigma_x\sigma_y\sigma_z + 2\tau_{xy}\tau_{yz}\tau_{zx} - \sigma_x\tau_{yz}^2 - \sigma_y\tau_{zx}^2 - \sigma_z\tau_{xy}^2. \end{aligned} \tag{3.16}$$

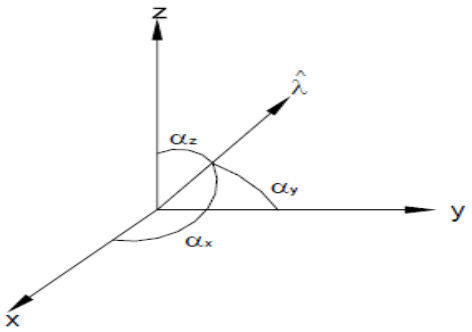

Figure 3.11 Direction Cosines

The three solutions of this equation are the principal stresses σ1, σ2 and σ3 (i.e., the eigenvalues). The quantities I1, I2 and I3 are called stress invariants, which are uniquely defined regardless of the choice of the co-ordinate axes.

The direction cosines λ1x, λ1y and λ1z identifying the principle axis corresponding to σ1 are found by the solution of the equations (Jaeger and Cook, 1979, p. 20):

$$\begin{aligned}
\lambda_{1x}(\sigma_x - \sigma_1) + \lambda_{1y}\tau_{xy} + \lambda_{1z}\tau_{xz} &= 0,\\
\lambda_{1x}\tau_{xy} + \lambda_{1y}(\sigma_y - \sigma_1) + \lambda_{1z}\tau_{yz} &= 0,\\
\lambda_{1x}\tau_{xz} + \lambda_{1y}\tau_{yz} + \lambda_{1z}(\sigma_z - \sigma_1) &= 0.
\end{aligned} \tag{3.17}$$

Similarly, the principle axes corresponding to σ2 and σ3 are found by the solution of the following equations:

$$\begin{aligned}
\lambda_{2x}(\sigma_x - \sigma_2) + \lambda_{2y}\tau_{xy} + \lambda_{2z}\tau_{xz} &= 0,\\
\lambda_{2x}\tau_{xy} + \lambda_{2y}(\sigma_y - \sigma_2) + \lambda_{2z}\tau_{yz} &= 0,\\
\lambda_{2x}\tau_{xz} + \lambda_{2y}\tau_{yz} + \lambda_{2z}(\sigma_z - \sigma_2) &= 0.
\end{aligned} \tag{3.18}$$

$$\begin{aligned}
\lambda_{3x}(\sigma_x - \sigma_3) + \lambda_{3y}\tau_{xy} + \lambda_{3z}\tau_{xz} &= 0,\\
\lambda_{3x}\tau_{xy} + \lambda_{3y}(\sigma_y - \sigma_3) + \lambda_{3z}\tau_{yz} &= 0,\\
\lambda_{3x}\tau_{xz} + \lambda_{3y}\tau_{yz} + \lambda_{3z}(\sigma_z - \sigma_3) &= 0.
\end{aligned} \tag{3.19}$$

Consequently, Equations (3.15-3.19) provide the principal stresses and their orientations at a point, which is adequate to specify the state of stress in three dimensions. If the co-ordinate system is oriented so that the x-axis is parallel to the first principal axis, the y-axis parallel to the second and the z-axis parallel to the third, the stress tensor will take the form presented in Eq(3.11). Relative to this set of co-ordinate axes, the stresses σ and τ in a general direction λ1,λ2 and λ 3 are determined by (Fjaer et al., 1992, p. 12):

$$\lambda_1^2\sigma_1 + \lambda_2^2\sigma_2 + \lambda_3^2\sigma_3 = \sigma,$$
$$\lambda_1^2\sigma_1^2 + \lambda_2^2\sigma_2^2 + \lambda_3^2\sigma_3^2 = \sigma^2 + \tau^2. \qquad (3.20)$$

Eq. (3.20) can then be utilized to construct the Mohr's circle in three dimensions. Consider the plane in the cube in Figure 3.12a. For this plane λ3 = 0, and so the normal and shear components (σ and τ) on the plane are not affected by σ3, but by σ1 and σ2, and σ and τ are located on the circle spanning from σ2 to σ1 as shown in Figure 3.9 b (i.e., σ1– σ2 Mohr's circle). If the plane was perpendicular to σ1, that is, λ1 = 0, then the relationship between σ and τ can be plotted on the σ2 –σ3 Mohr's circle. Similarly, if λ2 = 0, σ and τ are located on the σ1–σ3 Mohr's circle. For all other directions, the stress conditions lie in the shaded region between the circles in Figure 3.12 b.

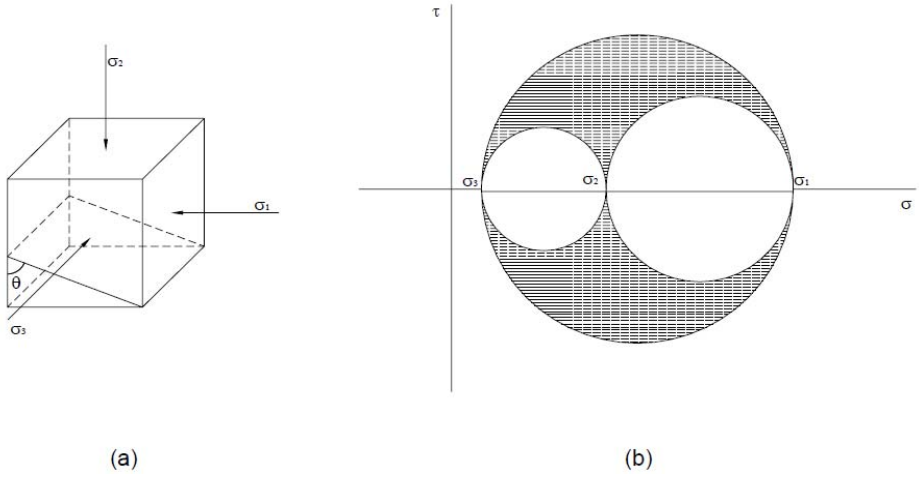

Figure 3.12 Mohr's circle for three dimensional state of stress.

3.8.2 Octahedral stress

The direction for which the plane in Figure 3.12a is equally inclined to the principal axes, that is:

$$\lambda_1 = \lambda_2 = \lambda_3 = \frac{1}{\sqrt{3}}, \tag{3.21}$$

is called the octahedral plane, since it is parallel to a face of an octahedron with vertices on the principal axes. The normal and shear stresses acting on this plane are called the octahedral normal stress (σoct) and the octahedral shear stress (τoct). By substituting Eq. (3.21) in Eq. (3.20), the octahedral normal stress is found to be given by

$$\sigma_{oct} = \frac{1}{3}(\sigma_1 + \sigma_2 + \sigma_3) = \frac{1}{3} I_1. \tag{3.22}$$

To determine the octahedral shear stress, introduce Eq. (3.21) into (3.20) to give

$$\tau_{oct} = \frac{1}{3}\sqrt{(\sigma_1 - \sigma_2)^2 + (\sigma_2 - \sigma_3)^2 + (\sigma_3 - \sigma_1)^2},$$

or
$$\tau_{oct} = \frac{\sqrt{2}}{3}\sqrt{\sigma_1^2 + \sigma_2^2 + \sigma_3^2 - \sigma_1\sigma_2 - \sigma_2\sigma_3 - \sigma_3\sigma_1}, \tag{3.23}$$

which can be written in terms of stress invariants as

$$\tau_{oct} = \frac{\sqrt{2}}{3}(I_1^2 - 3I_2)^{\frac{1}{2}}. \tag{3.24}$$

3.8.3 Deviatoric stress

The octahedral normal stress (σoct) defined in Eq. (3.22) is apparently the mean normal stress (σm) which remains unaltered during any change of co-ordinate axes, that is, the invariant I1/3. The mean normal stress is also known as the spherical or hydrostatic stress. It essentially causes uniform

compression or dilatation. In contrast, distortion is essentially determined by the so-called deviatoric stress (stress deviator or stress deviation). The deviatoric stress (s) estimates the deviation of stress from the mean normal stress by subtracting σm from the normal stress components

$$\boldsymbol{s} = \begin{bmatrix} s_x & s_{xy} & s_{xz} \\ s_{xy} & s_y & s_{yz} \\ s_{xz} & s_{yz} & s_z \end{bmatrix} = \begin{bmatrix} \sigma_x - \sigma_m & \tau_{xy} & \tau_{xz} \\ \tau_{xy} & \sigma_y - \sigma_m & \tau_{yz} \\ \tau_{xz} & \tau_{yz} & \sigma_z - \sigma_m \end{bmatrix}. \quad (3.25)$$

The principal axes of the deviatoric stress will be the same as those of stress. The deviatoric principle stresses (s1,s2,s3) can be established from the principle stresses and the spherical stress and is given by

$$\begin{aligned} s_1 &= \sigma_1 - \sigma_m = (2\sigma_1 - \sigma_2 - \sigma_3)/3, \\ s_2 &= \sigma_2 - \sigma_m = (2\sigma_2 - \sigma_1 - \sigma_3)/3, \\ s_3 &= \sigma_3 - \sigma_m = (2\sigma_3 - \sigma_1 - \sigma_2)/3, \end{aligned} \quad (3.26)$$

where s1 ≥ s2 ≥ s3.

Many failure criteria are concerned with distortion. As these criteria must be independent of the choice of co-ordinate axes, the invariants of the deviatoric stress will be involved in failure criteria. These will be denoted by J1, J2, and J3 and are found to be (Jaeger and Cook, 1979, p. 33)

$$\begin{aligned} J_1 &= s_x + s_y + s_z = 0, \\ J_2 &= -(s_x s_y + s_y s_z + s_z s_x) + s_{xy}^2 + s_{yz}^2 + s_{zx}^2, \\ J_3 &= s_x s_y s_z + 2 s_{xy} s_{yz} s_{zx} - s_x s_{yz}^2 - s_y s_{zx}^2 - s_z s_{xy}^2. \end{aligned} \quad (3.27)$$

Using the above equations and rearranging, the octahedral shear stress can be given as

$$\tau_{oct} = (2J_2/3)^{\frac{1}{2}}. \quad (3.28)$$

Chapter 4
STRESSES AROUND BOREHOLE:BOREHOLE INSTABILITY CRITERIA

4.1 NEAR WELLBORE STRESS- STATE

Before drilling, rock stress is described by the in-situ stresses and effective stresses. As the hole is drilled, the support provided by the rock is removed and replaced by hydrostatic pressure. This change alters the stresses. The stress at any point on or near the wellbore can now be described in terms of:

1. radial stress σ_{rr} acting along the radius of the wellbore
2. hoop stress $\sigma_{\theta\theta}$ acting around the circumference of the wellbore
3. axial stress σ_{zz} acting parallel to the well path and
4. the additional shear stress components designated by ($\tau_{r\theta}, \tau_{\theta z}, \tau_{z\theta}$)

These stresses are perpendicular to each other and for mathematical convenience, are used as a borehole coordinate system.

4.1.1 Hoop stress ($\sigma_{\theta\theta}$)

Hoop stress is dependent upon wellbore pressure (p_w), stress magnitude and orientation, pore pressure, and hole inclination and direction. Wellbore pressure (p_w) is directly related to mud weight/Equivalent Circulating Density(ECD).

For a vertical wellbore with equal horizontal stresses, hoop stress is dependent upon the mud weight and the magnitude of the horizontal stresses and is equally distributed around the wellbore.A deviated well creates unequal distribution of hoop stress around the wellbore due to the redistribution of the horizontal and vertical stresses. Hoop stress acting on a cross-section of the wellbore is maximum at the sides of the wellbore perpendicular to the maximum stress.

The same is true when drilling a vertical well in an in-situ environment of unequal horizontal stress. Hoop stress is maximum at the side of the wellbore perpendicular to the maximum horizontal stress.

4.1.2 Axial stress- (σ_{zz})

Axial stress is oriented along the wellbore path and can be unequally distributed around the wellbore. Axial stress is dependent upon; in-situ stress magnitude and orientation, pore pressure, and hole inclination and direction. Axial stress is not directly affected by mud weight.

For a vertical well with equal horizontal stress ($S_{Hmax} = S_{hmin}$), axial and vertical stress are the same. Axial stress in a deviated well is the resolution of the overburden and horizontal stresses.

4.1.3 Radial stress-(σ_{rr})

Radial stress is the difference in wellbore pressure and pore pressure and acts along the radius of the wellbore.

4.2 Mechanical Stability

Hoop, radial and axial stress describes the near wellbore stress-state of the rock. Mechanical Stability is the management of these stresses in an effort to prevent shear or tensile rock failure. Normally the stresses are compressive and create shear stress within the rock. The more equal these stresses, the more stable the rock.

4.2.1 Controlling Parameters

Mechanical stability is achieved by controlling the following parameters that affect hoop, axial and radial stress

i. Mud Weight/ECD
ii. Mud Filter Cake
iii. Well Path- Inclination and Azimuth
iv. Drilling/Tripping Practices

4.2.2 Uncontrollable Parameters

i. Unfavorable In-Situ condition.
ii. Adverse Formations like (reactive shale, unconsolidated or fractured formations, abnormal or subnormally pressured zones.
iii. Constrained Wellbore Trajectory

Mechanical stability of the well is also impacted by drilling fluid/formation interaction. Chemical instability eventually results in mechanical failure of the rock in shear or tension. Time is also an important consideration. The longer the formation is exposed to the drilling mud, the more near-wellbore pore pressure increases. The rock looses support provided by the mud weight.

4.3 EFFECT OF MUD WEIGHT/ECD

Mud weight, ECD and pressure surges on the wellbore directly effect hoop and radial stress.

- An increase in MW decreases hoop stress and increases radial stress.
- Similarly, a decrease in MW increases hoop stress and decreases radial stress.
- The result on wellbore stability is dependent upon the magnitude of the mud weight increase/decrease.

4.4 HOLE INCLINATION AND DIRECTION

The inclination and direction of the wellbore greatly impacts the stability of the well. Unequal distribution of hoop and axial stress around the circumference of the well tends to make the wellbore less stable.

4.5 EQUAL HORIZONTAL STRESSES

Before drilling from vertical, the hoop stress is equally distributed. As angle increases to horizontal, the hoop stress on the high and low side of the wellbore decreases, but the hoop increases greatly on the perpendicular sides. The radial stress remains fixed but the increasing hoop stress increases the stress-state.

4.6 STRESSES AROUND BOREHOLES

Underground formations are subjected to a vertical compressive stress caused by the weight of the overlying strata, and horizontal stresses due to the confining lateral restraints. Under the action of these *in situ* stresses, prior to drilling a borehole, the rock mass is in a state of equilibrium that will be destroyed by the excavation. When a borehole is drilled, the load carried by the removed rock is then taken by the adjacent rock to re-establish equilibrium. As a result, a stress concentration is produced around the well, and so the *in situ* stresses are modified. If there is no support pressure introduced into the borehole, failure in the formation may take place. Therefore, maintaining equilibrium in the field to prevent rock failure requires the use of a support pressure which is usually provided by a pressurized fluid called “mud”.

Moreover, the critical mud pressures are not significantly affected by elastic anisotropy for commonly encountered oilfield rocks (Aadnoy, 1988; Aadnoy, 1989a; Chen et al., 1996; Tan et al., 1999; Chen et al., 2002). Therefore, for wellbore stability analysis, we assume that rocks obey isotropic elastic behaviour. In this chapter, an isotropic linear elastic constitutive model is described. The model consists of a three dimensional analyses of stress

concentration around an arbitrarily oriented borehole, due to anisotropic *in situ* stress combined with internal wellbore pressure.

4.6.1 Stresses in cylindrical co-ordinates

A cylindrical co-ordinate system is used to assess the potential mechanical instability of a borehole; a constitutive model is needed in order to know the magnitude of the stresses around a borehole. The literature is rich with such constitutive models. Westergaard (1940) published one of the early works contributing to the knowledge of stress distribution around a borehole, in which an elasto-plastic model was developed. After that, many works using elasto-plastic models have been published (e.g., Gnirk, 1972; Risnes and Bratli, 1981; Mitchell et al., 1987; Anthony and Crook, 2002). On the other hand, there have been other efforts to develop a linear elastic constitutive model (e.g., Paslay and Cheatham, 1963; Fairhurst, 1965b; Bradley, 1979; Aadnoy, 1989b). Out of the numerous published models, linear elastic analysis may be the most convenient approach. This is due to its requirement of fewer input parameters compared to other more intricate models.

For instance, Risnes and Bratli (1981), and McLean and Addis (1990a) recommended the use of elasto-plastic model in wellbore stability analysis. Some of those authors, however, in other publications (McLean and Addis, 1990b; Svennekjaer and Bratli, 1998), applied a linear elastic model to carry out the stability analysis for field cases. In practice, the required input data for sophisticated models are rarely available (e.g., Maury and Sauzay, 1987; Fuh et al., 1988; Fleming et al., 1990; Woodland, 1990; Garrouch and Ebrahim, 2001).

Consideration convenient system for studying the state of stress around boreholes. Cartesian (x,y,z) and cylindrical (r,θ,z) co-ordinate systems are shown in Figure 4.1. The co-ordinate transformation between Cartesian and cylindrical co-ordinates is defined by the following equations:

$$r = (x^2 + y^2)^{1/2}, \quad \theta = \arctan(y/x). \tag{4.1}$$

and

$$x = r\cos\theta, \quad y = r\sin\theta. \tag{4.2}$$

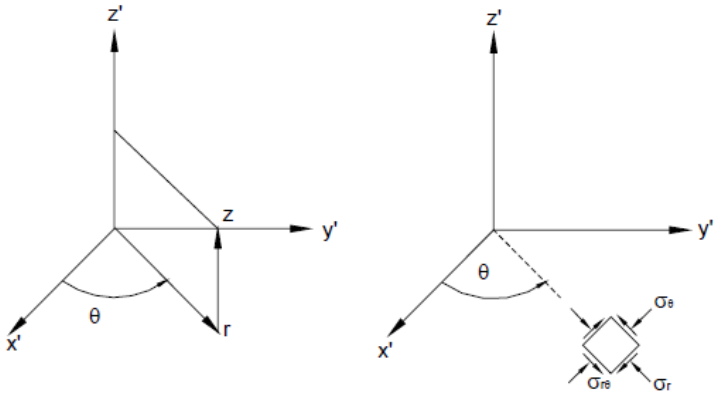

(a) (b)

Figure 4.1. Transformation between Cartesian and cylindrical co-ordinates. (a) Rotation about z axis. (b) Stresses in cylindrical co-ordinates.

In the cylindrical co-ordinate system, at any point, the stress tensor becomes

$$\begin{pmatrix} \sigma_r & \sigma_{r\theta} & \sigma_{rz} \\ \sigma_{r\theta} & \sigma_\theta & \sigma_{\theta z} \\ \sigma_{rz} & \sigma_{\theta z} & \sigma_z \end{pmatrix}, \tag{4.3}$$

where $\boldsymbol{\sigma_r}$ is called the *radial stress*, $\boldsymbol{\sigma_\theta}$ the *tangential stress* and $\boldsymbol{\sigma_z}$ the *axial stress*. Note that the same designation σ is used for all the stress components. This notation will be adopted in this chapter and the following ones. These stresses can be related to the Cartesian co-ordinate stresses by the aid of stress transformation equation that have the general form (Harrison and Hudson)

$$\begin{pmatrix} \sigma_x & \sigma_{xy} & \sigma_{xz} \\ \sigma_{yx} & \sigma_y & \sigma_{yz} \\ \sigma_{zx} & \sigma_{zy} & \sigma_z \end{pmatrix} = \begin{pmatrix} \lambda_{xx'} & \lambda_{xy'} & \lambda_{xz'} \\ \lambda_{yx'} & \lambda_{yy'} & \lambda_{yz'} \\ \lambda_{zx'} & \lambda_{zy'} & \lambda_{zz'} \end{pmatrix} \begin{pmatrix} \sigma_{x'} & \sigma_{x'y'} & \sigma_{x'z'} \\ \sigma_{y'x'} & \sigma_{y'} & \sigma_{y'z'} \\ \sigma_{z'x'} & \sigma_{z'y'} & \sigma_{z'} \end{pmatrix} \begin{pmatrix} \lambda_{xx'} & \lambda_{xy'} & \lambda_{xz'} \\ \lambda_{yx'} & \lambda_{yy'} & \lambda_{yz'} \\ \lambda_{zx'} & \lambda_{zy'} & \lambda_{zz'} \end{pmatrix}^T, \tag{4.4}$$

where the stress components on the right-hand side of this expression are assumed known, that is, in the (x, y, z') co-ordinate system, and are required in

the (x,y,z) co-ordinate system that is inclined with respect to the first. The transformation from (x',y',z') to (x,y,z) is described by the direction cosines ($\lambda_{xx'},\lambda_{xy'},\lambda_{xz'}$), *etc*. The term $\lambda_{xx'}$, for instance, is the direction cosine of the angle between the x-axis and x'-axis.

The first matrix on the right-hand side of the equation is called the *rotation matrix*, and the last matrix is its transpose. The transformation from (x, y, z') to (r,θ,z) can be obtained by a rotation θ around the z'-axis, as shown in Figure 4.3. The corresponding rotation matrix is

$$\begin{pmatrix} \cos\theta & \sin\theta & 0 \\ -\sin\theta & \cos\theta & 0 \\ 0 & 0 & 1 \end{pmatrix}. \qquad 4.5$$

Proceeding with the matrix multiplication on the right hand side of the stress transformation equation, using the above rotation matrix, and replacing the matrix on the left-hand side by Eq. (4.3), produces the following formulae for the stress components in cylindrical coordinate:

$$\begin{aligned}
\sigma_r &= \sigma_{x'}\cos^2\theta + \sigma_{y'}\sin^2\theta + 2\sigma_{x'y'}\sin\theta\cos\theta, \\
\sigma_\theta &= \sigma_{x'}\sin^2\theta + \sigma_{y'}\cos^2\theta - 2\sigma_{x'y'}\sin\theta\cos\theta, \\
\sigma_z &= \sigma_{z'}, \\
\sigma_{r\theta} &= (\sigma_{y'} - \sigma_{x'})\sin\theta\cos\theta + \sigma_{x'y'}(\cos^2\theta - \sin^2\theta), \\
\sigma_{rz} &= \sigma_{x'z'}\cos\theta + \sigma_{y'z'}\sin\theta, \\
\sigma_{\theta z} &= \sigma_{y'z'}\cos\theta - \sigma_{x'z'}\sin\theta.
\end{aligned} \qquad 4.6$$

4.7 STRESSES AROUND DEVIATED BOREHOLES

In this section, the stresses around a deviated borehole with anisotropic horizontal stresses are described. Assume that the in situ principal stresses are vertical stress σ_v, major horizontal stress σ_H, and minor horizontal stress σ_h. These stresses are associated with the co-ordinate system (x, y, z′), as

illustrated in Figure 4.4a. The z′-axis is parallel to σ_v, x′-axis is parallel to σ_H, and y′-axis is parallel to σ_h.

These virgin formation stresses should be transformed to another co-ordinate system (x,y,z), to conveniently determine the stress distribution around a borehole. Figure 4.4b shows the (x,y,z) co-ordinate system, where the z-axis is parallel to the borehole axis, the x-axis is parallel to the lowermost radial direction of the borehole, and the y-axis is horizontal. This transformation can be obtained by a rotation α around the z′-axis, and then a rotation i round the y′-axis (Figure 4.2).

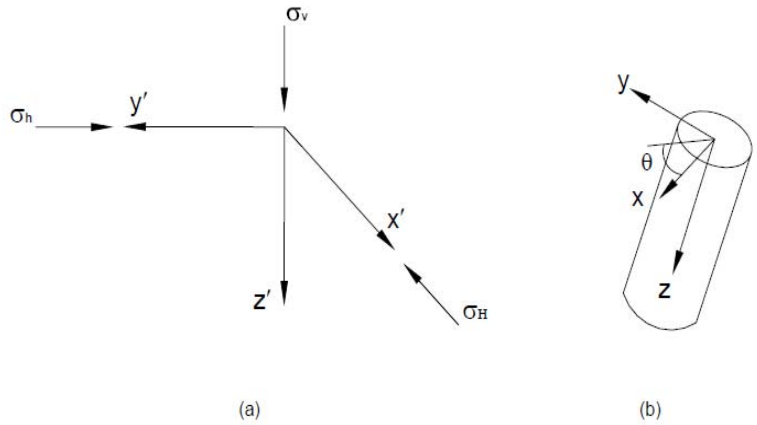

Figure 4.2 In situ stress co-ordinate system

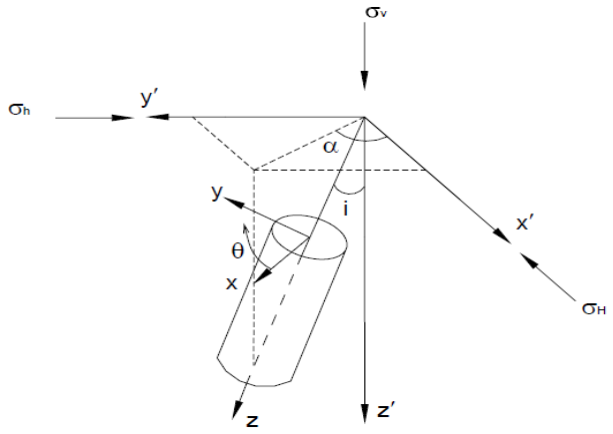

Figure 4.3 Stress transformation system for deviated borehole

The direction cosines associated with the z-axis can be determined by the projection of a unit vector parallel to the z-axis onto the ($x'y'z'$) axes. This result in

$$\lambda_{zx'} = \cos\alpha \sin i, \ \lambda_{zy'} = \sin\alpha \sin i, \ \lambda_{zz'} = \cos i. \tag{4.7}$$

For the direction cosines associated with the x-axis, the result will be the same as Eq. (4.5), with i by $i + (\pi / 2)$, so that

$$\lambda_{xx'} = \cos\alpha \cos i, \ \lambda_{xy'} = \sin\alpha \cos i, \ \lambda_{xz'} = -\sin i. \tag{4.8}$$

Finally, the y-axis is horizontal and makes angles α and $\alpha + (\pi / 2)$ with the x' and y'-axes, respectively. Therefore the direction cosines associated with the y-axis are

$$\lambda_{yx'} = -\sin\alpha, \ \lambda_{yy'} = \cos\alpha, \ \lambda_{yz'} = 0. \tag{4.9}$$

These nine direction cosines will form the rotation matrix

$$\begin{pmatrix} \cos\alpha\cos i & \sin\alpha\cos i & -\sin i \\ -\sin\alpha & \cos\alpha & 0 \\ \cos\alpha\sin i & \sin\alpha\sin i & \cos i \end{pmatrix}, \tag{4.10}$$

and together with the known stress tensor

$$\begin{pmatrix} \sigma_H & 0 & 0 \\ 0 & \sigma_h & 0 \\ 0 & 0 & \sigma_v \end{pmatrix}, \tag{4.11}$$

using the stress transformation equation, the virgin formation stresses expressed in the (x,y,z) co-ordinate system become:

$$\sigma_x^o = (\sigma_H \cos^2\alpha + \sigma_h \sin^2\alpha)\cos^2 i + \sigma_v \sin^2 i,$$

$$\sigma_y^o = \sigma_H \sin^2\alpha + \sigma_h \cos^2\alpha,$$

$$\sigma_z^o = (\sigma_H \cos^2\alpha + \sigma_h \sin^2\alpha)\sin^2 i + \sigma_v \cos^2 i,$$

$$\sigma_{xy}^o = 0.5(\sigma_h - \sigma_H)\sin 2\alpha \cos i,$$

$$\sigma_{yz}^o = 0.5(\sigma_h - \sigma_H)\sin 2\alpha \sin i,$$

$$\sigma_{xz}^o = 0.5(\sigma_H \cos^2\alpha + \sigma_h \sin^2\alpha - \sigma_v)\sin 2i.$$

4.12

The superscript "*o*" on the stresses denotes that these are the virgin formation stresses. As mentioned before, the excavation of a wellbore will alter the *in situ* stresses that are given in the above equation. The complete stress solutions, in cylindrical co-ordinate system, around an arbitrarily oriented wellbore are as shown below.

Formulae Set 2

$$\sigma_r = \left(\frac{\sigma_x^o + \sigma_y^o}{2}\right)\left(1 - \frac{a^2}{r^2}\right) + \left(\frac{\sigma_x^o - \sigma_y^o}{2}\right)\left(1 + 3\frac{a^4}{r^4} - 4\frac{a^2}{r^2}\right)\cos 2\theta$$
$$+ \sigma_{xy}^o\left(1 + 3\frac{a^4}{r^4} - 4\frac{a^2}{r^2}\right)\sin 2\theta + P_w\frac{a^2}{r^2},$$

$$\sigma_\theta = \left(\frac{\sigma_x^o + \sigma_y^o}{2}\right)\left(1 + \frac{a^2}{r^2}\right) - \left(\frac{\sigma_x^o - \sigma_y^o}{2}\right)\left(1 + 3\frac{a^4}{r^4}\right)\cos 2\theta$$
$$- \sigma_{xy}^o\left(1 + 3\frac{a^4}{r^4}\right)\sin 2\theta - P_w\frac{a^2}{r^2},$$

$$\sigma_z = \sigma_z^o - \nu\left[2\left(\sigma_x^o - \sigma_y^o\right)\frac{a^2}{r^2}\cos 2\theta + 4\sigma_{xy}^o\frac{a^2}{r^2}\sin 2\theta\right],$$

$$\sigma_{r\theta} = \left[-\left(\frac{\sigma_x^o - \sigma_y^o}{2}\right)\left(1 - 3\frac{a^4}{r^4} + 2\frac{a^2}{r^2}\right)\sin 2\theta\right] + \sigma_{xy}^o\left(1 - 3\frac{a^4}{r^4} + 2\frac{a^2}{r^2}\right)\cos 2\theta,$$

$$\sigma_{\theta z} = \left(-\sigma_{xz}^o \sin\theta + \sigma_{yz}^o \cos\theta\right)\left(1 + \frac{a^2}{r^2}\right),$$

$$\sigma_{rz} = \left(\sigma_{xz}^o \cos\theta + \sigma_{yz}^o \sin\theta\right)\left(1 - \frac{a^2}{r^2}\right),$$

4.13

where "*a*" is the radius of the wellbore, P_w is the internal wellbore pressure, and ν is a material constant called Poisson's ratio. The angle θ is measured clockwise from the *x*-axis, as shown in Figure 4.2.

Eq. (4.13) is derived under the assumption that there is no displacement along the *z*-axis, that is, a plain strain condition, in order to estimate σ_r, σ_θ, σ_z and $\sigma_{r\theta}$. The longitudinal shear stresses, $\sigma_{\theta z}$ and σ_{rz}, however, are determined assuming that all plane sections normal to the *z*-axis undergo the same deformations as a result of longitudinal shears. The equations for stresses around a circular opening were first published by Kirsch , where the opening is assumed to be parallel to a principle stress axis (Charlez, 1991, p. 87). The stress field around a circular opening in any direction was first presented by Hiramatsu and Oka (1968) and Fairhurst (1968).

4.8 STRESS DISTRIBUTION AROUND A WELLBORE

It is usually assumed that the major principal in-situ stress, σ1, is vertical and the intermediate and minor principal in-situ stresses, σ2 and σ3 respectively are horizontal. However, in tectonically active areas the principal stresses may be inclined to the vertical and horizontal.

When a borehole is drilled into a rock mass, drilling fluid of a different density replaces the excavated rock, and the natural stress field redistributes locally around the borehole. The stress distribution in the borehole wall depends on the magnitude of the in-situ principal stresses and the stress strain response of the rock material. Borehole stability studies have assumed a homogeneous, isotropic, linear elastic rock.

Hence the drilling of a hole in the ground disturbs the in-situ stresses around the wellbore and induces additional stresses. In particular, hoop or circumferential stresses $\sigma_{\theta\theta}$ are induced which act around the wellbore. The mud pressure creates radial stresses σ_{rr} which provide support for the walls of the wellbore. As σ_{rr} increases, the induced hoop stresses decrease and may

become negative resulting in rock failure in tension, i.e. wellbore burst. A third stress σ_{zz}, longitudinal stress acts along the axis of the wellbore.

Hence at any point near the wellbore there will be three induced stresses $\sigma_{\theta\theta}$,σ_{rr} and σ_{zz}. Theses stresses are mutually perpendicular to each other at any point within the vicinity of the wellbore as shown in fig 4.4a below, the rock core is subjected to

- A high axial stress $\sigma_{\theta\theta}$
- A confining pressure provided by the longitudinal stress, σ_z
- A second confining pressure provided by wellbore pressure, σ_r

As we move away from the wellbore, the induced stresses will revert back to the in situ stresses. In drilling, wellbore stability is influenced by the stresses around and near the wellbore.

The expression for $\sigma_{\theta\theta}$ (hoop stress) depends on the wellbore pressure (Pw). At high wellbore pressure, the tangential stresses goes into tension resulting in axial fractures. In fact if the minimum effective $\sigma_{\theta\theta}$ (at angle = 180 deg) was set to zero, then equation below for tensile failure will be obtained.

$$T=\sigma_2 - 3\sigma_3 + P_f + P_w$$

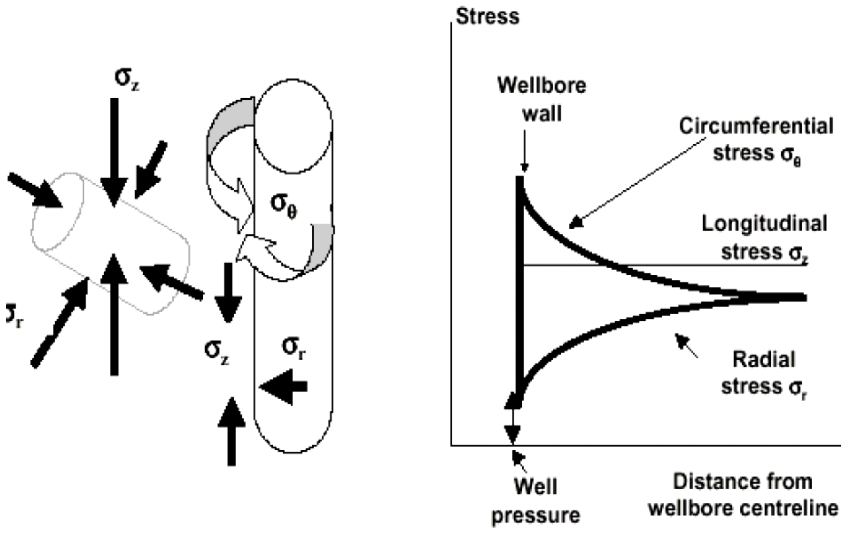

Fig 4.4a Stress distribution around the wellbore

At low wellbore pressure, the tangential stress is high and if the difference between $\sigma\theta$ and σr (i.e. deviatoric stress $\sigma 1 - \sigma 3$) in some areas around the wellbore is large enough then shear failure will occur. This failure is known as borehole collapse. The zone surrounding the wellbore which undergoes collapse failure is known as the yield zone or plastic zone. The plastic zone will not be circular, but may be ellipse or may be limited to small failure zone on each side of the well due to the variation of wellbore stresses around the wellbore.

The type of wellbore collapse depends on the type of rock being drilled. For elastic rocks such as soft shale, the failed material remains intact and would extend slightly into the wellbore (partial closure causing tight hole) or in some cases complete closure. For brittle rocks such as brittle shales, wellbore collapse manifest itself in the form of wellbore enlargement where rocks break away from the walls of the hole. In some soft sandstones, rock failure occurs as sand production and the individual sand grains are effectively being produced into the wellbore.

4.9 STRESS TRANSFORMATION FOR DEVIATED WELLS

The stability of the wellbore depends on the magnitude of the induced stresses due to the creation of the borehole. For a vertical well, the induced stresses can be easily calculated using the equation presented in Formula Set 2. The stresses induced are transformed into principal stresses and are compared with a failure criterion to determine the minimum mud weight required to prevent hole collapse.

However, for inclined and horizontal wells, the in-situ earth stresses must first be transformed into axes aligned with the wellbore before one can calculate the induced stresses. The in-situ principal stresses are first transposed relative to a co-ordinate system with one of the axes parallel to the borehole axis, and one in the horizontal plane. The process of transforming stresses is as follows.

1. Transform the in-situ stresses to stresses aligned with the wellbore using the equations in Formula Set 3 and shown in figure 4.4b This process transforms the stresses from a global system to wellbore coordinates. The stresses σ1, σ2, σ3 in Formula Set 3 are the in-situ earth principal stresses. Angle α is the hole inclination of the well from the vertical. The angle β is the horizontal angle (azimuth) between the wellbore and σ3.
2. Calculate the induced stresses due to the creation of the wellbore using the equations in Formula Set 2 and shown in figure 4.4b shows the angle where these stresses are measured from. The stresses σθθ, σrr, σzz vary with the position around the wellbore. The angle θ takes any value from 0-90, corresponding to different points on the well circumference, Figure 4.7 b. Hence the equations in Formula Set 2 do not provide a unique solution as they vary with angle θ and distance from the wellbore wall.
3. At the wellbore walls, the equations in Formula Set 2 are reduced to the equation in Formula Set 4. Note that σx, σy, σz depend on hole inclination, azimuth and on the magnitude of σ1,σ2,σ3.
4. The equations in Formula Set 4 give maximum stresses when cos 2θ = 1, or when θ = 0
5. In Formula Set 4, only σrr is a principal stress since τrz and τrθ are zero. Both σθθ and σzz have shear stresses (τθz) associated with them. Hence we need to find the principal stresses associated with σθθ and σzz. This is done as follows:

Formula Set 3: Stresses around an Inclined Well

$$\sigma_x = \sigma_2 \sin^2 \beta + \sigma_3 \cos^2 \beta$$
$$\sigma_y = \cos^2 \alpha \left(\sigma_2 \cos^2 \beta + \sigma_3 \sin^2 \beta\right) + \sigma_1 \sin^2 \alpha$$
$$\sigma_z = \sin^2 \alpha \left(\sigma_2 \cos^2 \beta + \sigma_3 \sin^2 \beta\right) + \sigma_1 \cos^2 \alpha \qquad 4.14$$
$$\tau_{xy} = \cos \alpha \sin \beta \cos \beta \left(\sigma_2 - \sigma_3\right)$$
$$\tau_{xy} = \sin \alpha \cos \alpha \left(\sigma_1 - \sigma_2 \cos^2 \beta - \sigma_3 \sin^2 \beta\right)$$
$$\tau_{zx} = \sin \alpha \sin \cos \beta \left(\sigma_3 - \sigma_2\right)$$

Formula Set 4: Stress at the wellbore walls

$$\sigma_{rr} = P_w$$

$$\sigma_{\theta\theta} = (\sigma_x + \sigma_y) - P_w - 2(\sigma_x - \sigma_y)\cos 2\theta$$

$$\sigma_{zz} = \sigma_z - \nu\{2(\sigma_x - \sigma_y)\}\cos 2\theta \qquad 4.15$$

$$\tau_{r\theta} = 0$$

$$\tau_{\theta z} = \tau_{yz}\cos\theta$$

$$\tau_{zr} = 0$$

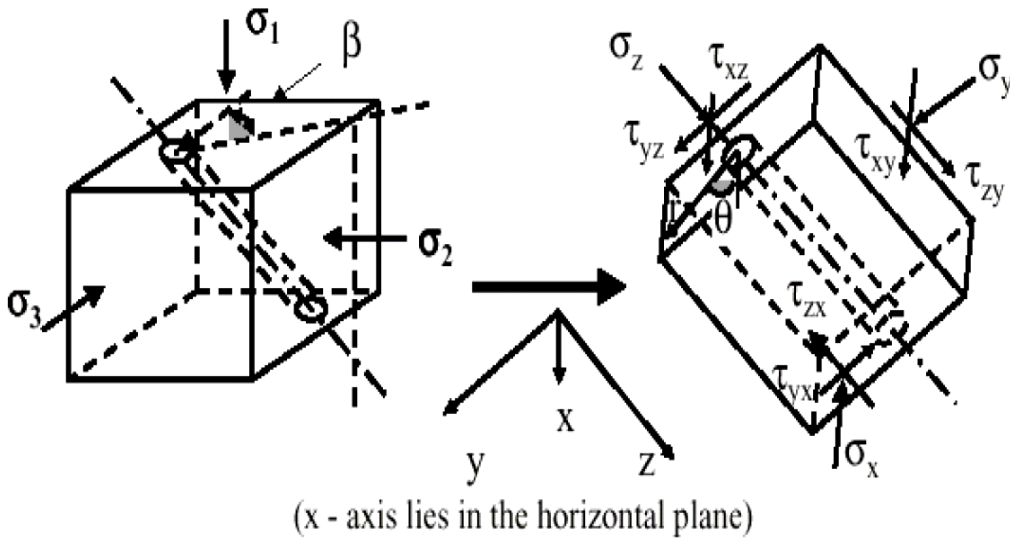

Figure 4.4b Stress Transformation

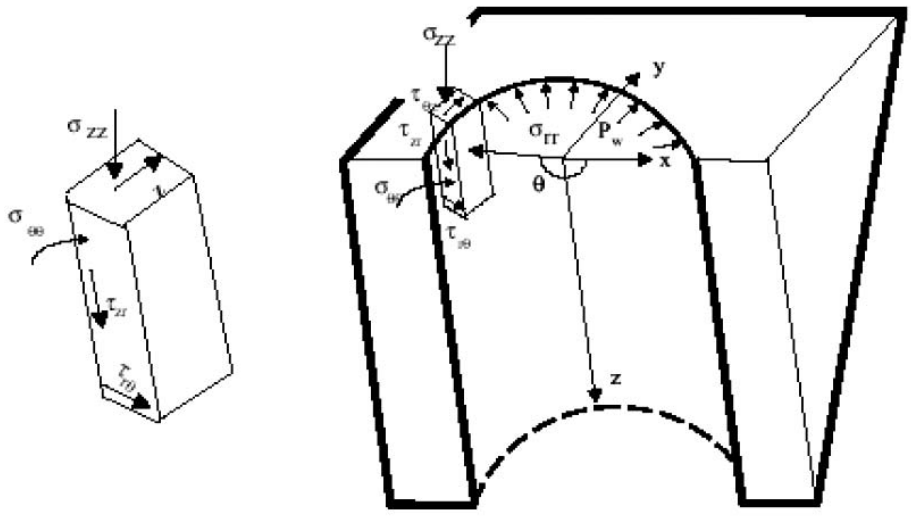

Figure 4.5 Stresses around Wellbore

The two principal stresses can be calculated by referring to Mohr's circle, centred at ½ (σθθ + σzz) and with a radius of

$$\left\{\left[\frac{\sigma_{\theta\theta}-\sigma_{zz}}{2}\right]^2+\tau_{\theta z}{}^2\right\}$$

Hence the three principal stresses are given by equation shown below

$$\left\{\begin{array}{l}\dfrac{\sigma_{\theta\theta}+\sigma_{zz}}{2}+\left\{\left[\dfrac{\sigma_{\theta\theta}-\sigma_{zz}}{2}\right]^2+\tau_{\theta z}{}^2\right\}^{0.5}\\ \dfrac{\sigma_{\theta\theta}+\sigma_{zz}}{2}-\left\{\left[\dfrac{\sigma_{\theta\theta}-\sigma_{zz}}{2}\right]^2+\tau_{\theta z}{}^2\right\}^{0.5}\\ P_w\end{array}\right\}$$

The above transformation to principal stresses is necessary before theses stresses are used in the failure criteria. The induced principal stresses in equations shown above at the walls of the borehole should then be arranged in ranking order:

σ1 (maximum) = psi

σ2 (intermediate) = psi

σ3 (minimum) = psi

4.10 VERTICAL WELLBORE

In order to determine the stresses at wall of a vertical borehole, we set the inclination angle $i = 0$ in Eq. (4.12). For simplicity, we orient the horizontal axes so that the direction $\theta = 0$ is parallel to σ_H (*i.e.*, $\alpha = 0$), as shown in Figure 4.9. Consequently, the stresses become:

$$\sigma_r = P_w,$$

$$\sigma_\theta = \sigma_H + \sigma_h - 2(\sigma_H - \sigma_h)\cos 2\theta - P_w,$$

$$\sigma_z = \sigma_v - 2\nu(\sigma_H - \sigma_h)\cos 2\theta,$$

$$\sigma_{\theta z} = 0,$$

$$\sigma_{r\theta} = 0,$$

$$\sigma_{rz} = 0.$$

4.16

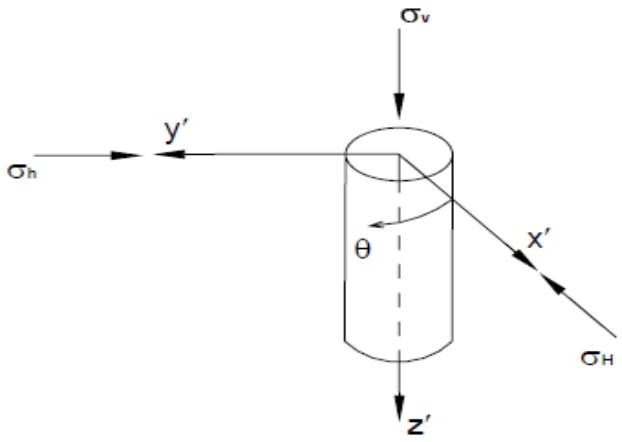

Figure 4.6. Stress transformation system for a vertical borehole

4.11 HORIZONTAL WELLBORE

To estimate the stresses at the wall of a horizontal borehole, we put i = π/2 in Eq. (4.12), which gives

$$\sigma_x^o = \sigma_v,$$

$$\sigma_y^o = \sigma_H \sin^2\alpha + \sigma_h \cos^2\alpha,$$

$$\sigma_z^o = \sigma_H \cos^2\alpha + \sigma_h \sin^2\alpha,$$

4.17

$$\sigma_{xy}^o = 0,$$

$$\sigma_{yz}^o = 0.5(\sigma_h - \sigma_H)\sin 2\alpha,$$

$$\sigma_{xz}^o = 0.$$

Introducing Eq. (4.16) into Eq. (4.14), the stresses at borehole wall will be

$$\sigma_r = P_w,$$
$$\sigma_\theta = \left(\sigma_v + \sigma_H \sin^2\alpha + \sigma_h \cos^2\alpha\right) - 2\left(\sigma_v - \sigma_H \sin^2\alpha - \sigma_h \cos^2\alpha\right)\cos 2\theta - P_w,$$
$$\sigma_z = \sigma_H \cos^2\alpha + \sigma_h \sin^2\alpha - 2\nu\left(\sigma_v - \sigma_H \sin^2\alpha - \sigma_h \cos^2\alpha\right)\cos 2\theta, \qquad 4.18$$
$$\sigma_{\theta z} = (\sigma_h - \sigma_H)\sin 2\alpha \cos\theta,$$
$$\sigma_{r\theta} = 0,$$
$$\sigma_{rz} = 0.$$

Figure 4.7 illustrates the stress transformation system corresponding to a horizontal wellbore. In this configuration, notice that the angle θ is measured anticlockwise from the *x*-axis.

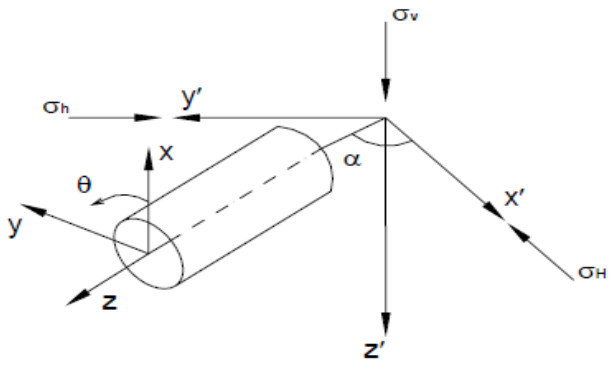

Figure 4.7 Stress transformation system for a horizontal borehole.

For the case in which the wellbore axis lies along the maximum horizontal principal stress (*i.e.,* α = *0*), the stresses at borehole wall are:

$$\sigma_r = P_w,$$
$$\sigma_\theta = \sigma_v + \sigma_h - 2\left(\sigma_v - \sigma_h\right)\cos 2\theta - P_w,$$
$$\sigma_z = \sigma_H - 2\nu\left(\sigma_v - \sigma_h\right)\cos 2\theta, \qquad 4.19$$
$$\sigma_{\theta z} = 0,$$
$$\sigma_{r\theta} = 0,$$
$$\sigma_{rz} = 0,$$

4.12 ROCK FAILURE

Understanding the fundamental principles of rock failure in compression, tension and shear is very important in establishing the rock failure criteria.

If a rigid body is subjected to normal stresses as shown in Figure 4.8, then these stresses will generate both shear and normal stresses within the body. An imaginary plane at angle θ to stress σ1 will have a normal stress σ and a shear stress τ acting on it. The normal stress pushes the surface of the plane together. The induced shear stress τ tends to cause the surfaces of this imaginary plane to slide relative to each other.

If the induced shear stress is greater than the rock's inherent shear strength then the rock will fail in shear. Conjugate shear planes at angle θ to σ1 can occur throughout the rock. If these failures surfaces connect then massive failure occurs. Shear failure occurs on a surface inclined at angle θ to σ1. On Mohr's circle, this angle plots as 2θ.

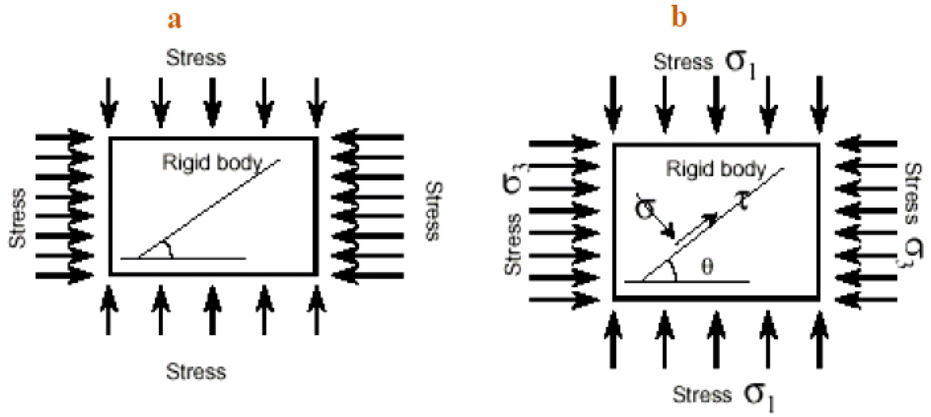

Figure 4.8 Stresses in a Rigid Body

If rock cores are tested in a triaxial testing machine (Figure 4.9) where axial stress (σ1) is applied in one direction and a confining stress (σ3), then by varying the magnitude of the confining pressure the rock will fail in shear at different values of σ1.

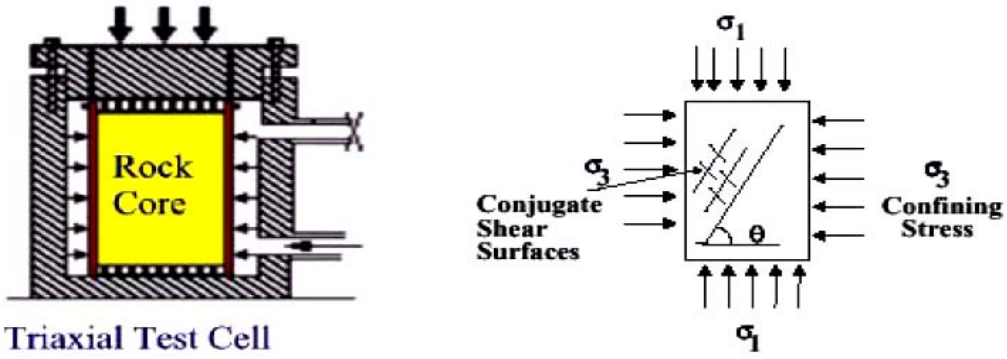

Figure 4.9 Triaxial Rock Testing

A convenient way of describing rock failure is to produce a Mohr plot where shear stress is plotted against principal stress. In practice, the shear stress is not measured, only the applied stresses σ1,σ3 are measured.

The principal stresses (σ1 and σ3) are plotted on the horizontal axis as shown in Figure 4.10. A circle is then drawn through these values with a diameter equal to (σ1 - σ3) and centre equal to ½ (σ1 + σ3). The vertical axis becomes automatically the shear stress.

4.12.1 Failure Envelope

A tangent to this circle is then drawn which represents the failure envelope. This tangent can be linear or a curve. The rock is stable below this envelope. The rock can not exist above this envelope as the combination of shear and principal stresses above this envelope result in rock failure.

The Mohr envelope describes shear failure in rocks. Shear failure occurs if the difference between the effective stress in one direction is much greater the effective stress acting at right angles to it. Shear failure also occurs if the pore pressure reduces by a large amount (i.e. more effective stress or if one of the acting stresses become significantly large). This can be easily seen with reference to Mohr circle.

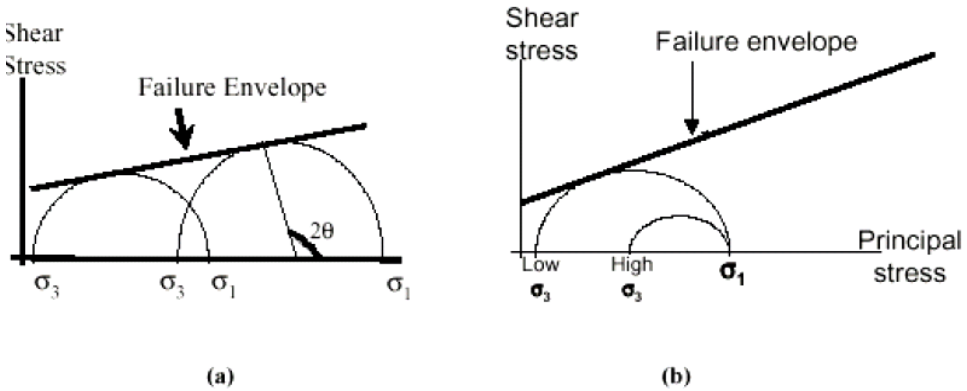

Figure 4.10 Mohr Envelope

Thus results in large shear stresses developing within the rock which if exceed the rock inherent shear strength would result in shear failure. A tangent to this circle is then drawn which represents the failure envelope. This tangent can be linear or a curve. The rock is stable below this envelope. The rock cannot exist above this envelope as the combination of shear and principal stresses above this envelope result in rock failure.

4.12.2 Effects of Pore Pressure on Wellbore Failure

In the oilfields, the majorities of rocks we encounter are porous and contain some pore fluid. Because of this a modified term is used to describe rock failure is known as effective stress. Shear failure can occur when one of the applied stresses become sufficiently large or the effective stress in one direction becomes significantly larger than the effective stress at right angles to it. This situation induces a shear stress which is greater than the inherent shear strength of the rock causing failure by sliding of rock surfaces.

The pore pressure helps to support part of the overburden stress and also resists any lateral loading as may be seen in fracturing operations. Without the pore pressure, the rock matrix transmits the applied loads through grain contacts and the cementing material throughout the rock which is being stressed.

In porous rocks, if the applied stress is sufficiently large, rock failure may occur by Pore Pressure around localized areas near the wellbore due to

crushing of rock grains. Hence it is seen that rock failure will be controlled by the applied stress and by changes in pore pressure. In a depleted reservoir, therefore, the fracture pressure will be less than before depletion as there is less pore pressure to provide support against fracturing pressures.

The effect of pore pressure on the failure envelope is to move the failure circle to the left if the pore pressure increases and to the right if it decreases, as shown in Figure 4.11. A reduction in pore pressure results in an increase in the effective stress acting on grain boundaries. While shear failure may be prevented by reduction of pore pressure, the resulting effective stress may be large enough to crush the rock and cause pore collapse.

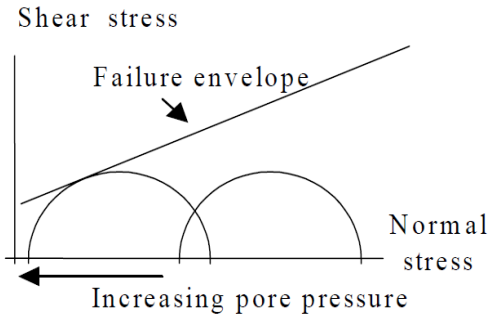

Figure 4.11 Effect of Pore Pressure on Wellbore Failure

If the rock confinement around the wellbore is increased by increasing the wellbore pressure (with pore pressure constant) then shear failure can be inhibited or prevented. This is clearly seen where σ3 increases towards the right. The circle height will reduce and fall below the failure envelope. This is the basis for preventing brittle shale failure by increasing the mud weight. With the exception of a few rocks, most porous rock become stronger as the confining pressure σ3 is increased.

4.12.3 Rock Failure under Compression

The borehole fails in compression when the pressure of the drilling mud is insufficient to keep the shear stresses in the borehole wall below the shear strength of the formation. When the borehole fails in compression, broken

rock falls into the borehole and the borehole diameter increases at the point of failure. Both the increase in borehole diameter and the volume of rock debris falling into the borehole sometimes make it difficult or impossible to move drilling equipment into or out of the borehole. Certain rock types, such as salt, creep rather than fail when compressed and may close around equipment in the borehole or reduce borehole diameter, again making it difficult or impossible to move drilling equipment into or out of the hole.

4.12.4 Rock Failure under Tension

The borehole fails in tension when the pressure exerted by the drilling mud induces stresses in the borehole wall that exceed the tensile strength of the rock. The failure takes the form of cracks, typically starting from the borehole wall and running radially into the formation. Drilling mud may then penetrate and propagate these cracks, leading to a fall in mud level in the borehole. If this continues, the borehole stability will eventually be restored by the resulting reduction in the hydrostatic loading of the hole at depth.

The wellbore pressure required to fracture (burst) the wellbore walls for any given hole angle may be derived from the equation given for $\sigma_{\theta\theta}$ by setting the effective stress to zero. Remember the effective stress is the total stress minus the pore pressure. We shall call this wellbore pressure as the formation breakdown gradient (FBG) to distinguish it from the fracture gradient which is related to overcoming the earth horizontal stress component. The failure envelope for any given mud weight may be determined for a series of hole angles.

4.13 FAILURE CRITERIA

A rock failure criterion is required to predict whether the rock is going to fail or not depending on the applied stresses. Our aim in the oil industry is to prevent rock failure around the wellbore. The discussion below applies to shear failure.

Failure criteria were originally developed for solid masses containing no pore pressure. Most rocks encountered in the oil industry contain pore pressure, hence for rocks with a connected system of pores, failure is controlled by the effective stress, where:

Effective stress, $\sigma' = \sigma - P_f$

We shall examine two failure criteria which are widely used in the oil industry: Mohr- Coulomb and Druker-Prager criteria.

4.13.1 Mohr-Coulomb Criterion

The failure criterion states that the shear stress across a plane is resisted by the material cohesion (C) and normal stress (σ') such that:

$$|\tau| = C + \sigma' \tan \varnothing$$

In terms of the principal effective stresses, the failure criterion is:

$$2C = \sigma'_1 \left[\left(\tan^2 \phi + 1 \right)^{1/2} - \tan \phi \right] - \sigma'_3 \left[\left(\tan^2 \phi + 1 \right)^{1/2} + \tan \phi \right]$$

Extrapolation of the failure envelope to a zero value of shear stress gives a predicted value of the uni-axial tensile strength. Experimentally determined strengths are usually less than predicted values, and a tensile cut-off is typically applied.

The criterion is shown graphically in Figure 4.12. The plot in Figure 4.12b is very useful as it will be utilised later to establish wellbore stability. Simply stated, for a given rock a Mohr- Coulomb envelop is established as shown in Figure 4.12 b using rock properties from triaxial tests from offset wells. Then for the well under investigation, the wellbore stresses are compared with the envelope to establish rock stability.

All rocks to the right of the line in Figure 4.12 b are stable and those to the left are unstable. In practice, wellbore stresses are calculated for a range of mud weights to establish the minimum mud weight required to prevent hole collapse.

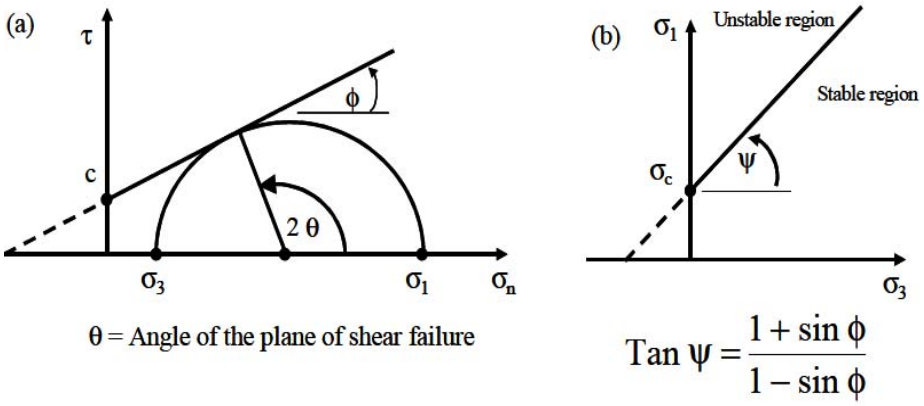

Figure 4.12 Coulomb Strength Envelopes in terms of (a) shear and normal stresses (b) Principal Stresses

Although widely used in borehole stability studies, there are drawbacks to the Mohr-Coulomb criterion. These are:

- The criterion does not take into account the intermediate principal stress, which is known to affect failure.
- It implies that a major shear fracture occurs at peak strength. Experimental work suggests that this is not always the case.
- It implies a direction of shear, relative to the major and minor principal stresses, σ1 and σ3, that is not always seen in experimental observations.
- Experimental peak strength envelopes derived using the Mohr construction ar generally non-linear. This possibly explains the poor correlation between the uni-axial tensile strength obtained by extrapolating a linear Mohr-Coulomb failure surface and that obtained by experiment.

4.13.2 Drucker-Prager Criterion

An approximation to the Mohr-Coulomb law was proposed by Drucker and Prager. The Drucker-Prager criterion is given by:

$$\gamma I_1 + (J_2)^{1/2} = K$$

Where

I1 = first invariant of stress = σx +σy +σz

J2 = second invariant of stress deviation

J2 =- (SySz + SzSx + SxSy) + Syz2Szx2+ Sxy2

$$S_x = \sigma_x - S,\ S_y = \sigma_y - S,\ S_z = \sigma_z - S$$
$$S_{yz} = \tau_{yz},\ S_{zx} = \tau_{zx},\ S_{xy} = \tau_{xy}$$
$$S = 1/3\ (\sigma_x + \sigma_y + \sigma_z)$$

γ and K vary according to where the criterion intersects the Mohr-Coulomb failure surface. The geometrical representation of the Drucker-Prager failure surface is given in Figure 4.13

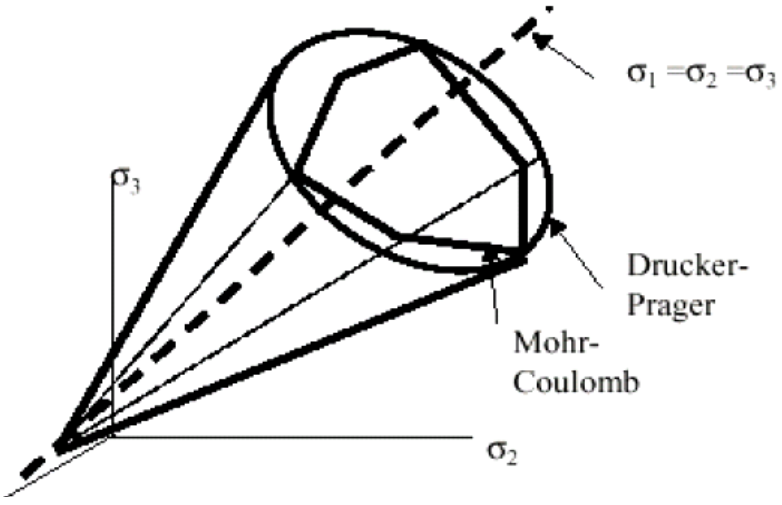

Figure 4.13 Drucker-Prager Criteria of Rock Failure

The Drucker-Prager failure criterion is sometimes expressed in terms of the octahedral shear stress, τoct, and the octahedral normal stress, σoct, where:-

$$\tau_{oct} = \frac{2J_2}{3}$$

$$\sigma_{oct} = \frac{I_1}{3}$$

Sandstone cores from the reservoir were tri-axially tested and gave the following results:

Cohesion, C = 6 MPa

Internal friction angle, φ = 43.8°

Poisson's Ratio = 0.2

The major principal stress, σ1, is considered to be vertical and equal the overburden stress. The overburden stress gradient is 1 psi/ft and the reservoir depth is 8530 ft. The intermediate and minor principal stresses are considered horizontal and equal to each other. No direct measurements of the horizontal stress are available therefore an arbitrary value of 0.75 psi/ft was assumed.

The tensile strength is considered negligible and tensile failure is assumed to occur when the effective compressive stress at the borehole wall is zero.

The comparison was presented in the form of hole inclination vs. safe mud weight for the four criteria examined. The Mohr- Coulomb plot is shown in Figure 4.14. The actual mud weight used to drill the horizontal section of the Cyrus reservoir was 1.17 SG.

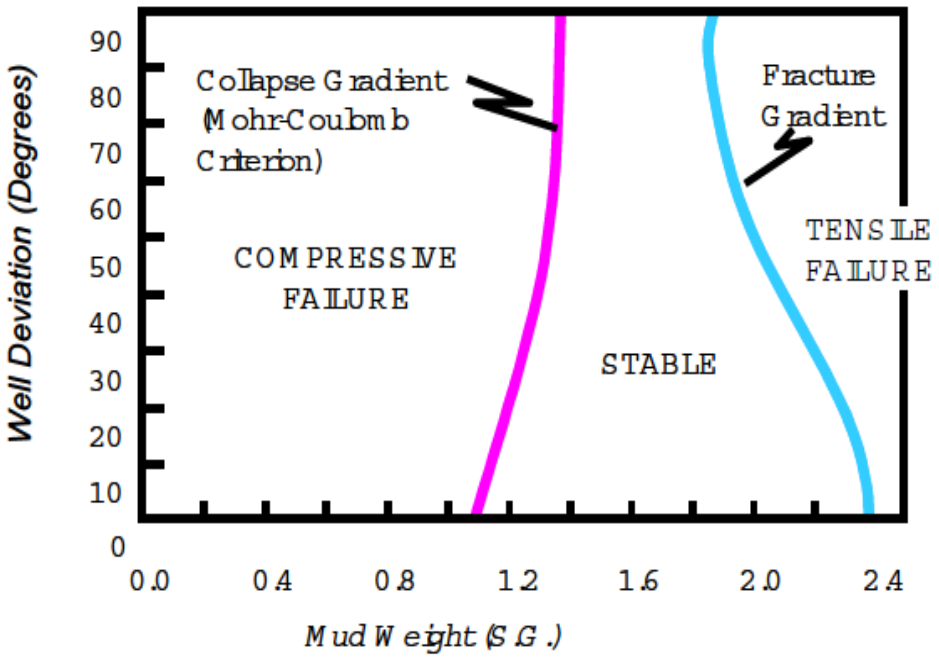

Figure 4.14 Safe Mud Weight as predicted by Mohr-Coulomb Criterion

The Mohr-Coulomb criterion circumscribing the inner apices of the Mohr-Coulomb plot and that inscribing the Mohr-Coulomb plot all recommend minimum mud weights significantly higher than this. Mohr-Coulomb plot predicts that 1.17 SG is within a safe mud weight range (Figure 4.14), implying it is the best criterion to use. However, this criterion gives unrealistic minimum mud weight recommendations for lower borehole inclinations.

Figure 4.15 Envelope of Safe Mud Weights as predicted by Drucker-Prager Criteria , concluded that:

- When using a linear elastic analysis, the failure criteria give extreme differences in predicted minimum mud weights.
- The criteria do not give consistently realistic minimum mud weight predictions as conditions, e.g. borehole inclination, change.

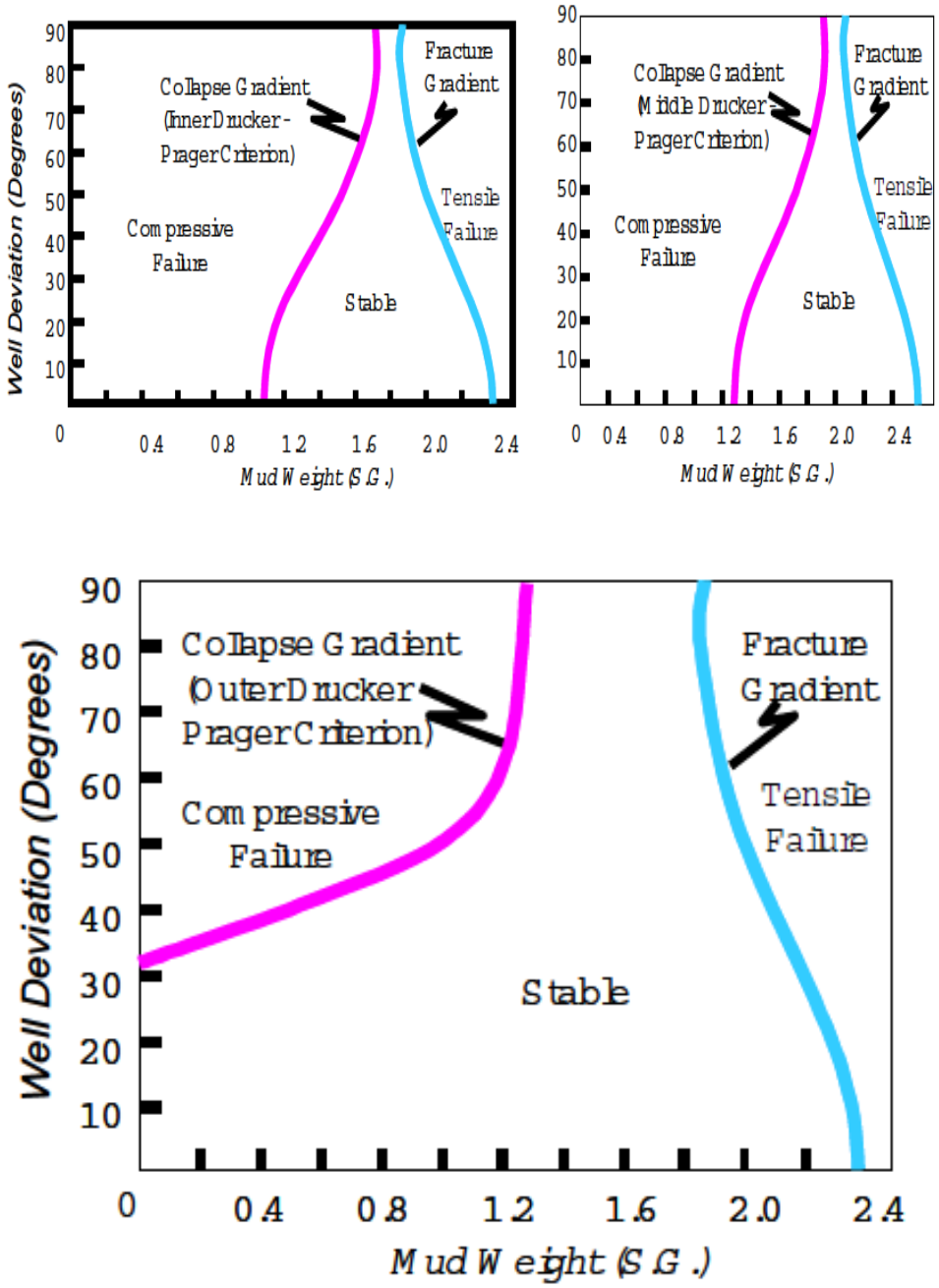

Fig 4.15

The Mohr-Coulomb criterion is recommended as the most realistic due to its good fit to experimental data. However, it is recognized that a Mohr-Coulomb failure criterion, coupled with linear elasticity, does not always give reliable predictions of minimum mud weights used in practice.

Linear Elastic Analysis coupled with any of the failure criteria studied is considered a useful qualitative tool for studying borehole instability problems .By using the wellbore data to determine the safe mud weight window which gives an in-depth idea to construct Mud Weight vs Well Deviation Plot .This work is done in the chapter 7th employing the use of C-Programming.

4.13.3 Hoek-Brown Criterion

Laboratory results of triaxial tests on rocks often show a curved strength envelope (Hoek and Brown, 1980; Hoek, 1983). Various researchers have therefore proposed non-linear criteria, based on laboratory investigations (Sheorey, 1997). The most representative and commonly used one is the Hoek-Brown criterion (Bieniawski, 1996; Hoek and Brown, 1997; Sheorey, 1997). This criterion was originally developed for estimating the strength of rock masses for application to excavation design. Hoek and Brown (1980) proposed that at failure the relationship between the maximum and minimum principal stresses is given by

$$\sigma_1 = \sigma_3 + \sqrt{m C_0 \sigma_3 + s C_0^2},$$

where m and s are material constants, s takes the value 1 for intact rock, and less than unity for disturbed rock (Hoek and Brown, 1997). The values for m are different from rock to rock, with a range between about 1.4 and 40.7 (Sheorey, 1997).

Chapter 5
METHODS TO DETERMINE HORIZONTAL INSITU STRESSES

5.1 DETERMINING S_{hmin} FROM LEAK-OFF TEST

One can also determine the least principal stress from a leak-off test: after the casing has been cemented in place at a given depth and the well is drilled a short distance (usually 10–20 ft) the open section of the well is pressurized to the point that a hydraulic fracture is created, and the magnitude of the least principal stress can be determined.

When leak-off tests are carried out fully, they are referred to as extended leak-off tests. When significant mud losses are noted during drilling, it can denote the accidental hydraulic fracturing of a well, requiring that the mud weight be reduced to a value less than the least principal stress, or frac-gradient. Finally, wellbore ballooning noted during logging-while-drilling (LWD) operations indicate that the wellbore pressure is very close to the least principal stress.

5.2 COULD S_{Hmax} BE DETERMINED DIRECTLY?

In many problems encountered in geomechanics, knowledge of the magnitude of the maximum horizontal principal stress at depth, SHmax, is especially important. For example, an accurate determination of SHmax is usually very important in problems related to wellbore stability such as the determination of optimal mud weights, well trajectories, casing set points

Despite the importance of the determination of SHmax in geomechanics, it has long been recognized that this is the most difficult component of the stress tensor to accurately estimate, particularly as it cannot be measured directly.[27]

The widespread use of wellbore imaging devices has been an important development that has made possible the application of the techniques for estimating SHmax.

5.3 THEORY BEHIND HYDRAULIC FRACTURING

Hubbert and Willis (1957) presented a compelling physical argument that hydraulic fractures in the earth will always propagate perpendicular to the orientation of the least principal stress, S3. Because the work done to open a Mode I fracture a given amount is proportional to the product of the stress acting perpendicular to the fracture plane times the amount of opening (i.e. work is equal to force times distance), hydraulic fractures will always propagate perpendicular to the least principal stress because it is the least energy configuration. They confirmed this with simple sand-box laboratory tests (Figure 5.1) and pointed out that igneous dike propagation is also controlled by the orientation of the least principal stress.

5.4 FRACTURE PROPAGATION IN VARIOUS FAULTING ENVIRONMENTS

This fundamental point is the basis for using hydraulic fracturing to measure the magnitude of the least principal stress as discussed below. In strike-slip and normal faulting environments where S3 ≡ Shmin, hydraulic fracture (and dike) propagation will be in a vertical plane perpendicular to Shmin (and parallel to SHmax). In reverse faulting environments where S3 ≡ Sv, hydraulic fracture propagation will be in a horizontal plane. At the time that the Hubbert and Willis (1957) paper was written, their arguments put to rest a great deal of argument and debate over whether hydraulic fractures in oil wells and gas were propagating in vertical or horizontal planes and whether they were following pre-existing fractures and faults.

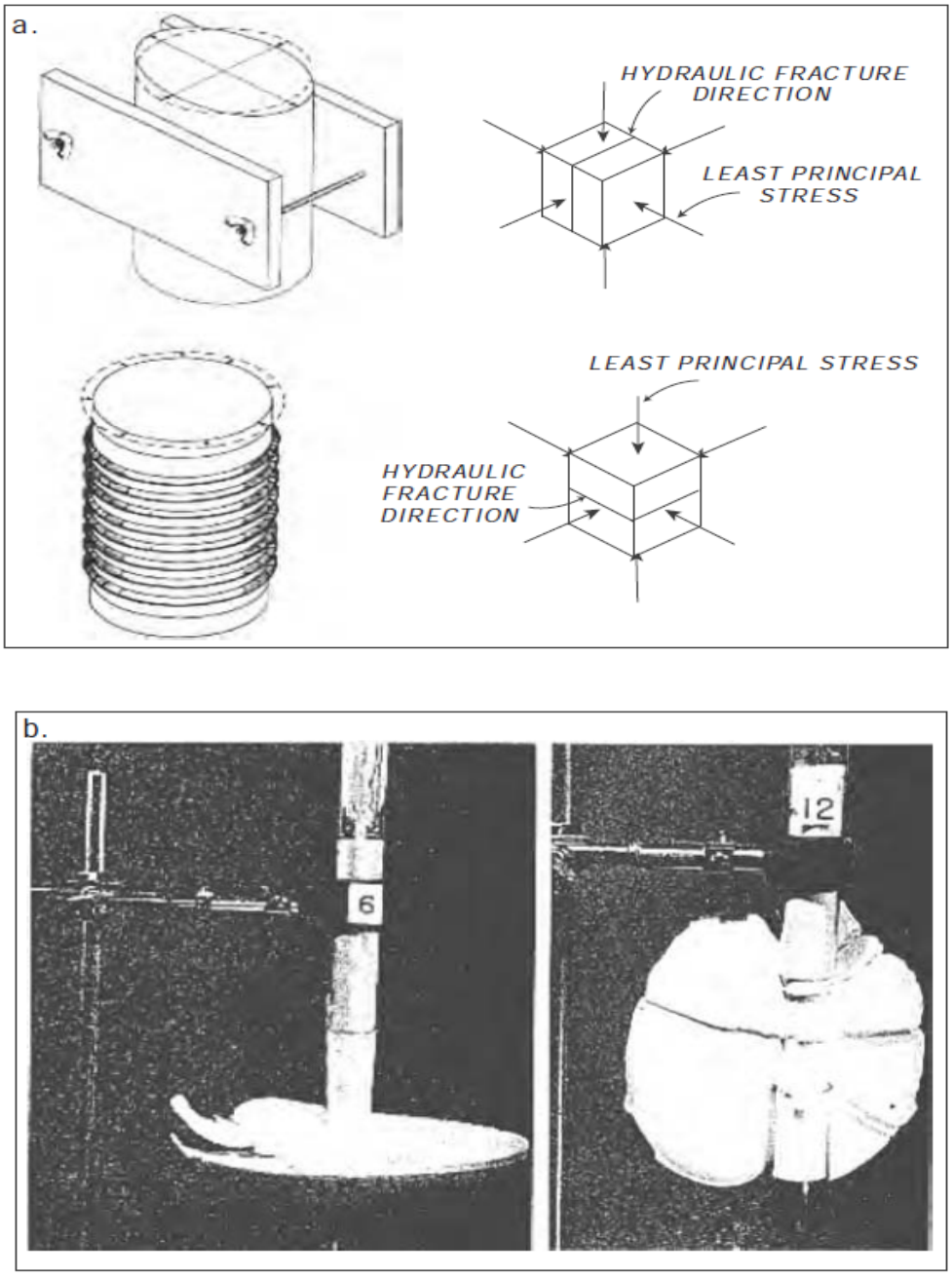

Figure 5.1. Schematic diagram of the laboratory sand-box experiments that illustrated that hydraulic fractures will propagate perpendicular to the orientation of the least principal stress. The photographs illustrate hydrofracs made with plaster of Paris as a frac fluid in a stressed container of unconsolidated sand. From Hubbert and Willis (1957). C1957 Society Petroleum Engineers

Dike studies and hydrofrac mine-back experiments (Warren and Smith 1985) have shown that while pre-existing fractures and faults have some influence on fracture propagation, the overall trajectory of fracture propagation is controlled by the orientation of the least principal stress.

The other issue addressed by Hubbert and Willis (1957) is the manner of hydraulic fracture initiation at the wellbore wall. They were the first to note that a tensile wall fracture will be induced when equation below

$$\sigma_{\theta\theta}^{\min} = 3S_{\text{hmin}} - S_{\text{Hmax}} - 2P_0 - \Delta P - \sigma^{\Delta T}$$

equals −T0, the tensile strength of the rock. Because T0 ~ 0, a tensile fracture

will form at the wellbore wall when the hoop stress goes into tension, as in the formation of a drilling-induced tensile fracture.

5.5 DIFFERENCE BETWEEN DRILLING INDUCED FRACTURE AND HYDRAULIC FRACTURE

What distinguishes a drilling-induced tensile fracture from a hydraulic fracture is the fact that during hydraulic fracturing, the fluid pressure in the wellbore is above the magnitude of the least principal stress so that the fracture will propagate away from the wellbore. In some cases, the wellbore pressure required to initiate a tensile fracture is greater than the least principal stress so that the pressure drops after fracture initiation. In other cases, the fracture initiation pressure is significantly lower than the least principal stress such that the wellbore pressure slowly climbs to the value of the least principal stress after a tensile fracture initiates at the wellbore wall (see Hickman and Zoback 1983). This point should now be obvious in the context of the formation of drilling-induced tensile fractures. It is obvious that if the interval

being hydraulically fractured already has drilling-induced tensile fractures present, no additional pressurization is needed to initiate them.

5.6 XLOT

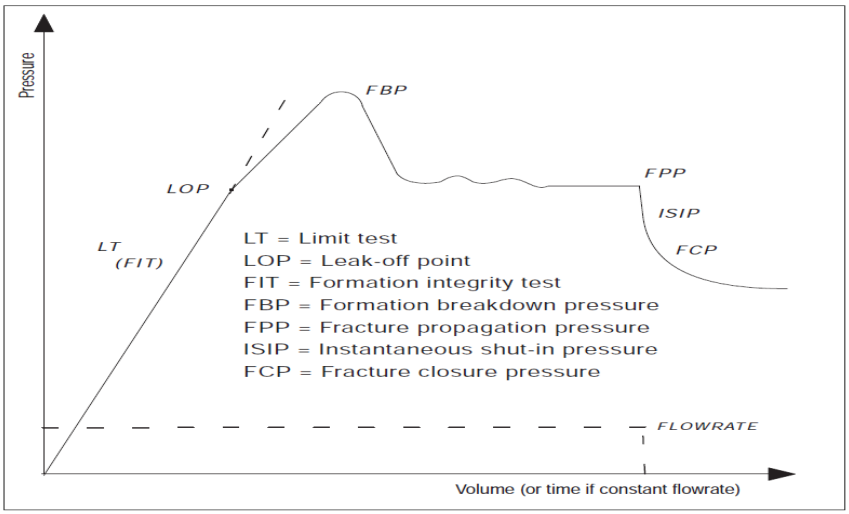

Figure 5.2. A schematic mini-frac or extended leak-off test showing pressure as a function of volume, or equivalently time (if the flow rate is constant). Modified after Gaarenstroom, Trompet al. (1993). The significance of the various points indicated on the pressure record is discussed inthe text.

In the schematic example shown in Figure 5.2, the pumping rate into the well is constant. Thus, the pressure should increase linearly with time as the volume of the wellbore is fixed. At the pressure where there is a distinct departure from a linear increase of wellbore pressure with time (referred to as the LOP, the leak-off point) a hydraulic fracture must have formed. The reason for this is that there cannot be a noticeable decrease in the rate of wellbore pressurization unless there is a significant increase in the volume of the system into which the injection is occurring.

In other words, the pressure in the wellbore must be sufficient to propagate the fracture far enough from the wellbore to increase system volume enough to affect the rate of wellbore pressurization. Thus, there must be a hydraulic fracture propagating away from the wellbore, perpendicular to the least principal stress in the near-wellbore region, once there is a noticeable change in the pressurization rate. Thus, a clear LOP (a distinct break-in-slope) is approximately equal to the least principal stress (as shown in Figure 5.2) although the wellbore pressure may also reflect some near-wellbore resistance to fracture propagation. If the hydrofrac is being made through perforations in a cased and cemented wellbore (as is the case in mini- or micro-fracs), the tortuosity of the perforation/fracture system may cause the pressure to increase in the wellbore above the least principal stress. The same is true if the injection rate is high or if a relatively high viscosity fluid is used.

It should be noted that Figure 5.2 represents pressure at the surface during a mini-frac or LOT (note that the pressure is zero at the beginning of the test). To determine the magnitude of the least principal stress at the depth of the test, it is necessary to add the pressure in the wellbore due to the column of wellbore fluid. In fact, it is always preferable to measure pressure downhole during such tests.

If the LOP is not reached, a limit test, or formation integrity test (LT, or FIT), is said to have been conducted. Such tests merely indicate that at the maximum pressure achieved, the fluid pressure did not propagate away from the wellbore wall, either because the maximum wellbore pressure did not exceed the least principal stress or was not sufficient to initiate a fracture of the wellbore wall in the case of an open-hole test. The peak pressure reached during a LOT or mini-frac is termed the formation breakdown pressure (FBP) and represents the pressure at which unstable fracture propagation away from a wellbore occurs (fluid flows into the fracture faster from the wellbore than the pump supplies it; hence the pressure drops). The difference between the LOP and FBP is a complex function of the conditions immediately

surrounding the well (especially when a frac is being initiated through perforations).

If pumping continues at a constant rate, the pumping pressure will drop after the FBP to a relatively constant value called the fracture propagation pressure (FPP). This is the pressure associated with propagating the fracture away from the well. In the absence of appreciable near-wellbore resistance mentioned above (i.e. if the flow rate and fluid viscosity are low enough), the FPP is very close to the least principal stress (e.g. Hickman and Zoback 1983). Hence, the FPP and LOP values should be similar. It should be emphasized that a distinct FBP need not be present in a reliable mini-frac or XLOT. This correspondence between the LOP and FPP is the reason why, in typical oil-field practice, leak-off tests are taken only to the LOP, rather than performing a complete, extended leak-off test.

5.7 IMPORTANT FEATURES ABOUT S_{hmin}

There are three important features to note about the least principal stress values at depth. First, the measurements are repeatable and indicate a consistent trend throughout the field. Second, the measurements clearly indicate a compressional stress state because even at relatively shallow depth (where pore pressure is hydrostatic), the magnitude of the least principal stress is extremely close to the vertical stress. We show below that the magnitude of SHmax is greater than Sv such that a strike-slip faulting regime exists in this region. However, because Shmin is extremely close to Sv if the magnitude of Sv was slightly over-estimated (due to uncertainties in density), or if S3 is slightly higher than the values shown (if the measurements were not carefully made), it might be the case that S3 would appear to be equal to Sv such that a reverse-faulting regime would be indicated. As noted above, if S3 ≡ Shmin, vertical hydrofracs would be initiated at the wellbore wall. However, if S3 ≡ Sv, vertical fractures would be expected to form at the wellbore wall (when the increase in wellbore pressure causes $\sigma\theta\theta$ to go into tension).However, the hydraulic fracture will rotate into a horizontal plane (perpendicular to Sv) as

the fracture propagates away from the wellbore (Baumg¨artner and Zoback 1989).

After fracture propagation away from the wellbore, the FPP or ISIP can be used to determine S3. In cases where S3 ~ Sv it is particularly important to carefully integrate density logs to determine Sv and to determine if S3 corresponds to Sv or Shmin with confidence. In fact, in the Visund field, considerable effort was taken to estimate rock density at extremely shallow depth to derive the curve shown.

5.8 FIELD REQUIREMENTS FOR S_{hmin}

When trying to analyze such tests, two questions must be kept in mind to know whether the test can be used to obtain a measure of the least principal stress. First, is there an indication that the LOP was reached? If so, the LOP can be considered an approximate measure of the least principal stress. If not, then the test must be considered a FIT and the maximum pressure achieved cannot be used to estimate the least principal stress. Second, was a stable FPP achieved? If so, the fracture clearly propagated away from the well and the shut-in pressure is likely a good measure of S3. While these two questions are straightforwardly answered when there is a good record of the test, it is sometimes necessary to rely on a single reported value, not knowing whether it refers to a reasonable estimate of the least principal stress. In fact, in some cases the pressure–time record is approximated by a few distinct data points only, obtained by reading pressure on a fluctuating gauge and estimating flow rate by counting pump strokes.

In such cases, determination of accurate LOT values is essentially impossible. Values of LOT's that are markedly lower than the expected trend for a given area should also be treated with extreme caution as these tests may simply

indicate a poor-quality cement job rather than an anomalously low value of the least principal stress.

Chapter 6

MODELING OF INDUCED STRESS CONDITION TO PREDICT WELLBORE STABILITY

6.1 BACKGROUND TO WELLBORE STABILITY MODELING

Before a well is drilled, compressive stresses exist within the rock formations. With the exception of structurally complex areas like salt diapirs the in-situ stresses can be resolved into a vertical or overburden σ_v and two horizontal stresses σ_H (maximum horizontal stress), σ_h (minimum horizontal stress) which are generally unequal. When the well is drilled, the rock stresses in the vicinity of the wellbore are redistributed as the support originally offered by the drilled out rock is replaced by the hydraulic pressure of the mud. The redistributed stresses are normally referred to as the hoop stress $\sigma_{\theta\theta}$, which acts circumferentially around the wellbore wall, the radial stress σ_{rr} and the axial stress σ_{zz}, which acts parallel to the wellbore axis. In deviated wells an additional shear component $\tau_{\theta z}$ is generated.(shown in fig 6.1)

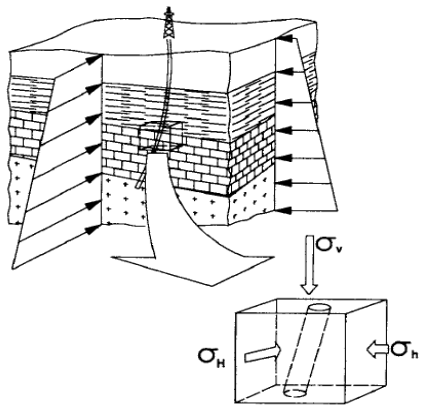

Fig 6.1 In-situ Stress Field

6.2 DETERMINATION OF BOREHOLE STRESS STATE

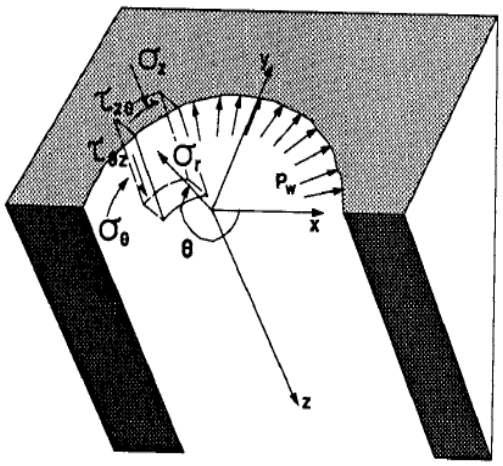

Fig 6.2 Stress state at the wall of the Deviated wellbore

The ease with which the borehole stresses can be computed is highly dependent on the stress-strain behavior chosen to model the formation response to loading. The most common behavior assumed is that formations are homogenous, isotropic and linear elastic which allows the stresses to be determined from a set of equations. In general, a linear elastic analysis is the most common approach due to its ease of application. Also, more complex models frequently suffer from an exhaustive list of input parameters, many of which cannot be realistically determined in field cases. The equations required to compute the redistributed stress state at the wellbore wall are given below. Using a linear- elastic approach the stress state at the wellbore wall will normally be the most critical.

Formula to calculate Radial, Hoop and Axial Stress at the wellbore wall

$$\sigma_{rr} = P_w$$

$$\sigma_{\theta\theta} = (\sigma_x + \sigma_y) - P_w - 2(\sigma_x - \sigma_y)cos2\,\theta - 4\tau_{xy}\,sin2\theta$$

$$\sigma_{zz} = \sigma_z - 2V\{(\sigma_x - \sigma_y)\,cos2\,\theta + 2\tau_{xy}\,sin2\theta\}$$

$$\tau_{r\theta} = 0\,;\,\tau_{\theta z} = 2\{\tau_{yz}\,cos\theta - \tau_{zx}\,sin\theta\}$$

$$\tau_{zr} = 0$$

6.3 IN-SITU STRESS TRANSPOSITION

Before determining the redistributed stress state at the wellbore wall it is necessary to transpose the in-situ stress tensor relative to a co-ordinate system with one of its axes parallel to the wellbore axis and another which lies in a horizontal plane (as shown in fig below). The transposed stress state is given as:

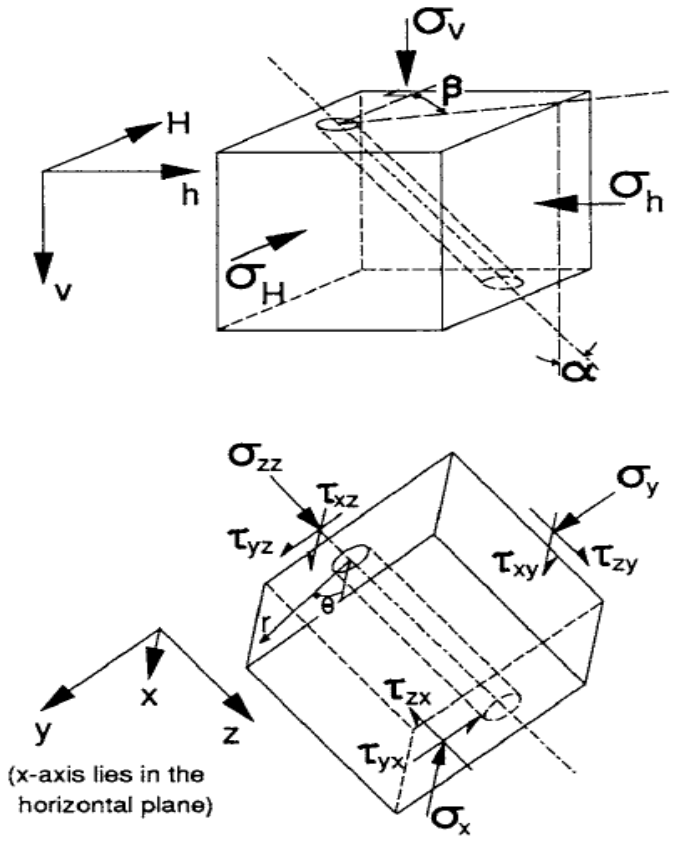

Fig 6.3 Transpose of the In-Situ Stress State

$$\sigma_x = \sigma_H \sin^2\beta + \sigma_h \cos^2\beta$$

$$\sigma_y = \cos^2\alpha\,(\sigma_H \cos^2\beta + \sigma_h \sin^2\beta) + \sigma_v \sin^2\alpha$$

$$\sigma_z = \sin^2\alpha\,(\sigma_H \cos^2\beta + \sigma_h \sin^2\beta) + \sigma_v \cos^2\alpha$$

$$\tau_{xy} = \cos\alpha \sin\beta \cos\beta\,(\sigma_H - \sigma_h)$$

$$\tau_{xy} = \sin\alpha \cos\alpha\,(\sigma_V - \sigma_H \cos^2\beta - \sigma_h \sin^2\beta)$$

$$\tau_{zx} = \sin\alpha \sin\cos\beta\,(\sigma_h - \sigma_H)$$

6.4 THE FAILURE MODEL

Having determined the stresses at points around the wellbore wall, it is then necessary to compare the computed stresses against the formation strength. At points where the stress states exceed the formation strength (either tension or compression) failure is considered to have initiated.

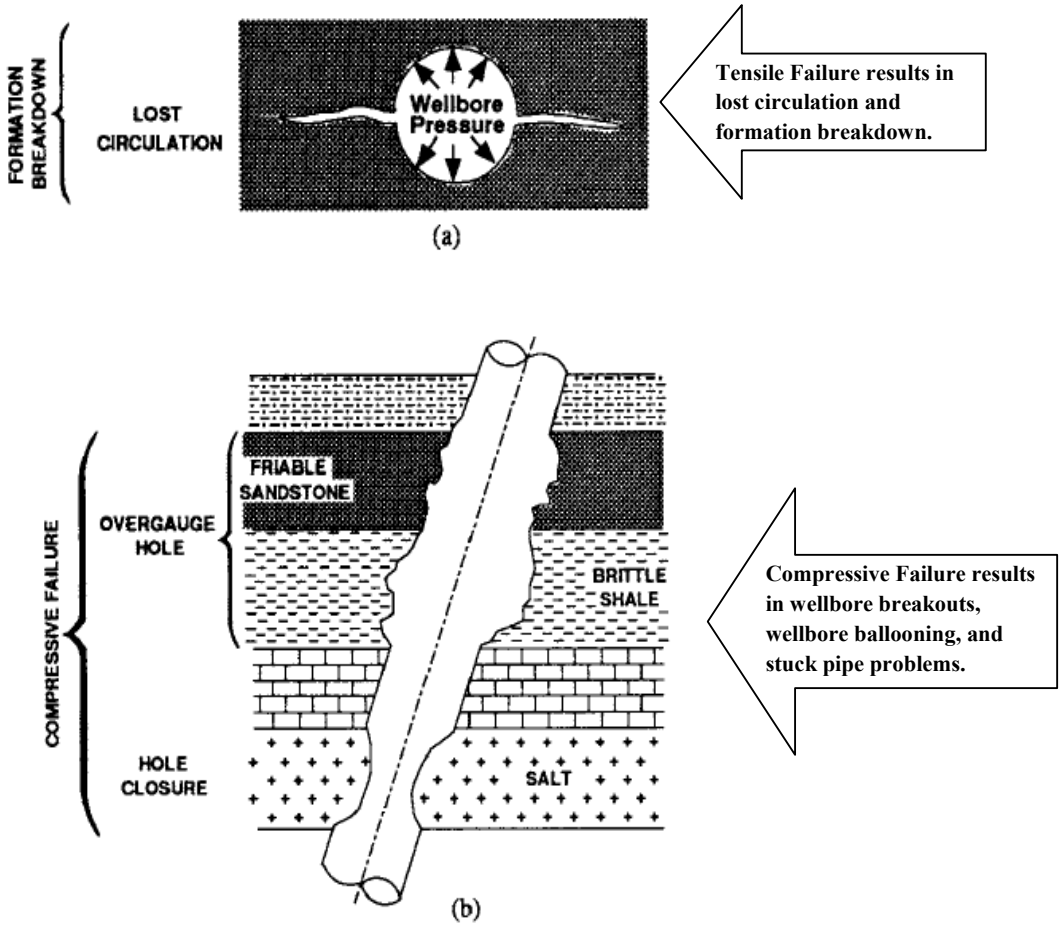

Fig 6.4 Types of stress induced Wellbore Instability

Most strength criterion are expressed in terms of the principal stresses (σ_1, σ_2, and σ_3,).One of the principal stress acts perpendicular to the wellbore and is simply given by the well pressure , Pw. The remaining two are found by transposing the hoop stress, axial stress and shear stress into principal stresses.

Thus the three induced principal stresses can be expressed as

$$\sigma_1, \sigma_2, \text{ and } \sigma_3, = \begin{Bmatrix} \frac{\sigma_{\theta\theta}+\sigma_{zz}}{2} + \left\{\left[\frac{\sigma_{\theta\theta}+\sigma_{zz}}{2}\right]^2 + \tau_{\theta z}{}^2\right\}^{0.5} \\ \frac{\sigma_{\theta\theta}+\sigma_{zz}}{2} - \left\{\left[\frac{\sigma_{\theta\theta}+\sigma_{zz}}{2}\right]^2 + \tau_{\theta z}{}^2\right\}^{0.5} \\ P_w \end{Bmatrix}$$

The ranking shown above indicates that $\mathbf{P_w} = \sigma_3$, This is the most common situation, however Pw may also be the intermediate or maximum principal stress, depending on the conditions. The order of ranking should be $\sigma_1 > \sigma_2 \geq \sigma_3$.

6.5 TENSILE FAILURE MODEL

The criterion for tensile failure initiation is simply determined by whether the minimum effective stress at the wall is less than the tensile strength of the formation assuming compression is positive. Thus failure occurs when

$$\sigma'_3 \leq -\sigma_t$$

Where σ_t the tensile strength of the rock and the effective normal stress is is given by total normal stress minus pore pressure

$$\mathbf{\sigma' = \sigma - p_f}$$

In certain instances the well pressure required to initiate fracturing at the wellbore wall is less than the minimum principal in-situ stress. In these cases the tensile fracture will only propagate a few radii from the wellbore resulting in only minor fluid losses, which is unlikely to constitute a problem. Thus when tensile failure is initiated we must also check to see if the fracture will propagate. Assuming the minimum horizontal principal stress is less than the overburden stress, then the propagation criterion can be expressed as

$$\mathbf{Pw} \geq \sigma_h$$

6.6 COMPRESSIVE FAILURE MODEL

There are numerous criterion proposed to define the failure of rock in compression. Here only the two most commonly used criteria with respect to wellbore stability analysis are reviewed, namely the Mohr-Coulomb and the Drucker-Prager (also known as extended Von Mises)

6.6.1 Mohr-Coulomb Model

The Mohr-Coulomb failure criterion can be expressed in terms of principal stresses as

$$\sigma_1 - P_f = \frac{1+\sin\emptyset}{1-\sin\emptyset}(\sigma_3 - P_f) + \frac{2C\cos\emptyset}{1-\sin\emptyset}$$

where c and $\emptyset$ are material parameters

6.6.2 Drucker-Prager Model

The Drucker-Prager Criterion is expressed in terms of principal stresses as

$$\tau_{oct} = \tau_0 + \mathrm{m}\,(\sigma_{oct} - Pf)$$

where

$$\tau_{oct} = \frac{1}{3}\sqrt{(\sigma_1-\sigma_2)^2 + (\sigma_2-\sigma_3)^2 + (\sigma_3-\sigma_1)^2}$$

$$\sigma_{oct} = \frac{1}{3}(\sigma_1 + \sigma_2 + \sigma_3)$$

and τ_0, m are material properties

It could be shown that the relationship between the three Drucker-Prager options are given by

Outer circle: $m = \frac{2\sqrt{2}\sin\phi}{3-\sin\phi}$ and $\tau_0 = \frac{2\sqrt{2}\,c\cos\phi}{3-\sin\phi}$

Middle circle: $m = \frac{2\sqrt{2}\sin\phi}{3+\sin\phi}$ and $\tau_0 = \frac{2\sqrt{2}\,c\cos\phi}{3+\sin\phi}$

Inner Circle: $m = \frac{\sqrt{6}\sin\phi}{\sqrt{9+3\sin^2\phi}}$ and $\tau_0 = \frac{\sqrt{6}\,c\cos\phi}{\sqrt{9+3\sin^2\phi}}$

Rock strength in the laboratory is frequently determined using triaxial test equipment, provided core is available. When using a Mohr-Coulomb criterion one will fit a strength criterion to the laboratory data. When using a Drucker-Prager criterion one is faced with three choices when fitting the criterion to the test data. These choices have come about through comparing the Drucker-Prager Criterion with the Mohr-Coulomb criterion. So the projection of Mohr-Coulomb criterion and one of the Drucker-Prager criterions in principal stress space is very important. In general outer Drucker-Prager circle coincides with the outer apices of the Mohr-Coulomb hexagon and the middle one with the inner space. Thus only the outer Drucker-Prager circle actually fits the test data.

Chapter 7

CALCULATIONS FOR STRESS CONDITION AROUND BOREHOLE

The successful completion of gas and oil wells involves the selection of mud weight to maintain hole stability, avoid formation fluid intrusion into the wellbore and minimize mud loss to the formation. Borehole instability is caused by the tensile or compressive failure of the borehole wall. The wellbore tensile failure takes the form of cracks, typically starting from the borehole wall and running radially into the formation. Drilling mud may then penetrate and propagate into these cracks, leading to a fall in mud level in the borehole. The borehole fails in compression, when broken rock falls into the borehole and the borehole diameter increases at the point of failure.

Both the increase in borehole diameter and the volume of rock debris falling into the borehole sometimes make it difficult or impossible to move drilling equipment into or out of the borehole. This is particularly true for long reach, highly deviated and horizontal wells where the cost of downtime is very high. Here I address the manual step by step geomechanical calculation procedures involved in carrying out wellbore stability analysis.

7.1 SAFE MUD WEIGHT DETERMINATIONS

By computing the stresses at points around the circumference of the wellbore using equations in sections 6.2, 6.3 & 6.4 and comparing them with various failure criterions given in sections 6.5 and 6.6, I calculated at what mud weights, either tensile or compressive failure is initiated. The critical stress

points are manually calculated around the periphery of the wellbore wall by varying angle θ from 0 to 90.

7.2 FIELD DATA ASSUMPTIONS

When no direct measurements of the horizontal stresses (minimum & maximum principal horizontal in-situ stresses) in the reservoir were available, an arbitrary value equivalent to 0.75 psi/ft was chosen for both horizontal stresses. The vertical stress is assumed to be equivalent to the weight of the overburden taken at 1 psi/ft. The formations were normally pressured equivalent to 0.45 psi/ft.

7.3 STEP BY STEP MANUAL CALCULATION OF STRESS CONDITION AROUND BOREHOLE FOR DIFFERENT ORIENTATION

Given well data

Vertical depth=8530 ft

Azimuth =30 degree

Inclination=0, 20, 30, 40, 50, 60, 70, 80, 90(0-90 degrees)

Poisson ratio=0.2

Internal friction angle=43.8 degrees

Cohesion=860 psi

Pore pressure=3839 psi

Vertical stress=8530 psi (σ_1)

Maximum horizontal stress=6398 psi (σ_2)

Minimum horizontal stress=6398 psi (σ_3)

Find the safe mud weights for wellbore stability.

Solution

Vertical stress=8530 psi

σ_1= (8530/8530) (psi/ft) = 1 psi/ft

Overburden gradient= 1 psi/ft

σ_3=$\sigma_{H\ min}$=6398 psi=(6398/8530)=.75 psi/ft

σ_2=$\sigma_{H\ max}$ = 6398 psi

σ_3=0.75 psi/ft(fracture gradient)

σ_2=intermediate principal stress=$\sigma_{H\ max}$

But here

(σ_2=σ_3) as per Mohr criterion

P_f=3839 psi

Step 1:

σ_1=8530 psi

σ_3=6398 psi

Step 2:

To determine the failure envelope

Mohr – coulomb criterion:

$$\sigma_1 - p_f = \frac{1+\sin\phi}{1-\sin\phi}\ (\sigma 3 - pf) + \frac{2\,C\cos\phi}{1-\sin\phi}$$

σ_1-σ_f=5.4947(σ_3-σ_f)+4033.2

σ_1=5.4974-4.4974+4033.2 ---------- (1)

Equation (1) represents a failure envelope for a rock sample under laboratory triaxial testing where confining stress (σ_3) and axial stress (σ_1) are applied. Assuming values of (σ_3) of 2000 to 6000 psi to solve equation (1), using a formation pressure of 3839 psi, the results are:

σ_1=5.4974 σ_3-4.4974 p_f+4033.2

Table 7.1

σ_3(confining stress),psi	σ_1(applied stress),psi
2000	-2237.51
3000	3259.89
4000	8757.29
5000	14254.69
6000	19752.09
7000	25249.49

Pore pressure=3839 psi

p_f=3839 psi

σ_1=5.4974 σ_3-13232.31 ---------- (2)

Step 3:

Transposition of in situ stress

Here we are transposing in situ stress in global earth co-ordinates into well bore co-ordinates:

$\sigma_2=\sigma_3$

$\sigma_3=\sigma_{H\ min}$

$\sigma_1=\sigma_v$

$\sigma_2=\sigma_{H\ max}$

The in situ stress in wellbore co-ordinates can be given by equations below:

$\sigma_x=\sigma_2 \sin^2\beta+\sigma_3\cos^2\beta$

$\sigma_y=\cos^2\alpha(\sigma_2\cos^2\beta+\sigma_3\sin^2\beta)+\sigma_1\sin^2\alpha$

$\sigma_z=\sin^2\alpha(\sigma_2\cos^2\beta+\sigma_3\sin^2\beta)+\sigma_1\cos^2\alpha$

$\tau_{xy}=\cos\alpha\sin\beta\cos\beta(\sigma_2-\sigma_3)$

$\tau_{yz}=\sin\alpha\cos\alpha(\sigma_1-\sigma_2\cos^2\beta-\sigma_3\sin^2\beta)$

$\tau_{zx}=\sin\alpha\sin\beta\cos\beta(\sigma_2-\sigma_3)$

Here

α= well deviation or inclination (0-90 degrees)

β=well azimuth (measured from true north)

$\sigma_x = \sigma_3 \sin^2\beta + \sigma_3 \cos^2\beta$ $(\sigma_3=\sigma_2)$

$= \sigma_3 (\sin^2\beta + \cos^2\beta)$

$\sigma_x=\sigma_3$

Similarly,

$\sigma_y = \sigma_3 \cos^2\alpha + \sigma_1 \sin^2\alpha$

$\sigma_z = \sigma_3 \sin^2\alpha + \sigma_1 \cos^2\alpha$

$\tau_{xy}=0$

$\tau_{zx}=0$

$\tau_{yz} = \sin\alpha \cos\alpha (\sigma_1 - \sigma_3 \cos^2\beta - \sigma_3 \sin^2\beta)$

$= \sin\alpha \cos\alpha [\sigma_1 - \sigma_3(\cos^2\beta + \sin^2\beta)]$

$\tau_{yz} = \sin\alpha \cos\alpha (\sigma_1 - \sigma_3)$

When $\sigma_3=\sigma_2$: $\tau_{xy} = \tau_{zx}=0$

When α = 0 to 90 degrees

σ_1=8530 psi

σ_2=6398 psi

When α=0;

σ_x=6398 psi

σ_y=6398 psi

σ_z=8530 psi$_{xy}$ =0

τ_{yz}=0

τ_{zx}=0

Table 7.2

Well Inclination (degrees)							
Transposed Stress	**0**	**10**	**20**	**30**	**50**	**70**	**90**
σ_x(psi)	6398	6398	6398	6398	6398	6398	6398
σ_y(psi)	6398	6462.31	6647.39	6931	7649.1	8280.6	8530
σ_z(psi)	8530	8465.62	8280.6	7997	7278.9	6647.3	6398
τ_{xy}(psi)	0	0	0	0	0	0	0
τ_{yz}(psi)	0	364.59	685.21	923.83	1049.80	685.21	0
τ_{zx}(psi)	0	0	0	0	0	0	0

Step 4:

Now because of this transposed stresses $\sigma_x, \sigma_y, \sigma_z, \tau_{yz}$,find out the induced stresses at the borehole wall.

The stresses will be calculated at point a=r; where r is the radius of the borehole.

The induced stresses at the wellbore walls when a=r is given by

$$\tau_{xy}, \tau_{yz}, \tau_{xz} = p_w \quad (7.1)$$

$$\sigma_{\theta\theta}=\sigma_x+\sigma_y-p_w-2(\sigma_x-\sigma_y)\cos 2\theta- 4 (\tau_{xy} \sin 2\theta) \quad (7.2)$$

$$\sigma_{zz}= \sigma_z-\nu[2(\sigma_x-\sigma_y)\cos 2\theta+4 \tau_{xy} \sin 2\theta] \quad (7.3)$$

$$\tau_{\theta z}=2(\tau_{yz} \cos\theta- \tau_{xz} \sin\theta) \quad (7.4)$$

$$\tau_{r\theta}=0 \quad (7.5)$$

$$\tau_{rz}=0 \quad (7.6)$$

Here θ is the angle measured between the x-axis and the radial distance from the centre.

The above equations give maximum stresses when cos 2θ=1 or when θ=0 and θ=180

Now, $\sigma_x, \sigma_y, \sigma_z, \tau_{x\,y}, \tau_{y\,z}, \tau_{x\,z}$ are calculated and shown in table 7.2

p_w=well bore pressure at the bottom of the hole due to mud weight.

TVD=8530 ft

Consider mud weight= 9 ppg

p_w=TVD*0.052*9

=8530*0.052*9

p_w=3992.04 psi

When θ=0;

σ_x=6398 psi

σ_y=6398 psi

σ_z=8530 psi

$\tau_{x\,y}= \tau_{y\,z}= \tau_{x\,z}=0$

$\sigma_{rr}=p_w$

σ_{rr}=3992.04 psi

$\sigma_{\theta\theta}$=6398+6398-3992.04-2(0)cos 2(0)-0

=12796-3992.04

$\sigma_{\theta\theta}$=8803.96 psi

σ_{zz}=8530-0.2(2(0)cos(1)+0)

σ_{zz}=8530 psi

$\tau_{\theta z}$=2(0-0)

=0

Consider mud weight 12 ppg

p_w=8530*0.052*12

p_w=5322.72 psi

When θ=0,

$\sigma_{rr}=p_w$

σ_{rr}=5322.72 psi

$\sigma_{\theta\theta}=\sigma_x+\sigma_y- p_w$

=12796-5322.72

=7473.28 psi

$\sigma_{zz}=\sigma_z-\nu(0)$

σ_{zz}=8530 psi

$\tau_{\theta z}$=2(0-0) =0

Table 7.3

Inclination (θ)					
Hole angle		**0**	**0**	**30**	**30**
Mud weight		**9 ppg**	**12 ppg**	**9 ppg**	**12 ppg**
Stress	σ_{rr}	3992.04	5322.72	3992.04	5322.72
	$\sigma_{\theta\theta}$	8803.96	7473.28	9869.96	8539.28
	σ_{zz}	8530	8530	8103.6	8103.6
	$\sigma_{\theta z}$	0	0	1349.5	1349.5

When θ=30,MW=9 ppg , ν=0.2

σ_x=6398 psi

σ_y=6931 psi

σ_z=7997 psi

τ_{yz}=923.3 psi

$\sigma_{rr}=p_w$

$\sigma_{\theta\theta}=\sigma_x+\sigma_y-p_w-2(\sigma_x-\sigma_y)\cos 2\theta- 4\ \tau_{xy}\sin 2\theta$

$\sigma_{\theta\theta}=\sigma_x+\sigma_y-p_w-2(\sigma_x-\sigma_y)\cos 2\theta- 0 \quad (\tau_{xy}=\tau_{xy}=0)$

$=6398+6931-3992.04-2(6398-6931)\cos 60$

$\sigma_{\theta\theta}$ =9869.96 psi

$\sigma_{zz}=\sigma_z-\nu[2(\sigma_x-\sigma_y)\cos 2\theta+4\ T_{xy}\sin 2\theta]$

$=7997-0.2[2(-533)*\cos 60]$

σ_{zz} =8103.6 psi

$\tau_{\theta z}=2(\tau_{yz}\cos\theta-\tau_{xz}\sin\theta)$

$=2(923.2*\cos 60)$

$\tau_{\theta z}$=923.2 ps

When MW=12ppg

$\sigma_{\gamma\gamma} = p_w$ =5322.72 psi

$\sigma_{\gamma\gamma}$ = 5322.72 psi

$\sigma_{\theta\theta}$ = 9336.96 – 5322.72 – 2(-533) * 0.5

= 8006.28 + 533

$\sigma_{\theta\theta}$ = 8539.28 psi

σ_{zz} = 8103.6 psi

$\tau_{\theta z}$ = 923.2 psi

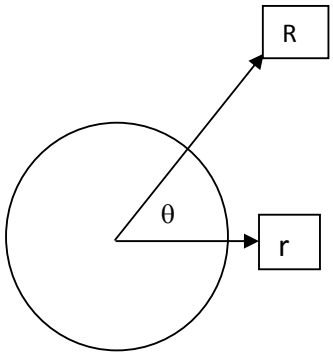

When θ =50; angle between R &r =50°

σ_x = 6398 psi MW = 9ppg

σ_y =7649.1 psi p_w = 3992.04

σ_z = 7278.9 psi

τ_{yz} = 1049.80 psi

$\sigma_{\gamma\gamma} = p_w$

$\sigma_{\gamma\gamma}$ = 3992.04

$\sigma_{\theta\theta} = \sigma_x +\sigma_y – p_w-2(\sigma_x - \sigma_y) \cos2\theta$

= 6398+ 7649.1 – 3992.04 – 2(6398-7649.1) cos100

= 14047.1 – 3992.04 -2(-1251.1)*cos100

= 14047.1 – 4426.54

$\sigma_{\theta\theta}$ = 9620.55 psi

$\sigma_{zz} = \sigma_z – v\ (2(\sigma_x - \sigma_y))\ \cos2\theta$

$= 7278.9 – 0.2(2(-1251.1))* \cos100$

$= 7278.9 – 86.9$

$\sigma_{zz} = 7192$ psi

$\tau_{\theta z} = 2(\tau_{yz} \cos\theta)$

$= 2*1049.8*\cos50$

$\tau_{\theta z} = 1349.59$ psi

Similarly when MW = 12ppg

$\sigma_{\gamma\gamma} = p_w$

$\sigma_{\gamma\gamma} = 5322.72$ psi

$\sigma_{\theta\theta} = 14047.1 – 5322.72 – 2(-1251.1)*\cos100$

$= 14047.1 – 5322.72 – 434.5$

$\sigma_{\theta\theta} = 8289.8$ psi

when $\theta = 70$; angle between R & r = 70°

$\sigma_x = 6398$ MW = 9ppg

$\sigma_y = 8280.6$ $p_w = 3992.04$ psi

$\sigma_z = 6647.3$

$\tau_{yz} = 685.21$

$\sigma_{\gamma\gamma} = p_w$

$\sigma_{\gamma\gamma} = 3992.04$ psi

$\sigma_{\theta\theta} = \sigma_x + \sigma_y – p_w – 2(\sigma_x-\sigma_y)\cos2\theta$

$= 6398 + 8280.6 – 3992.04 – 2(6398 – 8280.6) \cos140$

$= 14678.6 – 3992.04 – 2(-1882.6) \cos140$

$= 14678.6 – 3992.04 – 2884.3$

$\sigma_{\theta\theta} = 7802.25$

$\sigma_{zz} = \sigma_z –v(2(\sigma_x- \sigma_y)\cos120$

$= 6647.3 – 0.2(2884.3)$

$= 6647.3 – 576.86$

$\sigma_{zz} = 6070.44$ psi

$\tau_{\theta z} = 2 \tau_{yz} \cos\theta$

$= 2*685.21*\cos70$

$\tau_{\theta z} = 468.71$ psi

Similarly when 12ppg

$\sigma_{\gamma\gamma}$ = 5322.72 psi

$\sigma_{\theta\theta}$ = 14678.6 – 5322.72 – 2884.3

$\sigma_{\theta\theta}$ = 6471.58 psi

σ_{zz} = 6070.44 psi

when θ= 90 ; angle between R & r =90°

σ_x = 6398 psi MW = 9ppg

σ_y = 8530 psi $\sigma_{\gamma\gamma} = p_w$ = 3972.04

σ_z = 6398 psi

τ_{yz} = 0

$\sigma_{\theta\theta} = \sigma_x + \sigma_y - p_w - 2(\sigma_x - \sigma_y)\cos 2\theta$

= 6398+8530- 3992.04

= 14928 – 3992.04

$\sigma_{\theta\theta}$ = 10935.96

$\sigma_{zz} = \sigma_z - v(2(\sigma_x-\sigma_y)\cos 2\theta)$

σ_{zz} = 6398 psi

$\tau_{\theta z}$ = 0 (since τ_{yz} =0)

Therefore when ppg=12

$\sigma_{\gamma\gamma}$ = 5322.72 psi

$\sigma_{\theta\theta}$ = 14928 – 5322.72

$\sigma_{\theta\theta}$ = 9605.28 psi

σ_{zz} = 6398 psi

$\tau_{\theta z}$ = 0

Contd…..Table 7.3

Inclination (θ)							
Hole angle		50	50	70	70	90	90
Mud weight		9	12	9	12	9	12
Stress	$\sigma_{r\,r}$	3992.04	5322.72	3992.04	5322.72	3992.04	5322.72
	$\sigma_{\theta\theta}$	9620.55	8289.8	7802.25	6471.58	1035.96	9605.28
	σ_{zz}	7192	7192	6070.44	6070.44	6398	6398
	$\sigma_{\theta z}$	1349.59	1349.59	468.71	468.71	0	0

Step 5:

Now express the induced wellbore stresses as induced principal stresses using the Equation below:

$$\sigma_1, \sigma_2, \text{ and } \sigma_3, = \left\{ \begin{matrix} \frac{\sigma_{\theta\theta}+\sigma_{zz}}{2} + \left\{ \left[\frac{\sigma_{\theta\theta}+\sigma_{zz}}{2} \right]^2 + \tau_{\theta z}{}^2 \right\}^{0.5} \\ \frac{\sigma_{\theta\theta}+\sigma_{zz}}{2} - \left\{ \left[\frac{\sigma_{\theta\theta}+\sigma_{zz}}{2} \right]^2 + \tau_{\theta z}{}^2 \right\}^{0.5} \\ P_w \end{matrix} \right\}$$

NOTE: from equation 7.1 to 7.5

- Only $\sigma_{\gamma\gamma}$ is a principal stress since $\tau_{\gamma z}$ & $\tau_{\gamma z}$ are zero.
- Both $\sigma_{\theta\theta}$ & σ_{zz} have shear stress associated with them.
- Hence we need to find the induced principal stress associated with $\sigma_{\theta\theta}$ & σ_{zz}. This is given by above equations.
- The above two principal stress (induced) can be calculated by referring to Mohr circle, centred at ½($\sigma_{\theta\theta}$+ σ_{zz}) and with a radius of $\{((\sigma_{\theta\theta} - \sigma_{zz})/2)^2 + \tau_{\theta z}{}^2\}$

When θ =0; angle between R & r is zero

$\sigma_{\theta\theta}$ = 8803.96 ppg = 9

σ_{zz} = 8530 p_w = 3992.04

$\tau_{\theta z} = 0$

$= (8803.96 + 8530)/2 + \{((8803.96 – 8530)/2)^2 + 0\}^{1/2}$

$= 8666.98 + 136.98$

$\sigma_1 = 8803.96$

$\sigma_2 = 8666.98 – 136.98$

$= 8530$

$p_w = 3992.04 = \sigma_3$

when MW= 2ppg

$\sigma_{\theta\theta} = 7473.2$

$\sigma_{zz} = 8530$

$\tau_{\theta z} = 0$

Induced principal stress

$\sigma_1 = 7473.28$

$\sigma_2 = 8530$

$\sigma_3 = p_w = 5322.72$

when $\theta = 30$; angle between R & r= 30°

$\sigma_{\theta\theta} = 9869.96$

$\sigma_{zz} = 8103.6$

$\tau_{\theta z} = 923.6$

MW = 9ppg ; $p_w = 3992.04$

$\sigma_1 = ((9869.96+8103.6)/2) + \{((9869.96-8103.6)/2)^2 + 923.6^2\}^{1/2}$

$= 8986.78 + 1277.9$

$\sigma_1 = 10264.68$

$\sigma_2 = 8986.78 – 1277.9$

$\sigma_2 = 7708.88$

$\sigma_3 = p_w = 3992.04$

when $\theta = 30$; MW= 12ppg

$\sigma_{\theta\theta} = 8539.28$

$\sigma_{zz} = 8103.6$

$\tau_{\theta z} = 923.6$

$\sigma_3 = p_w = 5322.72$

$\sigma_1 = 8321.44 + ((217.84)^2 + (923.6)^2)^{1/2}$

$= 8321.44 + 948.94$

$\sigma_1 = 9270.38$

$\sigma_2 = 8321.44 - 948.94$

$\sigma_2 = 7372.5$

$\sigma_3 = 5322.72$

when $\theta=50$; MW = 9ppg

$\sigma_{\theta\theta} = 9620.55$

$\sigma_{zz} = 7192$

$\tau_{\theta z} = 1349.59$

$\sigma_1 = 8406.275 + \{(1214.225)^2 + (1349.59)^2\}^{1/2}$

$= 8406.275 + 1815.44$

$\sigma_1 = 10221.72$

$\sigma_2 = 6590.835$

$\sigma_3 = 3992.04$

when $\theta = 50$; MW= 12ppg

$\sigma_{\theta\theta} = 8289.8$

$\sigma_{zz} = 7192$

$\tau_{\theta z} = 1349.59$

$\sigma_1 = 7740.9 + \{(548.9)^2 + (1349.59)^2\}^{1/2}$

$= 7740.9 + 1456.9$

$\sigma_1 = 9197.84$

$\sigma_2 = 6284$

$\sigma_3 = 5322.72$

when $\theta = 70$; MW=9ppg

$\sigma_{\theta\theta} = 7802.25$

$\sigma_{zz} = 6070.44$

$\tau_{\theta z} = 468.71$

$\sigma_1 = 6936.345 + \{(865.905)^2 + (468.71)^2\}^{1/2}$

$= 6936.345 + 984.62$

$\sigma_1 = 7920.96$

$\sigma_2 = 5951.725$

$\sigma_3 = 3992.02$

when $\theta = 70$; MW = 12ppg

$\sigma_{\theta\theta} = 6471.58$

$\sigma_{zz} = 6070.44$

$\tau_{\theta z} = 468.71$

$\sigma_1 = 6271.01 + \{(200.72)^2 + (468.71)^2\}^{1/2}$

$= 6271 + 509.88$

$\sigma_1 = 67808.8$

$\sigma_2 = 5761.12$

$\sigma_3 = 5322.72$

when $\theta = 90$; MW = 9ppg

$\sigma_{\theta\theta} = 10935.96$

$\sigma_{zz} = 6398$

$\tau_{\theta z} = 0$

$\sigma_1 = 8666.98 + 2268.96$

$\sigma_1 = 10935.96$

$\sigma_2 = 6398$

$\sigma_3 = 3992.02$

when $\theta = 90$; MW= 12ppg

$\sigma_{\theta\theta} = 9605.28$

$\sigma_{zz} = 6398$

$\tau_{\theta z} = 0$

$\sigma_1 = 8001.64 + 1603.64$

$\sigma_1 = 9605.28$

$\sigma_2 = 6398$

$\sigma_3 = 5322.72$

TABLE: 7.4

INCLINED PRINCIPAL STRESSESS	HOLE ANGLE	ANGLE BETWEEN R & r ; INCLINATION									
		0	0	30	30	50	50	70	70	90	90
		MUD WEIGHT									
	σ_{stress}	9	12	9	12	9	12	9	12	9	12
	σ_1	8803.96	7473.28	10264.68	9270.38	10221.72	9197.84	7920.96	6780.8	10935.96	9605.28
	σ_2	8530	8530	7708.88	7372.5	6590.83	6284	5951.73	5761.12	6398	6398
	σ_3	3992	5322.72	3992	5322.72	3992	5322.72	3992	5322.72	3992	5322.72

Note: Two mud weights are required to develop a relationship between mud weight and wellbore stresses.

Step 6:

DRUCKER PRAGER FAILURE ENVELOPE CALCULATION:

$\tau_{oct} = (2*(2)^{½}c\cos\varphi) /(3-\sin\varphi) + ((2*(2)^{½}\sin\varphi)/(3-\sin\varphi))*(\sigma_{oct} - p_f)$

$= (2*(2)^{½}*860*\cos43.8) /(3-\sin43.8) + ((2*(2)^{½}\sin43.8)/(3-\sin43.8))*(\sigma_{oct} - p_f)$

$= 1755.64/2.3078 +0.8483*(\sigma_{oct} - p_f)$

$\tau_{oct}= 760 + 0.8483\sigma_{oct} - 0.8483p_f$

$\tau_{oct} = 0.8483\ \sigma_{oct} - 2496.62$

By putting different values of σ_{oct} from 2000 psi to 7000 psi, the different values of τ_{oct} are shown in the table below.

Table 7.5

σ_{oct}(psi)	τ_{oct}
2000	-800
3000	48.28
4000	896.58
5000	1744.88
6000	2593.18
7000	3441.48
8000	4289.78
9000	5138.08

NOTE: Tensile strength is normally 1/10 of the UCS (ultimate compressive strength) of the rock.[1]

- The Mohr's envelope and circle shown here only apply to the highest point of the wellbore cross section.
- A stable Mohr's circle at this point does not necessarily imply well bore stability of the material at that point.
- Breaking the Mohr's envelope does not necessarily imply wellbore instability because only the minimum safe mud weight is obtained from the Mohr-Coulomb criterion, while the maximum mud weight is from the maximum tensile strength criterion.
- There might be a situation in which the mud weight exceeds the upper limit of the Mohr-Coulomb criterion but still satisfies the maximum tensile stress criterion.

Step 7:

Determining the Tensile strength of the rock (T)

$$Co = \frac{2C\cos\emptyset}{1-\sin\emptyset}$$

$$Co - \frac{2*80*\cos 43.8}{1-\sin 43.8}$$

=4032.45 psi

T=403 psi

Step 8:

Determining the Formation Breakdown Pressure(FBP)

We have considered that formation breakdown pressure depends on Induced transposed stresses and given as

FBP=σ_3 (3-cos$^2\alpha$)-$\sigma_1$sin2α+T-p_f (for vertical well)

FBP= σ_x (3-cos$^2\alpha$)-$\sigma_y$sin2α+T-p_f (For deviated well)

When α=0

σ_x =6398 psi σ_y=6398 psi

FBP=2 σ_3 –p_f+ T

FBP=2 σ_x –p_f+ T

=(2*6398)-3839+403

=21.10 ppg

When α=30

FBP=σ_x (3-cos^{2}30)-$\sigma_y$sin2α+T-p_f

=20.8 ppg

When α=50

FBP=σ_x (3-cos^{2}30)-$\sigma_y$sin2α+T-p_f

σ_x=6398 psi; σ_y=7649.1 psi

FBP=17.493ppg

When α=70

FBP=σ_x (3-cos^{2}30)-$\sigma_y$sin2α+T-p_f

σ_x=6398 psi; σ_y=8280.6 psi

FBP=17.35 ppg

When α=90

σ_x=6398 psi; σ_y=8530 psi

FBP=16.295 ppg

*Above results shown in ppg after using conversion factor

Table 7.6 Maximum Mud Weight Comparison

Inclination (α)	SPE (20405)ppg	Manual result(ppg)	Error (%)
0	20.08	21.1	4.8
30	18.82	20.8	9.5
50	17.65	17.493	0.88
70	16.24	17.35	6.39
90	15.66	16.295	3.8

Table 7.7 Applying 5% error in the manual calculation

Well Inclination(α)	SPE(20405)ppg	Manual Result(ppg)
0	**20.08**	**20.045**
30	**18.82**	**19.76**
50	**17.65**	**17.793**
70	**16.24**	**16.48**
90	**15.66**	**15.4802**

Minimum Mud Weights Determination

- Plot the values of table 7.1 to obtain Mohr-Coulomb Failure Envelope keeping σ_3 in X-axis and σ_1 in Y-axis.
- Now Plot the stresses shown in Table 7.4 (σ_1 and, σ_3 alone) in this failure envelope plot for each hole angle .
- For each hole angle we will get two co-ordinate points, using this make a line and extend it.
- The intersection point between the failure envelope and the induced principal stresses at the wellbore gives the minimum mud weight required to prevent hole collapse.
- Actually this method gives the hole collapse pressure and it should be converted to equivalent ppg format.
- This method is recommended for well inclination values ranging from 0 to 30 degrees.
- For higher well inclination angles, Drucker-Prager Failure envelope is recommended.

Table 7.8 Minimum Mud Weight Comparison

Well Inclination (degrees)	Collapse Pressure (psi)	Minimum Mud Weight (ppg)manual	SPE 20405 (ppg)	Error (%)
0	3992	8.999	8.9964	0.3
30	4250	9.5815	9.8294	2.5
50	4422.6	9.9707	10.6624	6.48
70	4594.8	10.359	11.0789	6.5
90	4767.07	10.747	11.4121	5.8

Table 7.9 Applying 5% error in manual calculation

Well Inclination (degrees)	SPE 20405 (ppg)	Manual Calculation
0	8.99	8.99
30	9.83	9.58
50	10.66	10.47
70	11.1	10.877
90	11.41	11.285

7.4 WELLBORE STABILITY PLOT (MOHR COULOMB)

The calculated optimum mud weights are plotted against well inclination to obtain the wellbore stability plot.

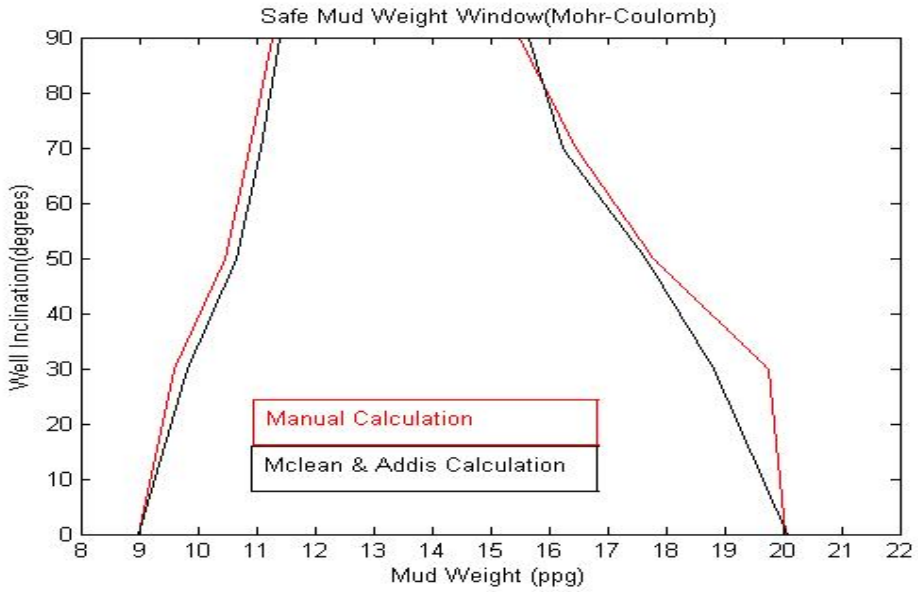

Fig 7.1

Discussions

- Referring to fig 7.1, the Minimum mud weight required is directly proportional to the well inclination and Maximum mud weight required is inversely proportional to the well inclination.

- Hoop stress contributes to collapse failure (ie, stress induced failure) whereas Radial stress contributes to tensile failure (ie, drilling induced failure).

7.5 WELLBORE STRESSES CALCULATIONS USING C-PROGRAM

Given well data

Vertical depth=1000ft

Mud Weight = 9 ppg and 12 ppg

Azimuth = 0 to 360 degrees (Keeping Inclination fixed)

Inclination= 0-90 degrees (Keeping Azimuth fixed)

Vertical stress=10000 psi (σ_1)

Maximum horizontal stress=8000 psi (σ_2)

Minimum horizontal stress=7000 psi (σ_3)

Here induced wellbore stresses are calculated using the developed C-Programs (available in the Appendix section)

Table 7.10 Calculation of Transpose In-Situ Stress using C-Program

Transposed Stresses (psi)	Well Inclination(degrees)									
	0	**5**	**10**	**15**	**20**	**25**	**30**	**35**	**40**	**45**
σ_x	7249.77	7249.77	7249.77	7249.77	7249.77	7249.77	7249.77	7249.77	7249.77	7249.77
σ_y	7750.23	7767.30	7818.00	7900.78	8013.14	8151.67	8312.15	8489.72	8678.99	8874.21
σ_z	10000	9982.93	9932.23	9849.44	9737.08	9598.55	9438.07	9260.50	9071.23	8876.01
τ_{xy}	432.88	431.23	426.31	418.144	406.8	392.36	374.94	354.67	331.70	306.21
τ_{xy}	0	195.24	384.55	562.18	722.76	861.39	973.88	1056.80	1107.65	1124.88
τ_{zx}	0	-37.708	-75.131	-111.98	-147.98	-182.85	-216.34	-248.18	-278.13	-305.97

Transposed Stresses	Well Inclination(degrees)								
	50	**55**	**60**	**65**	**70**	**75**	**80**	**85**	**90**
σ_x	7249.77	7249.77	7249.77	7249.77	7249.77	7249.77	7249.77	7249.77	7249.77
σ_y	9069.46	9258.81	9436.52	9597.18	9735.93	9848.54	9931.61	9982.61	9999.99
σ_z	8680.76	8491.41	8313.70	8153.04	8014.3	7901.68	7818.61	7767.61	7750.23
τ_{xy}	278.4	248.46	216.63	183.17	148.30	112.31	75.47	38.05	0.344
τ_{xy}	**1107.97**	**1057.42**	**974.75**	**862.54**	**724.12**	**563.73**	**386.23**	**197.00**	**1.800**
τ_{zx}	**-331.48**	**-354.47**	**-374.77**	**-392.21**	**-406.68**	**-418.05**	**-462.25**	**-431.20**	**-432.87**

Table 7.11 Calculation of Wellbore Stresses when MW-9PPG

Induced Stress	Induced Stresses									
	0	5	10	15	20	25	30	35	40	45
σ_{rr}	4680.00	4680.00	4680.00	4680.00	4680.00	4680.00	4680.00	4680.00	4680.00	4680.00
$\sigma_{\theta\theta}$	11320.92	11057.04	10872.81	10762.40	10708.06	10679.69	10646.85	10576.29	10440.63	10221.72
σ_{zz}	10200.18	10126.92	10029.24	9907.81	9762.05	9590.21	9391.09	9163.86	8909.61	8631.55
τ_{zr}	0.0	395.56	783.50	1144.02	1459.61	1716.02	1903.31	2016.31	2054.94	2023.99

MW-9PPG

Induced Stress	Induced Stresses								
	50	55	60	65	70	75	80	85	90
σ_{rr}	4680.00	4680.00	4680.00	4680.00	4680.00	4680.00	4680.00	4680.00	4680.00
$\sigma_{\theta\theta}$	9913.60	9523.75	9072.64	8591.51	8118.76	7695.41	7360.12	7144.51	7069.32
σ_{zz}	8335.63	8030.44	7726.97	7437.95	7176.91	6957.10	6790.36	6686.04	6650.14
τ_{zr}	1932.79	1794.40	1624.59	1440.7	1260.31	1100.01	974.12	893.71	865.76.76

Table 7.12 Calculation of Wellbore Stresses when MW-12PPG

Induced Stress	Induced Stresses									
	0	5	10	15	20	25	30	35	40	45
σ_{rr}	6240.00	6240.00	6240.00	6240.00	6240.00	6240.00	6240.00	6240.00	6240.00	6240.00
$\sigma_{\theta\theta}$	9760.92	9497.04	9312.82	9202.40	9148.06	9119.69	9086.85	9016.29	8880.63	8661.72
σ_{zz}	10200.19	10126.92	10029.24	9907.81	9762.05	9590.21	9391.06	9163.86	8909.61	8631.56
τ_{zr}	390.48	395.56	783.50	1144.02	1459.61	1716.02	1903.31	2016.32	2054.94	2023.99

MW-12PPG

Induced Stress	Induced Stresses								
	50	55	60	65	70	75	80	85	90
σ_{rr}	6240.00	6240.00	6240.00	6240.00	6240.00	6240.00	6240.00	6240.00	6240.00
$\sigma_{\theta\theta}$	8353.60	7693.75	7512.64	7031.51	6558.76	6135.41	5800.12	5584.51	5509.32
σ_{zz}	8335.63	8030.44	7726.97	7437.95	7176.91	6957.10	6790.36	6686.04	6650.14
τ_{zr}	1932.79	1794.40	1624.60	1440.70	1260.32	1100.01	974.12	893.70	865.76

Table 7.13 Transposed stresses with varying Azimuth

Transposed Stresses (psi)	Azimuth (degrees)										
	0	**20**	**40**	**60**	**80**	**90**	**100**	**120**	**140**	**160**	**180**
σ_x	7000.00	7116.00	7412.83	7749.54	7969.60	7999.90	7970.15	7750.92	7414.39	7117.88	7000.00
σ_y	8499.54	8411.86	8189.82	7937.21	7772.11	7747.31	7771.70	7936.17	8188.65	8411.09	8499.53
σ_z	9500.46	9471.27	9397.35	9313.24	9258.28	9250.68	9258.14	9312.90	9396.95	9471.01	9500.46
τ_{xy}	0.00	278.26	426.45	375.28	148.69	0.68	-147.40	-374.59	-426.68	-279.31	-1.30
τ_{xy}	**865.76**	**916.34**	**1044.46**	**1190.22**	**1285.48**	**1298.63**	**1285.71**	**1190.81**	**1045.14**	**916.79**	**865.76**
τ_{zx}	**0.00**	**-160.55**	**-246.05**	**-216.53**	**-85.79**	**-0.30**	**85.05**	**216.14**	**246.18**	**161.16**	**0.79**

Transposed Stresses (psi)	Azimuth (degrees)								
	200	**220**	**240**	**260**	**280**	**300**	**320**	**340**	**360**
σ_x	7115.84	7411.26	7748.11	7969.05	7970.68	7752.29	7415.96	7118.91	7000.01
σ_y	8412.63	8191.00	7938.24	7772.52	7771.30	7935.14	8187.47	8410.32	8499.53
σ_z	9471.52	9397.73	9313.59	9258.41	9258.01	9312.55	9396.56	9470.75	9500.45
τ_{xy}	277.20	426.20	375.93	149.99	-146.10	-373.90	-426.91	-280.36	-2.75
τ_{xy}	915.90	1043.78	1189.62	1285.24	1285.95	1191.41	1045.82	917.23	865.76
τ_{zx}	-159.94	-245.91	-216.93	-86.54	84.30	215.74	246.33	161.77	-1.59

Table 7.14 Induced wellbore stresses with varying azimuth when MW-9 ppg

Induced Stress	Induced Stresses					
	0	**20**	**40**	**60**	**80**	**90**
σ_{rr}	4680.00	4680.00	4680.00	4680.00	4680.00	4680.00
$\sigma_{\theta\theta}$	13818.62	12118.23	9513.92	9518.59	11228.46	11570.68
σ_{zz}	10100.28	9725.17	9115.60	9015.61	9291.63	9350.96
τ_{zr}	1731.51	1832	1916.88	1566.25	617.20	2.86

Table 7.15 Induced wellbore stresses with varying azimuth when MW-12 ppg

Induced Stress	Induced Stresses					
	0	**20**	**40**	**60**	**80**	**90**
σ_{rr}	6240.00	4680.00	4680.00	4680.00	4680.00	4680.00
$\sigma_{\theta\theta}$	12258.62	10558.23	7953.92	7958.59	9668.46	10010.68
σ_{zz}	10100.27	9725.17	9115.60	9015.61	9291.63	9350.96
τ_{zr}	1731.51	1832.02	1916.88	1566.25	617.20	2.86

Chapter 8
RESULTS AND DISCUSSION

In this chapter I have developed various wellbore stress plots using Matlab for different bore hole orientations to understand the stress effects cross over.

8.1 RESERVOIR DATA FOR STRESS PLOTS (VERTICAL AND HORIZONTAL WELL)

I am considering a typical wellbore in a reservoir having following information--

Wellbore Pressure Pw=5000psi

Poisson Ratio v= 0.2

Vertical In-situ Stress = 12000 psi

Max Horizontal Stress = 10000 psi

Min Horizontal Stress = 9000 psi

Using this field data we plotted Induced Tangential stress, Axial Stress Vs Circumferential Angle (θ) for a vertical and horizontal wellbore.

8.1.1 Stress Plot for Vertical Wellbore

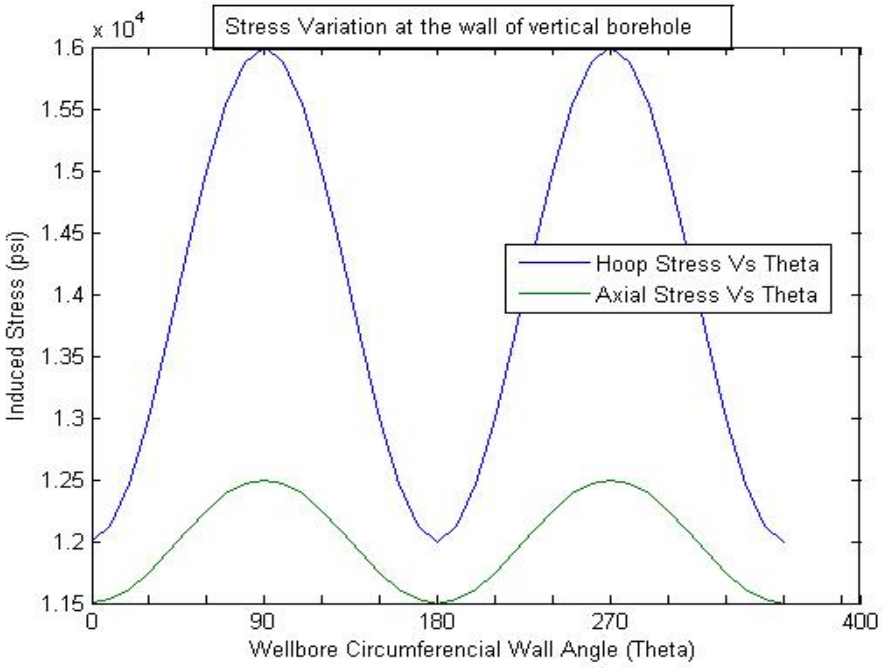

Fig 8.1

Discussions

- Referring to fig 8.1 for a vertical wellbore orientation, the induced wellbore hoop stress is always greater than the induced wellbore axial stress
- The induced wellbore stresses namely hoop stress and axial stress are independent of transposed wellbore in-situ stresses and are depending only on wellbore circumferential wall angle.

8.1.2 Stress Plot for Horizontal Wellbore

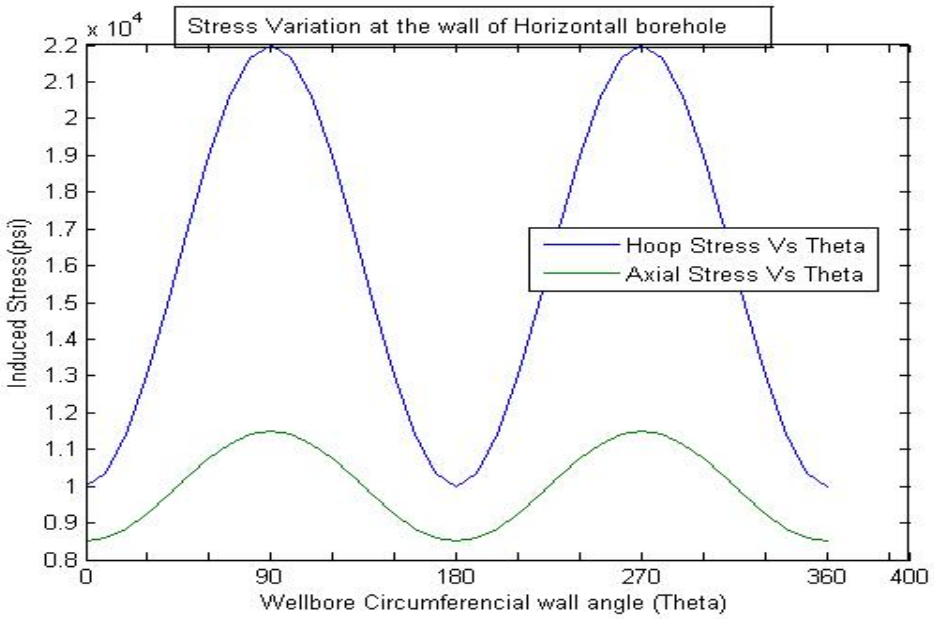

Fig 8.2

Discussions

- Referring to fig 8.2, for a Horizontal wellbore orientation, the induced wellbore hoop stress is always greater than the induced wellbore axial stress
- The induced wellbore stresses namely hoop stress and axial stress are dependent on transposed wellbore in-situ stresses and are depending on wellbore circumferential wall angle .

8.1.3 Comparision of Stresses-Vertical and Horizontal Wellbore

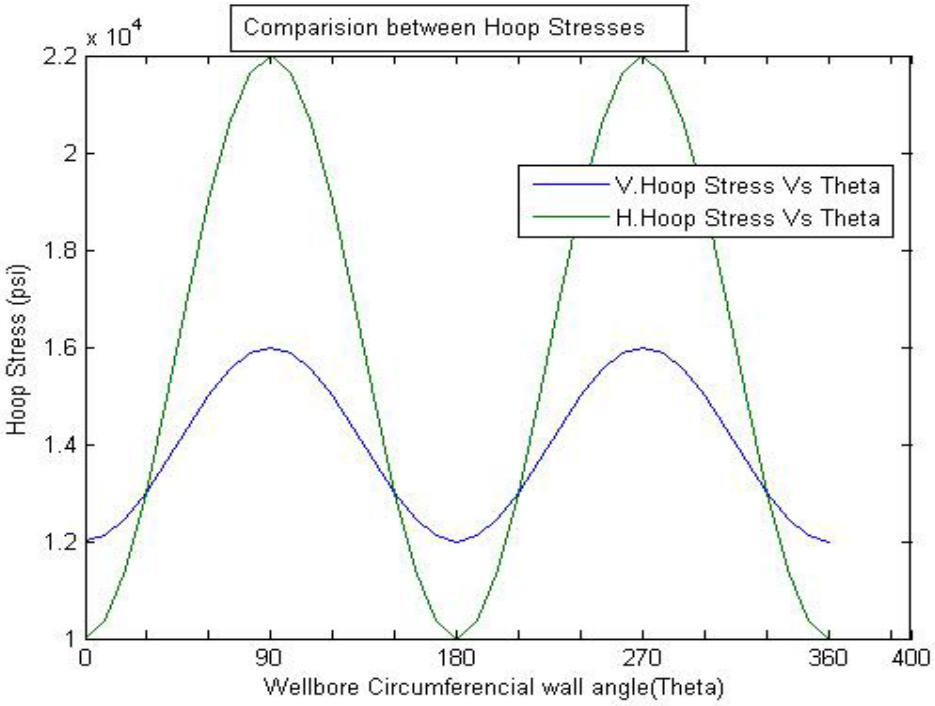

Fig 8.3

Discussions

- Referring to fig 8.3, when we compare a vertical wellbore orientation and horizontal wellbore orientation, the induced wellbore hoop stress in a vertical well is always greater than the induced wellbore hoop stress in a horizontal well.
- The in-situ stress acting along the horizontal well bore axis greatly influences the magnitude of induced hoop stress

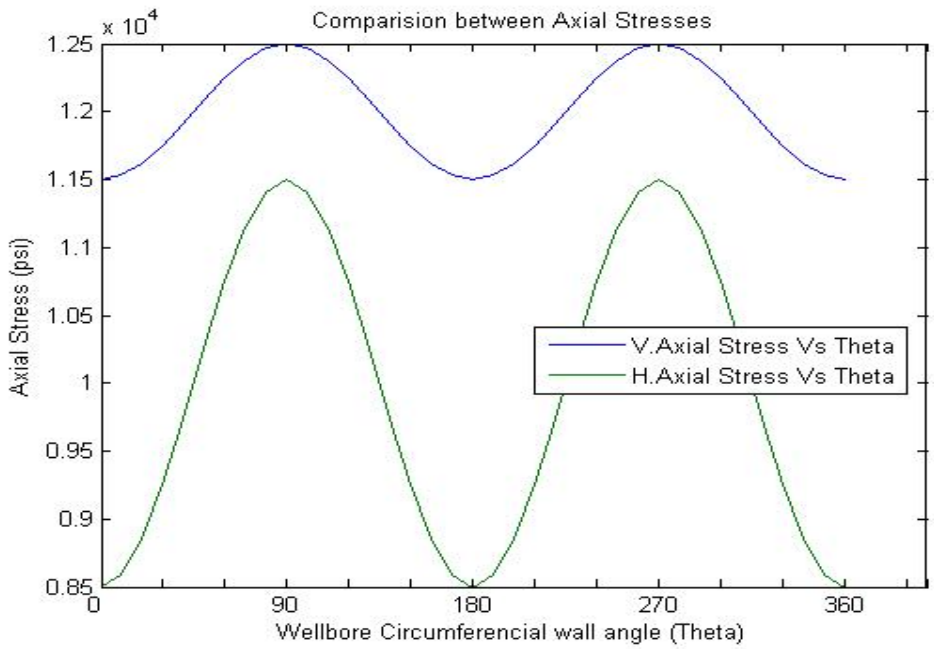

Fig 8.4

Discussions

- Referring to fig 8.4, when we compare a vertical wellbore orientation and horizontal wellbore orientation, the induced wellbore axial stress in a vertical well is always greater than the induced wellbore axial stress in a horizontal well.
- The in-situ stress acting along the horizontal well bore axis greatly influences the magnitude of induced axial stress.

8.2 STRESS PLOTS (Deviated Well $S_H = S_h$)

Given well data

Vertical depth=8530 ft

Azimuth =30 degree

Inclination=0, 20, 30, 40, 50, 60, 70, 80, 90(0-90 degrees)

Poisson ratio=0.2

Internal friction angle=43.8 degrees

Cohesion=860 psi

Pore pressure=3839 psi

Vertical stress=8530 psi (σ_1)

Maximum horizontal stress=6398 psi (σ_2)

Minimum horizontal stress=6398 psi (σ_3)

Using this data we have determined the safe mud weights plots for wellbore stability.

8.2.1 Various Stress Plots for Deviated well ($S_H = S_h$)

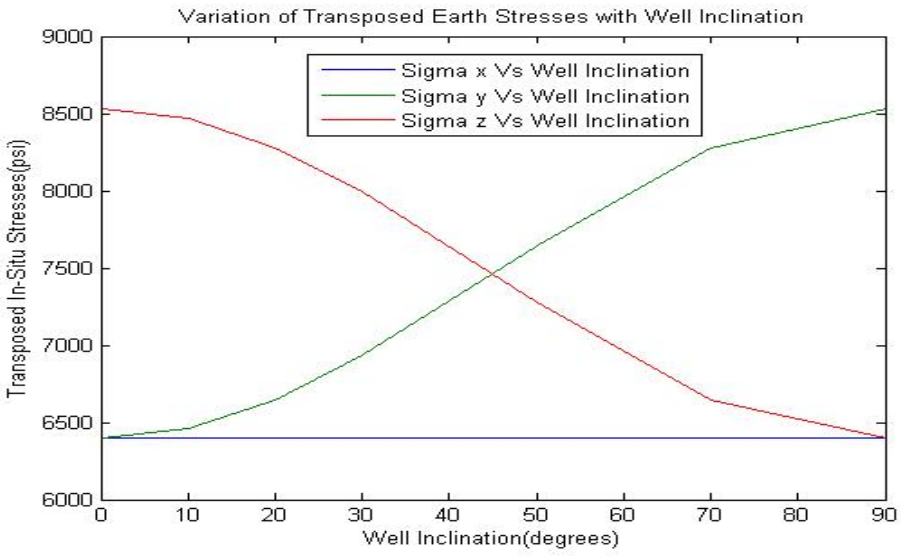

Fig 8.5

Discussions

- Referring to fig 8.5, for a Deviated wellbore orientation , the transposed in-situ stress σ_y acts in tangential direction and σ_z acts in axial direction
- Keeping azimuth as fixed constant value of 30 degree, the transposed in-situ stress acting in tangential direction (σ_y) to the deviated wellbore is directly proportional to well inclination from 0 to 90 degrees and transposed in-situ stress acting in axial direction (σ_z) is inversely proportional to the well inclination from 0 to 90 degrees.
- The transposed in-situ stress acting in radial direction(σ_x) remains constant for the condition $\sigma_h = \sigma_H$

8.2.2 Safe Mud Weight Window using Mohr - Coulomb Criterion

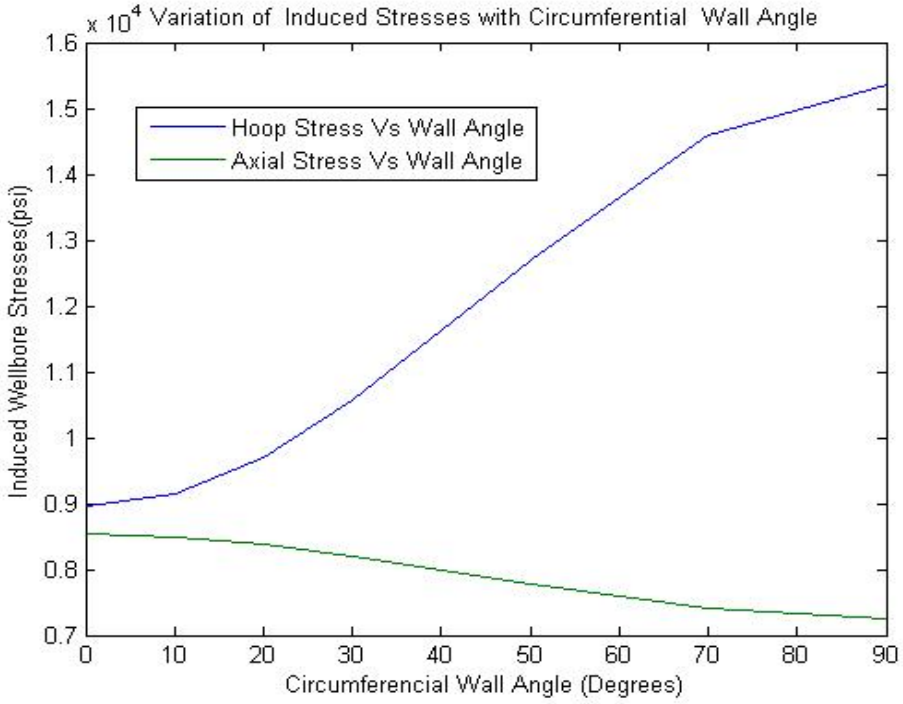

Fig 8.6

Discussions

- Referring to fig 8.6, for a Deviated wellbore orientation , the induced wellbore hoop stress $\sigma_{\theta\theta}$ is greater than the induced wellbore axial stress σ_{zz}
- The hoop stress acting in tangential direction ($\sigma_{\theta\theta}$) to the deviated wellbore is directly proportional to well inclination and the axial stress acting in axial direction (σ_{zz}) is inversely proportional to the well inclination.

Based on the stress plots, the hoop stress acting in any wellbore orientation is greater than the axial stress acting in any wellbore orientation.

8.3 STRESS PLOTS (DEVIATED WELL WHEN $S_H \neq S_h$)

TVD = 10000 ft

Mud Weight = 9 & 12 ppg

Vertical stress=10000 psi (σ_v)

Maximum horizontal stress = 8000 psi (σ_H)

Minimum horizontal stress = 7000 psi (σ_h)

Case (i)

Azimuth = 30 degrees

Inclination = 0 to 90 degrees

Case (ii)

Azimuth =0 to 360 degrees

Inclination=30 degrees

Using this data we have determined the Transposed Stress Vs Inclination, Transposed Stress Vs Azimuth Plots and subsequently Induced Stress Vs Circumferential Angle (θ) Plots.

8.3.1 Various Stress Plots Deviated Well ($S_H \neq S_h$)

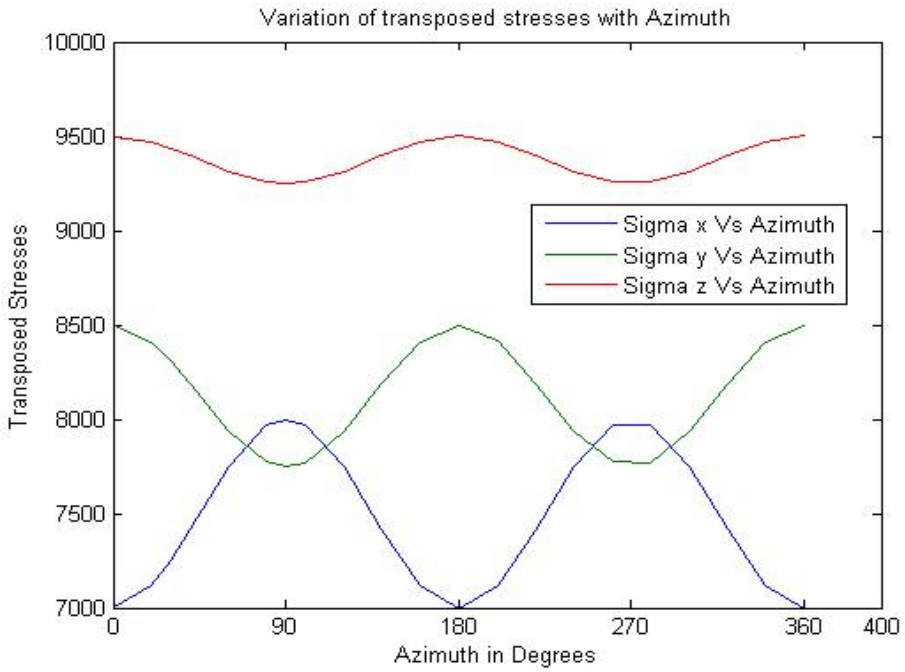

Fig 8.7

Discussions

- Keeping inclination as fixed constant value of 30 degrees, for a Deviated wellbore orientation , the transposed in-situ stress σ_y acts in tangential direction , σ_z acts in axial direction and σ_x acts in radial direction
- Referring to fig 8.7, the transposed in-situ stress acting in tangential direction (σ_y), axial direction (σ_z) is inversely proportional to the azimuth in NE and SW Quadrants.
- The transposed in-situ stress acting in tangential direction (σ_y), axial direction (σ_z) is directly proportional to the azimuth in SE and NW Quadrants.
- The transposed in-situ stress acting in radial direction (σ_x), is directly proportional to the azimuth in NE, SW Quadrants and inversely proportional to azimuth in SE, NW Quadrants.

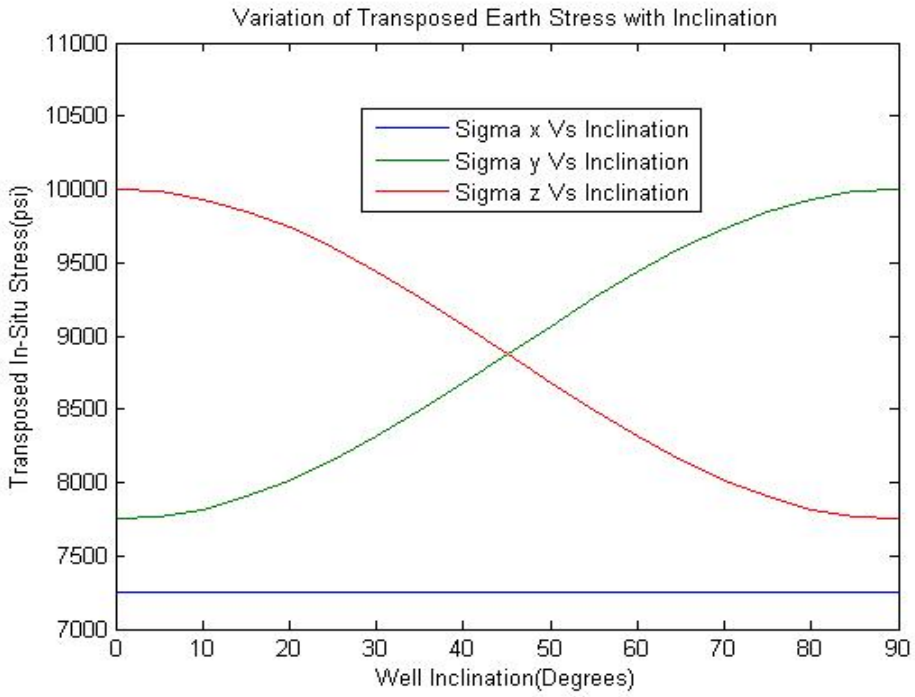

Fig 8.8

Discussions

- Referring to fig 8.8, keeping azimuth as fixed constant value of 30 degrees, the transposed in-situ stress acting in tangential direction (σ_y) to the deviated wellbore is directly proportional to well inclination and transposed in-situ stress acting in axial direction (σ_z) is inversely proportional to the well inclination.

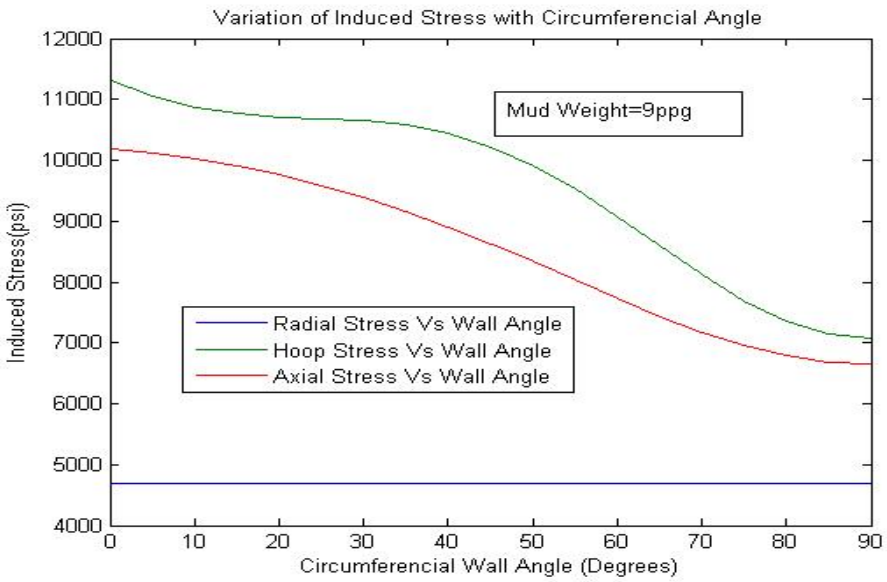

Fig 8.9

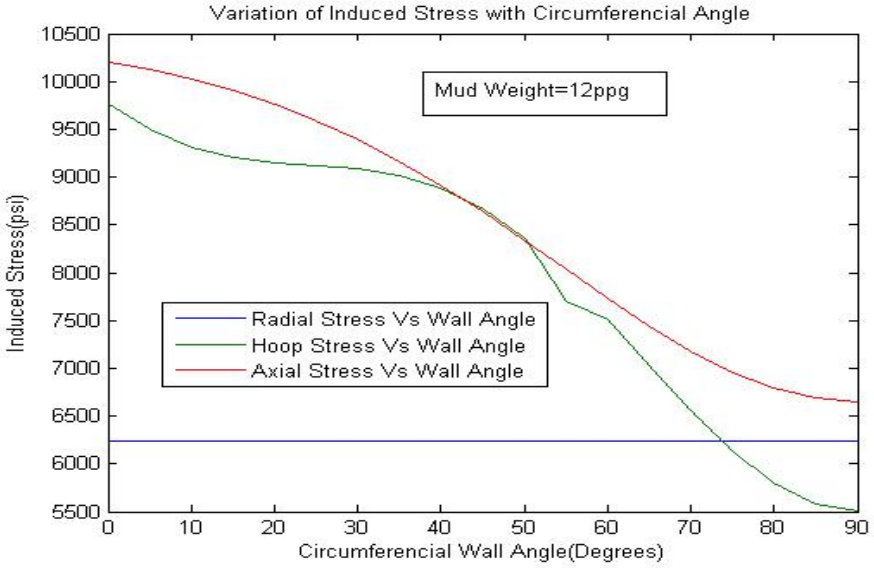

Fig 8.10

Discussions

- Referring to fig 8.9 and fig 8.10, the hoop stress concentration varies drastically with change in mud weights values. Hence more emphasize is given on Hoop Stress variation with respect to mud weights used.

8.3.2 Variation of Hoop Stress with mud weight and Circumferential wall Angle

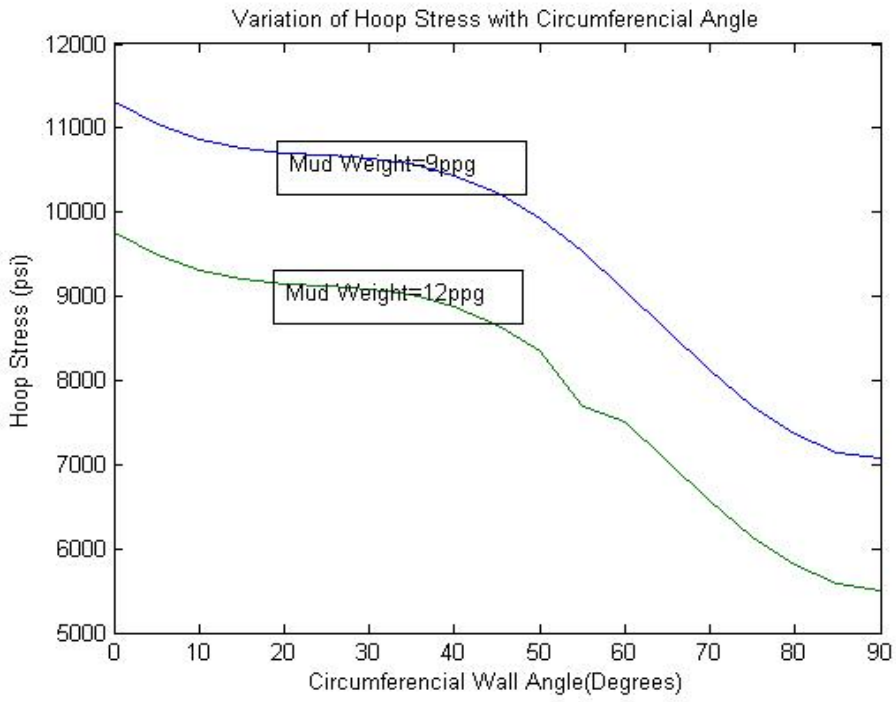

Fig 8.11

Discussions

- Referring to fig 8.11, Decrease in mud weight increases Hoop Stresses.

- Increase in mud weight increases Radial Stresses as radial stress is directly proportional to Mud Weight as seen from the previous mathematical expressions.

8.4 VALIDITY OF RESULTS

- The discussions in section 8.3.2 matches with Section 3 of Amoco's Wellbore Stability-Drilling Handbook.
- The pattern of various stress concentration plots around the wellbore wall obtained using Matlab are matching with pattern of stress concentration plots around the wellbore wall of section 6.3 & 6.5 of Reservoir Geomechanics by M.D.Zoback.
- The results of section 7.10 are matching with the published SPE Paper 20405 with a manual calculation error percentage of five.

Chapter 9

CONCLUSIONS AND RECOMMENDATIONS FOR FUTURE WORK

9.1 CONCLUSIONS

A number of conclusions are drawn from the material presented in this work.

- The investigation of borehole stress can provide increased understanding of the wellbore stability. Mud weights needed to control shear and tensile failure cross over.
- If the mud weight is cooler than the formation, it reduces the hoop stress as the formation is cooled. This reduction in hoop stress can prevent shear failure and stabilize the hole.
- If the mud weight is hotter than the formation exactly the opposition occurs as hoop stress is increased. This could promote spalling or shear failure.
- A more refined safe operating window between formation collapse and fracturing can be determined through the modeling approach used in this work.
- Rapid or frequent changes in wellbore pressure at the wellbore wall can have an effect on the effective radial stress and these changes can lead to circumferential tensile failure.

- When radial stress increases hoop stress decreases, under this condition the wellbore wall can go into tension and contribute to the occurrence of Drilling-Induced Tensile Fractures.
- A step by step method of analyzing wellbore stability using field-based drilling parameters is developed.
- The stress concentration varies rapidly with respect to position around the wellbore and distance from the wellbore wall.
- To increase borehole stability, the best direction is that which minimizes the principal stress difference normal to the axis.
- Inclined wells lose their relative stability very quickly with inclination. This is due to the fairly high overburden gradient.
- With respect to greater subsurface depth, the pore pressure never exceeds the overburden stress irrespective of the stress regime.
- Depending upon the stress regime, the minimum and maximum horizontal principal In-Situ Stress may exceed the Overburden In-Situ Stress.
- Stability model should never be considered as a purely deterministic.

9.2 RECOMMENDATIONS FOR FUTURE WORK

1. The limitations in this work includes experimental laboratory facilities for determining rock strength parameters, collecting core samples from greater subsurface depth for a particular field of study.
2. Better predictions are possible using geomechanical wellbore stability software.
3. Collaborative research work sponsored by some oil industry for particular field can be done based on the above work.
4. More case studies backed by field data are recommended for further research work.

REFERENCES

1. McLean, M. and Addis, M. A. (1990).Wellbore stability: the effect of strength criteria on mud weight recommendations. 65th Annual Technical Conference and Exhibition of the Society of Petroleum Engineers, New Orleans, Society of Petroleum Engineers.
2. M.A. Mohiuddin, K. Khan, A. Abdulraheem , A. Al-Majed, M.R. Awal, 'Analysis of wellbore instability in vertical, directional, and horizontal wells using field data' Journal of Petroleum Science and Engineering 55 (2007) 83–92
3. Abouzar Mirzaei Paiaman, Saman Azadbakht, Bandar Duraya Al-Anazi, 'Optimizing wellbore inclination and azimuth to minimize instability problems' Oil and Gas Business, 2008
4. Samantha Grandi, Rama Rao, and M. Nafi Tokoz , 'Geomechanical Modeling of In-Situ Stresses Around a Borehole'. Earth Resources Laboratory, Dept. of Earth, Atmospheric, and Planetary Sciences, Massachusetts Institute of Technology Cambridge, MA 02139.
5. Zhou Mingxin and Tang Xinguo, Dagang Oil Field, PetroChina; Wu Bailin, Chee Tan, Yang Shiduo and Wang Shunchang, Schlumberger, 'Comprehensive Geomechanics Study Helps Mitigate Severe Stuck Pipe Problems in Development Drilling in Bohai Bay, China' International Petroleum Technology Conference held in Doha, Qatar, 7–9 December 2009.
6. P.J. McLELLAN Shell Canada, 'Assessing the Risk of Wellbore Instability in Horizontal and Inclined Wells' JCPT, May 1996, Volume 35, No.5

7. Patrick M. Collins, SPE, CIM, CHOA, Petroleum Geomechanics Inc.' Geomechanics and wellbore stability design of an offshore horizontal well, North Sea '2002 SPE International Thermal Operations and Heavy Oil Symposium and International Horizontal Well Technology Conference held in Calgary, Alberta, Canada, November 2002.

8. J. Zhang, W. B. Standifird, K. Adesina Knowledge Systems, Inc., Sugar Land, Texas , USA, G. Keaney Norsk Hydro Produksjon AS, Bergen, Norway, "Wellbore stability with consideration of pore pressure and drilling fluid interactions'. Golden Rocks 2006, The 41st U.S. Symposium on Rock Mechanics (USRMS): June 17-21, 2006.

9. Ali S. Raba'a, Hazim H. Abass, and Drew E. Hembling, Saudi Aramco, and Thomas Finkbeiner, GeoMechanics International 'A Geomechanical Facies-Based Approach To Optimize Drilling and Completion Strategy of an Unconsolidated Sandstone Reservoir, Saudi Arabia'. the 2007 SPE Annual Technical Conference and Exhibition held in Anaheim, California, U.S.A., 11–14 November 2007.

10. Kaibin Qiu, SPE, Schlumberger; Julio Gonzalez Felgueroso, Gabino Lalinde, Abdulmagid Naas, and Bernard Coste, Akakus Oil Operations; and John Fuller, SPE, Schlumberger, 'Geomechanics Enables the Success of Horizontal Well Drilling in Libya: A Case Study . 2008 IADC/SPE Drilling Conference held in Orlando, Florida, U.S.A., 4–6 March 2008.

11. Warlick, L.M., Abass, H.H., Khan, M. R., Pardo Techa, C.H., Tahini, A.M., Shehri, D.A., Badairy, H.H., Shobaili, Y.M./Saudi Aramco, Finkbeiner, T and Perumalla, S./GeoMechanics International. Evaluation of Wellbore Stability during Drilling and Production of Open Hole Horizontal Wells in a Carbonate Field' 2009 SPE Saudi Arabia Section Technical Symposium and Exhibition held in AlKhobar, Saudi Arabia, 09–11 May 2009.

12. G.G. Donovan, P.E., and T.J. Bourgeois, Shell Exploration and Production Co. 'Applied rock mechanics in drilling of depleted

reservoirs in deepwater Gulf of Mexico. SPWLA 48th Annual Logging Symposium held in Austin, Texas, United States, June 3-6, 2007.

13. Donald Lee, SPE, Schlumberger, Juan Pablo Cassanelli, Pluspetrol, Marcelo Frydman, SPE, Schlumberger, Julio Palacio, Schlumberger, Roger Delgado, Pluspetrol, Bryan Collins, SPE, Schlumberger, 'Using a Dynamic Mechanical Earth Model and Integrated Drilling Team to Reduce Well Costs and Drilling Risks in San Martin Field'. SPE Annual Technical Conference and Exhibition held in Denver, Colorado, U.S.A., 5 - 8 October 2003.

14. Weiren Lin, Koji Yamamoto, Hisao Ito, Hideki Masago, and Yoshihisa Kawamura, 'Estimation of Minimum Principal Stress from an Extended Leak-off Test Onboard the Chikyu Drilling Vessel and Suggestions for Future Test Procedures'. Scientific Drilling, No. 6, July 2008.

15. A. Khaskar, GeoMechanics International, A.H. Warrington, Oil Search Ltd, M.E. Magee, GeoMechanics International, K.L. Burgdorff, GeoMechanics International, and D.A. Castillo, GeoMechanics International, 'Wellbore Breakout Analysis in the Southeast Moran Field , Papua New Guinea' SPE Asia Pacific Oil and Gas Conference and Exhibition held in Perth , Australia , 18-20 October 2004.

16. Matthews, W. and Kelly, J. (1967). How to predict formation pressure and fracture gradient. Oil and Gas Journal, February, 92-106.

17. Bradley, W.B. (1979). Failure of inclined boreholes. Transactions of the ASME, December, 101, 232-239.

18. Eaton B et al (1999) "Fracture gradient prediction for the new generation" SPR reprint series: pore pressure and fracture gradients.

19. J. Zhang, W. B. Standifird, K. Adesina (2006) "Wellbore stability with consideration of Pore pressure and drilling fluid interactions".

20. M. Frydman, J.D. Restrepo (2007) Reducing drilling risks in overpressurized formation.

21. Zhou Mingsin and Tang Xinguo, Dagang Oilfield, PetroChina-Schlumberger,(2009) Geomechanics study helps mitigate Stuck pipe problem.

22. Fjaer E et al (1992). Petroleum Related Rock Mechanics. Development in Petroleum Science 33,Elsevier.

23. Amoco-Wellbore Stability Manual.

24. John R Harrison and John A - Engineering Rock Mechanics, an Introduction to the principles.

25. Suping and Jincai Zhang "Engineering Geology for Underground Rocks"

26. Mark .D. Zoback " Reservoir Geomechanics"

27. Alan E. Mussett & M.Aftab Khan, 2000.Looking Into The Earth, Cambrdge University Press,UK

28. R.Pusch , 1995. Rock Mechanics on Geological Base, Developments in Geotechnical Engineering, 77, Elseveier, USA

29. Sadhu Singh, 2009.Applied Stress Analysis, Khanna Publishers, India

30. Ching H.Yew, 1997.Mechanics of Hydraulic Fracturing, Gulf Publishing Company, Houston Texas

31. French Oil Gas Industry Association Publications, Technical Committee, 1990.Directional Drilling and Deviation Control Technology

32. Ph.A.Charlez.1991.Rock Mechanics, Volume 1, Theoretical Fundamentals Editions Technip, Paris

33. Ph.A.Charlez.1997.Rock Mechanics, Volume 2, Petroleum Applcations, Editions Technip, Paris

34. Adam T. Bourgoyne Jr,Keith K .Millheim, Martin E.Chenevert & F.S.Young Jr.2001.Applied Drilling Engineering ,Society of Petroleum Engineering

35. www.rocscience.com
36. www.4shared.com
37. www.forced-balanced.net
38. www.LinkedIn.com
39. www.world-stress-map.org
40. www.spe.org
41. www.armarocks.org
42. http://pangea.stanford.edu/research/geomech/
43. www.isrm.net
44. www.carma-rocks.ca

Appendix A

C-Program to calculate the Transposed In-Situ Stress

```
#include<stdio.h>
#include<math.h>
#include<stdlib.h>
main()
{
double ar,br,alpha=30,beta=360,d1=10000,d2=8000,d3=7000;
double dx,dy,dz,txy,tyz,tzx;
fflush(stdin);
clrscr();
printf("Trigonametric functions \n");
ar=(double)alpha*3.14/180;
br=(double)beta*3.14/180;
dx=d2* sin(br)*sin(br) + d3*cos(br)*cos(br);
dy=cos(ar)*cos(ar) * (d2*cos(br)*cos(br) + d3*sin(br)*sin(br)) +
d1*sin(ar)*sin(ar);
dz=sin(ar)*sin(ar) * (d2*cos(br)*cos(br) + d3*sin(br)*sin(br)) +
d1*cos(ar)*cos(ar);
txy=cos(ar)*sin(br)*cos(br)*(d2-d3);
tyz= sin(ar)*cos(ar)* ( d1-d2*cos(br)*cos(br)-d3 *sin(br)*sin(br));
tzx= sin(ar)*sin(br)* cos(br)*(d3-d2);
printf(" The result of the following expressions are\n\n");
printf("dx= %f \t dy=%f \t dz= %f\n\n", dx,dy,dz);
printf("txy= %f \t tyz=%f \t tzx= %f\n\n", txy, tyz, tzx);
getch();
}
```

For the input data

TVD = 10000 ft

Mud Weight = 9 & 12 ppg

Vertical stress=10000 psi (σv)

Maximum horizontal stress = 8000 psi (σH)

Minimum horizontal stress = 7000 psi (σh)

Case (i)

Azimuth = 30 degrees

Inclination = 0 to 90 degrees

Case (ii)

Azimuth =0 to 360 degrees & Inclination=30 degrees

Output of the Program

When Azimuth = 30 ° & Inclination = 30 °

Trigonametric functions

The result of the following expressions are

dx= 7249.77; dy= 8312.155; dz= 9438.07

txy=374.94; tyz= 973.88; tzx= -216.18

C-Program to calculate the Induced Wellbore Stresses

```
#include<stdio.h>
#include<math.h>
#include<stdlib.h>
main()
{
double
tr,theta=0,pw,mw=9,tvd=10000,v=0.2,dx=7249.77,dy=7750.23,dz=10000,txy
=432.88,tyz=0,
tz =0;
double drr,dyy,dzz,trz;
fflush(stdin);
clrscr();
printf("Trigonametric functions \n");
tr=(double)theta*3.14/180;
pw=tvd*0.052*mw;
drr=pw;
dyy=dx+dy-pw-2*(dx-dy)*cos(2*(tr))-4*txy*sin(2*(tr));
dzz=dz-2*v*((dx-dy)*cos(2*(tr))+2*txy*sin(2*(tr)));
trz=2*(tyz*cos(tr)-tzx*sin(tr));
printf(" The result of the following expressions are\n\n");
printf("drr= %f \t dyy=%f \t dzz= %f\n\n", drr,dyy,dzz);
printf("trz= %f \n\n", trz);
getch();
}
```

Output of the Program

When Azimuth = 30 ° & Inclination = 30 °; Mud Weight= 9ppg

Trigonametric functions

The result of the following expressions are

drr= 4680; dyy= 10646.846; dzz= 9391.058

trz=1903.31

C- Program to calcute both transposed and induced wellbore stresses

```
#include<stdio.h>
#include<math.h>
#include<stdlib.h>
main()
{
double
ar,br,tr,alpha=30,beta=100,theta=100,pw,mw=9,tvd=10000,d1=10000,d2=800
0,d3=7000,v=0.2;
double dx,dy,dz,txy,tyz,tzx,drr,dyy,dzz,ttrz;
fflush(stdin);
clrscr();
printf("Trigonametric functions \n");
ar=(double)alpha*3.14/180;
br=(double)beta*3.14/180;
tr=(double)theta*3.14/180;
pw=0.052*tvd*mw;
dx=d2* sin(br)*sin(br) + d3*cos(br)*cos(br);
dy=cos(ar)*cos(ar) * (d2*cos(br)*cos(br) + d3*sin(br)*sin(br)) +
d1*sin(ar)*sin(ar);
dz=sin(ar)*sin(ar) * (d2*cos(br)*cos(br) + d3*sin(br)*sin(br)) +
d1*cos(ar)*cos(ar);
txy=cos(ar)*sin(br)*cos(br)*(d2-d3);
tyz= sin(ar)*cos(ar)* ( d1-d2*cos(br)*cos(br)-d3 *sin(br)*sin(br));
tzx= sin(ar)*sin(br)* cos(br)*(d3-d2);
drr=pw;
dyy=dx+dy-pw-2*(dx-dy)*cos(2*(tr))-4*txy*sin(2*(tr));
dzz=dz-2*v*((dx-dy)*cos(2*(tr))+2*txy*sin(2*(tr)));
ttrz=2*(tyz*cos(tr)-tzx*sin(tr));
printf(" The result of the following expressions are\n\n");
printf("dx= %f \t dy=%f \t dz= %f\n\n", dx,dy,dz);
```

```
printf("txy= %f \t tyz=%f \t tzx= %f\n\n", txy, tyz, tzx);
printf(" The result of the following expressions are\n\n");
printf("drr= %f \t dyy=%f \t dzz= %f\n\n", drr,dyy,dzz);
printf("ttrz= %f \n\n", ttrz);
getch();
}
```

Experimental exposure at NIRM, Bangalore

NIRM is equipped with modern laboratory facilities for determining the engineering properties of rocks as per international standards. I had completed basic experimental work at National Institute of Rock Mechanics (NIRM), Bangalore during 12th July to 24th July 2010.

Rock properties determined using Triaxial Setup

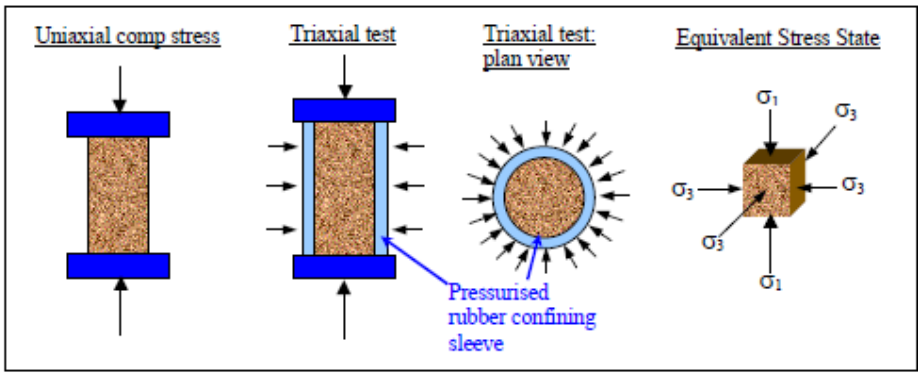

Tri-axial Test Result

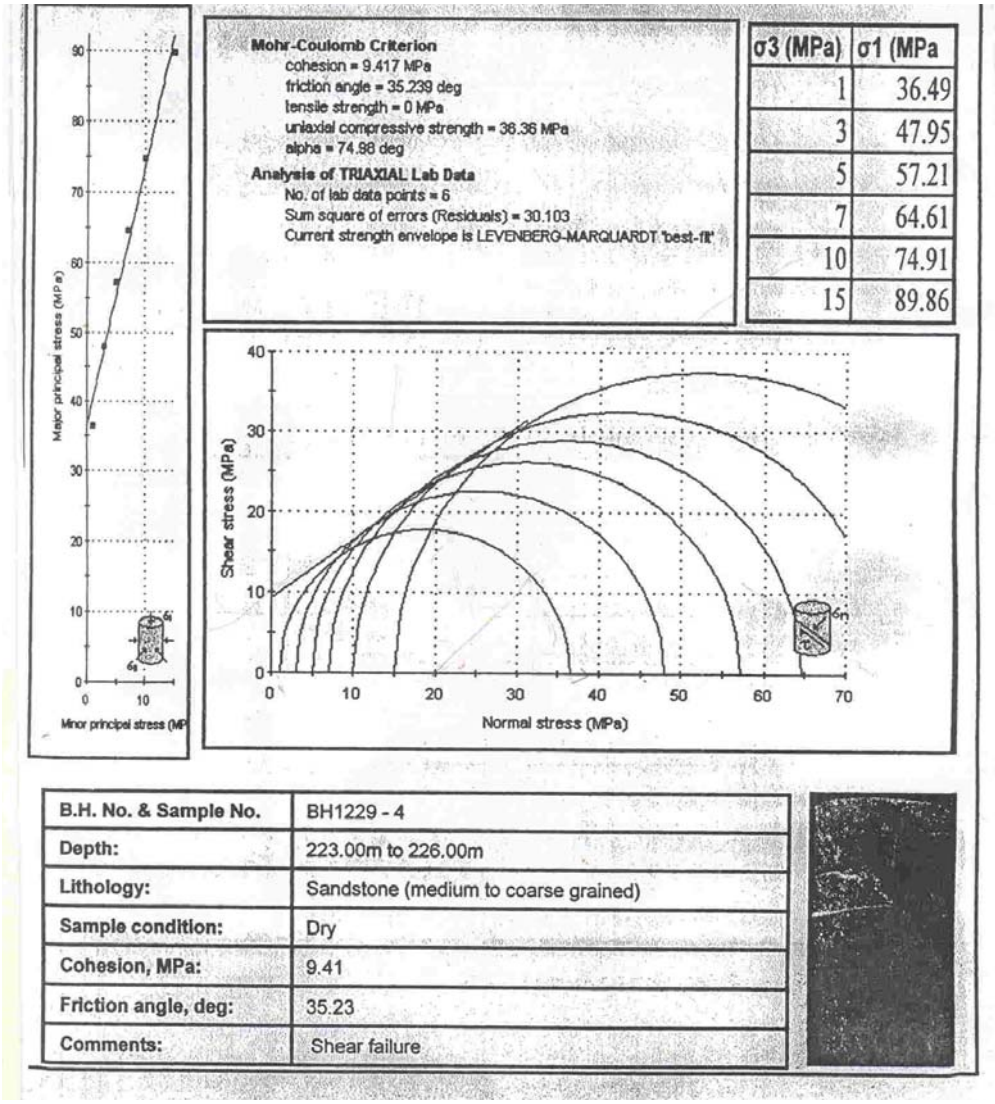

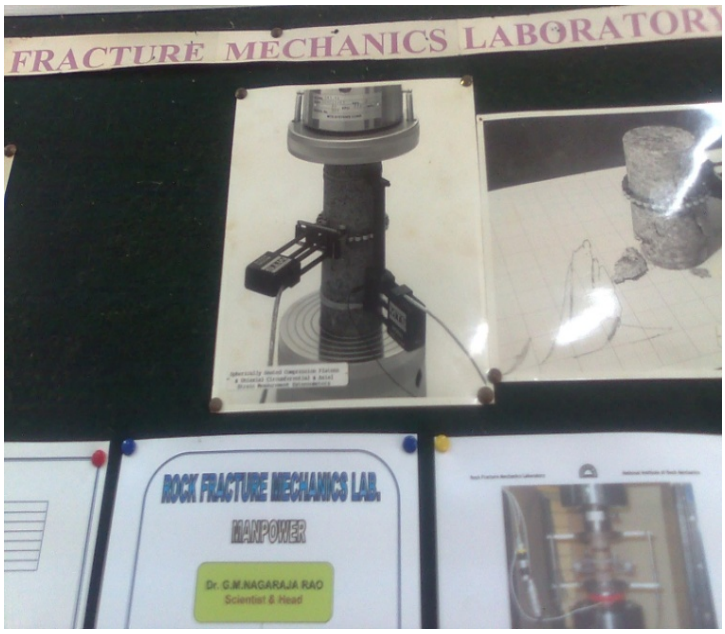
FRACTURE MECHANICS LABORATORY
ROCK FRACTURE MECHANICS LAB.
MANPOWER
Dr. G.M.NAGARAJA RAO
Scientist & Head


MTS
815
CAUTION

Dharmendra Kumar Gupta

BRIEF PROFILE

Dharmendra Kumar Gupta received a B. E. degree in *Mechanical Engineering* from Poona University, Pune (India) in 1992, M.E degree in *Analysis & Design of process Equipments* from Allahabad University, Allahabad (India) in 1997 and Ph. D. degree in *Study of Wellbore Stability With Varying Borehole Orientation Through Stress Condition Modeling* from University of Petroleum & Energy Studies, Dehradun (India) in 2011.

PROFESSIONAL EXPERIENCE:

- Proven record of *18 years performance oriented experience* in teaching, technical training, industry, research, publication & administration.
- Oil Field Equipment ***(BOP Accumulator Unit,Control Pannel, Hyd.Tongs, Swivel Joints , Flanges, Spools etc.)*** Design & Development as per international standards i.e.API-6A, 16 D, 7 K. at SARA *GROUP OF INDUSTRIES ,being HOD (R & D)Dehradun*

Subjects Handling

- Teaching *Drilling Engineering & Well Completion*, *Machine Design, MOS* to B.Tech. Students
- *Drilling Technology," Pumps, Compressors Selection, Sizing & Specifications"* to M Tech Students (Pipe Line Engg.)
- Short- term courses for GTs (E & P)

SPECIAL ACHIEVEMENT

- Excellent motivational ability to extract up to 100 % from students

RESEARCH ACTIVITIES:

1. Research paper on "*Orthotropic Pressure Vessels subjected to local Loads*" published in ***International Journal of Pressure Vessels and Piping*** 76 (1999) 387-392.
2. "The Analysis of Thermal Effects in Journal Bearings - *A Review*" published in *Fourth National Conference on Thermal Systems*. Feb 22-23, 2003 at BHU, Varanasi.
3. Research paper on '*Conical whirl Instability of Hydrodynamic Porous Journal Bearing in Turbulent Regime* ,published in **Institution Of Engineers India** ,Sep.2007
4. Research paper presented on '*Effect of Non –Homogeneous permeability on steady state performance of turbulent hybrid porous journal bearing*, at **International Tribology Conference ,Kobe, Japan ,** Feb.2005
5. Research paper "*A fresh look at Wellbore Stability Analysis to Sustainable Development of Natural Resources: Issues and Opportunities* "published in **International Journal of Science Technology & Management Vol. 2, Issue 1, February 2011**

BOOKS PUBLISHED:

1. "***Basic Mechanical Engineering***" (5th edition 2010) Dhanpat Rai & Co. (P) Ltd., Delhi.
2. "***Engineering Mechanics***" (4nd edition, 2010), Dhanpat Rai & Co. (P) Ltd., Delhi.

MEMBERSHIP OF PROFESSIONAL BODIES

- Life Member of "*Indian Society for Technical Education, Delhi*."
- Associate Member of "*The Institution of Engineers (India)*".
- Affiliate Member of the "Energy Institute", UK.
- Member of Society of Automotive Engineers ,USA

Contact Details: 0135-2776089 ext 218 (O)
9837717946 (Mob)
dkgupta@ddn.upes.ac.in